# Potentiation of anti-tumor immunity by RIPK1/RIPK3-dependent necroptosis

Annelise G. Snyder

A dissertation submitted in partial fulfillment of the
requirements for the degree of
Doctor of Philosophy

University of Washington
2019

Reading Committee:
Andrew Oberst, Chair
Marion Pepper
Anthony Rongvaux

Program Authorized to Offer Degree:
Immunology

## ABSTRACT OF THE DISSERTATION

Potentiation of anti-tumor immunity by RIPK1/RIPK3-dependent necroptosis

Annelise G. Snyder

Doctor of Philosophy in Immunology

University of Washington, 2019

Dr. Andrew Oberst, Chair

Programmed cell death (PCD) represents a set of signaling processes evolved as a mechanism to eliminate cells, both during turnover under homeostatic conditions as well as removal of cells that have been compromised by insults such as infection or injury. Distinct cell death modalities, such as apoptosis, necroptosis, and pyroptosis, differ with respect to their signaling requirements, morphological characteristics, and molecular species produced or released by dying cells. The immune system has evolved to recognize various types of signals associated with cell death, allowing it to distinguish between physiological cell death at equilibrium and potential threats to the host such as infection. The immune system can then respond to these signals appropriately in order to either (a) dampen responses to promote immune tolerance in the context of homeostatic cellular turnover, or (b) promote inflammation that potentiates pathogen clearance in the context of infection. The mechanisms underlying the downstream immune responses mounted against dying cells have been primarily studied in settings of autoimmunity or pathogenic infection. However, characterization of these responses has been relatively poorly defined in models of tumor immunology, as these studies are

complicated by the evasion of cell death signaling mechanisms commonly exhibited by transformed tumor cells.

Tumor immunotherapy encompasses a repertoire of clinical treatments that aim to stimulate immune cells such that they recognize and eliminate tumor cells, and has shown remarkable efficacy in patients. Many immunotherapeutic agents function by promoting inflammatory immune responses, either by stimulating innate immune signaling pathways or by enhancing the activation and expansion of tumor-specific cytotoxic $CD8^+$ T cells. Therefore, strategies to manipulate the immunogenicity of tumor cell death to more potently stimulate tumor-specific immunity constitutes an important target that could potentially synergize with existing immunotherapy treatments. Inflammatory forms of PCD are of particular interest in the context of tumor immunity, as the tumor microenvironment (TME) is typically viewed as a highly immunosuppressive tissue niche. Necroptosis is one such inflammatory form of PCD which occurs downstream of the receptor-interacting protein kinases RIPK1 and RIPK3. The activation of this complex leads to lytic cell death via MLKL-mediated pore formation, accompanied by *de novo* production of pro-inflammatory mediators such as chemokines and cytokines. Considering the potently inflammatory nature of necroptosis in comparison to other cell death modalities such as apoptosis, we sought to test how specific induction of necroptosis within the TME instructs anti-tumor immunity.

In this dissertation, we show that ectopic administration of necroptotic cells to the TME promotes $BATF3^+$ cDC1- and $CD8^+$ leukocyte-dependent anti-tumor immunity accompanied by increased tumor antigen loading by tumor-associated antigen presenting cells. Tumor control by necroptotic cells requires the activity of the RIPK1/RIPK3 signaling complex and its subsequent activation of NF-κB, but not the release of damage-associated molecular patterns (DAMPs) or

their ability to stimulate innate pattern recognition receptors (PRRs), highlighting a critical role for death-independent functions of the RIPK1/RIPK3 necrosome in determining the immunogenicity of necroptotic cells. Additionally, immune stimulation by necroptotic cells synergizes with co-administration of the immune checkpoint blockade (ICB) reagent α-PD-1, conferring durable tumor clearance in animals that received dual therapy. Furthermore, we report the development of constitutively-active forms of the necroptosis-inducing enzyme RIPK3, and show that delivery of a gene encoding this enzyme to tumor cells using recombinant adeno-associated viruses (AAVs) induces tumor cell necroptosis which synergizes with immune checkpoint blockade to promote durable tumor clearance. Collectively, these findings define a beneficial role for RIPK1/RIPK3 activation as a proximal target in the initiation of tumor-specific immune responses.

Although monotherapy with existing immunotherapy modalities such as ICB has shown great efficacy in a subset of cancer patients, restoration of neoangiten recognition alone is often insufficient to eliminate tumors in most individuals. Therefore, successful tumor immunotherapy regimens will likely require the rational selection of multiple treatment modalities aimed at orthogonal immune targets in order to achieve optimal clinical outcomes. Based on our findings, we propose that maximizing the immunogenicity of dying cells within the tumor microenvironment through specific activation of the necroptotic pathway represents one such beneficial treatment approach that may warrant further clinical development. This work has yielded additional insights regarding the relationship between PCD modalities and anti-tumor immune responses, and provides evidence that induction of alternate death pathways such as necroptosis could improve therapeutic outcomes in the context of tumor immunity.

## TABLE OF CONTENTS

## LIST OF FIGURES

## LIST OF TABLES

## ACKNOWLEDGEMENTS

I thank my advisor, Andrew, for his enduring support and optimism over the past 5 years. Working with Andrew has taught me immensely about scientific creativity, research independence, and effective communication, and has helped me developed confidence and happiness in my work that I didn't realize was possible when I started graduate school. He has always been an enthusiastic advocate for me in the pursuit of my professional goals, and his dedicated support in everything from grant applications, manuscript drafts, and advice on postdoc labs has played a critical role in my accomplishments as a graduate student. I am extremely fortunate to have worked for an advisor who allowed me to grow as a scientist and develop the skills that I need to be successful as an academic researcher, and will always be deeply appreciative of the opportunities that Andrew has given me.

I thank the members of my committee for their valuable support and feedback over the past few years. I always looked forward to our scientific discussions, as these helped me learn more about experimental design, data interpretation, and any conceptual background information that I needed to better understand my own research project. I'm truly grateful to have had a kind, respectful, and rigorous group of scientists show their investment in my project, and the suggestions that I received during my committee meetings undoubtedly strengthened the publications that I authored during my PhD. I particularly thank Marion, who has provided additional mentorship and support throughout my training; it has meant a lot to me to have worked with such a strong female scientist role model early on in my career.

I thank the past and present Oberst lab members that I've worked with throughout my training, mostly for dealing with my tyrannical views regarding lab cleanliness and flow antibody organization. They've also properly dragged me for my idiotic commitment to

completing my PhD using manual citations instead of a reference manager, which I fully deserve. Nick is one of the kindest and smartest people I've worked with, even if he still thinks it's okay to tell me when I look tired. I will fondly think of him any time I get angry watching a presentation that involves a poorly-executed joke slide, or anytime I encounter stereotypical PNW BS like a chair holding 4 different Patagonia jackets at once. Sigal increased my quality of life as soon as she joined our group, likely due to the positive energy fields her crystals established in our desk space. She is an inspiring, ambitious woman that serves relentless witch energy, and I'll miss her dearly when I leave. Brian is an incredible mentor, role model, and friend, who has taught me that you can be a demanding scientist that does high quality research while still being deeply empathetic and fiercely invested in improving the culture of the research community. Most importantly, he's taught me that using a well-placed Drag Race reaction gif or withering stare can say more than words ever could in certain conversations. I've been honored to work with some truly inspiring, brilliant, and thoughtful people during my time here, and I can't wait to see the amazing things that my former labmates do in the future.

I thank more friends and classmates than I have space to list in this section. The graduate student community in our department has grown stronger and more supportive during my PhD, and I am constantly impressed by the work that done by my peer group here at Washington. I'm so proud of my classmates for pursuing interesting research projects while also prioritizing supporting one another, since this attitude makes us all stronger together. I can only hope that the tradition of sketchily brown-bagging it in the park by MOHAI carries on each summer. I also have an amazing group of friends from my old east coast life that, despite all of us being spread out across the country, have made huge efforts to stay in touch ever since I moved to Seattle 5 years ago. In particular, I want to thank the Brodsky lab at the University of Pennsylvania for

being a close group of mentors and friends that set me on the path towards a research career. I also thank my Williams soccer teammates for being an incredible group of women that has given me so much love and inspiration over the past decade. These relationships have carried me through rough times here, and I am so lucky to have these people in my life to help keep me happy and grounded.

I thank my mother, Dr. Wendy Lehnert, who taught me to be unapologetically feisty, ambitious, and complex. She has made me into the woman that I am today. I also thank my brother, Michael Snyder, who will always be my first role model. I am remarkably privileged to have been raised in an academic family that prioritized education above all else, with parents who gave me all the tools that I needed to succeed in life and in my career. I took this for granted for far too long, but I fully appreciate it now. Our family has experienced pain, but I'm thankful that we've been able to invest our energy on healing together over the past few years.

I thank Duncan MacDiarmid, who has taught me patience, joy, and more than I would ever want to know about the mechanical nuances of Toyota 4Runner engines from 1989. He has brought me peace and lightness in times when I had none, and I am a calmer and happier person for having met him. I am profoundly grateful to have a truly equal partner to build a home with me here in the northwest, even though I'll always be terrible at every outdoor hobby that sustains his inner Oregonian core. Lastly, and most importantly of all, I thank Wallace. His tireless efforts in supervising my data analysis, practice presentations, and writing sessions throughout the entirety of my PhD have kept me on the path towards professional success. My little family in this upper left hand corner means the world to me.

Annelise Snyder
University of Washington
May 2019

## DEDICATION

This dissertation is dedicated to the memory of my late father, Dr. Mark Snyder. He gave me my obsessive work ethic, my cursing problem, my scientific curiosity, my dark humor, and my drive to care for others, all of which have served me well during my PhD. He fiercely dedicated his life to teaching, and I can only hope to have a fraction of his influence on any future mentees or students of mine. He showed me that the most fulfilling thing in life is to find a career in a field that you love, and to pursue that passion in a way that empowers and supports others along the way. Although I struggled to find this for several years, I am so grateful to have found my purpose here at Washington, even if he was no longer here to see me fully realize it. I carry him with me in everything that I do in research and teaching, and a day hasn't gone by in lab without me thinking of him in moments of bittersweet silence. My world has been sadly less strange without him.

"Do you know the story of the Russian cosmonaut?
He goes up in this big spaceship,
and he's got this portal window.
He's looking out of it,
and he sees
the curvature of the Earth
for the first time.

All of a sudden, this strange
*ticking*
begins coming out of the dashboard.
But he can't find it.
He can't stop it.
It keeps going.
A few hours into this… begins to feel like torture.
What's he going to do?
He's up in space.

So the cosmonaut decides:
The only way to save his sanity,
is to fall
in love
with this sound."

Brit Marling, Another Earth

# Chapter 1

Introduction

This chapter is adapted from the following publication:

Messmer MN*, Snyder AG*, Oberst A. Comparing the effects of different cell death programs in tumor progression and immunotherapy. *Cell Death Differ*. 2019; **26**: 115-129.

**Denotes equal contribution authorship.*

## 1.1 Introduction

Programmed cell death (PCD) refers to the signaling mechanisms that control distinct forms of cellular suicide. A growing body of literature has sought to determine the underlying mechanisms of how the immune system differentially responds to distinct cell death modalities, which has classically centered on studies in the context of homeostatic dying cell clearance or elimination of infected cells during pathogenic infection[1-9]. One such cell death program, termed necroptosis, has been shown to more potently stimulate antigen-specific immune responses in the context of vaccination[10], viral infection[12,13], and inflammation[14], though application of these findings to the tumor immunology field has yielded conflicting results. Considering the remarkable success of cancer treatments that stimulate anti-tumor immune responses, elucidation of mechanisms by which distinct PCD modalities can differentially instruct immunity represents an important area of study both in the cell death and tumor immunology fields.

This dissertation describes a protective role for inflammatory necroptosis in the context of tumor immunity. Specifically, our work identifies a role for death-independent signals derived from necroptotic signaling components in potently stimulating anti-tumor immune responses. This introductory chapter will provide a broad overview of PCD pathways and their downstream immunological effects, primarily focusing on the current state of the PCD field with respect to the tumor microenvironment. As the field of tumor immunotherapy necessitates the discovery and characterization of novel therapeutic targets, we stress the need to identify novel strategies for manipulating the relative immunogenicity of key events involved in the generation of a tumor-specific immune response, including cell death.

## 1.2 Programmed cell death in host defense and immunity

Programmed cell death (PCD) is required for normal development and maintenance of tissue homeostasis; in these contexts, cell death generally occurs via classical apoptosis. Additionally, evolution has selected for alternate forms of PCD not engaged during development, but instead occur in response to pathogen exposure or during cellular stress. Such PCD include necroptosis, pyroptosis, ferroptosis and others, though importantly apoptosis can also be triggered by similar stimuli. Distinct forms of PCD are defined by both specific signaling molecules activated downstream of death-inducing stimuli as well as characteristic morphologies of dying cells following initiation of these distinct programs. This is in contrast to unprogrammed lytic necrosis, or cell death due to loss of plasma membrane integrity mediated by physical stress which releases cellular contents into the extracellular space independent of any signaling cascades. Several reviews have extensively covered the signaling requirements for distinct PCD pathway[1-9].

Although distinct molecular mediators of each PCD pathway have been identified, the field has only recently focused on how the immune system mechanistically differentiates between these death modalities. In particular, the effects of inflammatory or immunogenic PCD on the initiation of anti-tumor immune responses are just beginning to be defined. This dissertation focuses primarily on comparing apoptosis and necroptosis as 1) they represent two extremes on the PCD spectrum in terms of inflammation, 2) they often directly antagonize each other, and 3) there is a strong body of evidence for their roles in cancer. Abbreviated discussion of the signaling pathways for these two forms of PCD are included below and summarized in **Figure 1**.

*Apoptotic Signaling*

Apoptosis is the major cell death pathway engaged during development and tissue homeostasis, but can also be induced downstream of certain cellular stresses such as infection. There are two pathways for apoptosis engagement - either extrinsic or intrinsic – that are summarized in **Figure 1** and extensively reviewed elsewhere[1,2,14-19]. Both result in activation of cysteine proteases, termed caspases, which trigger cell death with characteristic morphology involving nuclear condensation and membrane blebbing.

Extrinsic apoptosis can be engaged downstream of death receptor (DR) signaling at the plasma membrane, including binding of TNF to TNFR1/2, FasL-Fas interactions, or TRAIL-TRAIL-R activation, though the exact signaling pathways they engage are distinctive. Extrinsic apoptosis requires recruitment of the adaptor protein Fas-associated death domain protein (FADD) which activates the apical signaling enzyme caspase-8 through formation and autocatalytic stabilization of caspase-8 homodimers. Cleaved caspase-8 homodimers can then directly activate executioner caspases, caspase-3 and caspase-7, or activate mitochondrial apoptosis via cleavage of Bid. Executioner caspases-3 and-7 cleave aspartate residues in a wide variety of intracellular proteins, leading to catastrophic loss of cellular function and cellular dismantling[14]. DR signaling does not exclusively trigger apoptosis; indeed, NF-κB and MAPK-dependent transcription downstream of DR ligation can actively suppress DR-induced apoptotic signaling. The caspase paralog cFLIP is another notable target of DR-mediated transcriptional signaling[20]. In some contexts, it forms a suppressive heterodimer with caspase-8, preventing further pro-apoptotic signaling[21]. DR-induced apoptosis can also be blocked by inhibitor of apoptosis (IAP) E3 ligases or by Fas apoptosis inhibitory molecules (FAIMs). Taken together, a

paradigm emerges that DR engagement triggers diverse inflammatory transcriptional programs; apoptosis occurs upon relief of cFLIP-, IAP- and/or FAIM-mediated inhibition.

Intrinsic apoptosis converges on the same executioner caspases, caspases -3 and -7, but differs from extrinsic apoptosis with respect to upstream signaling[1,2]. Intrinsic apoptosis can be initiated by a variety of cellular stressors such as growth factor withdrawal, replication stress, DNA damage, and ER stress. Such stressors modulate Bcl-2 proteins. The Bcl-2 family includes both pro- and anti-apoptotic members, and the balance between these constituents determines cellular commitment to apoptosis. Pro-apoptotic Bcl-2 family members Bax, Bak and/or Bok mediate mitochondrial outer membrane permeabilization (MOMP), which releases cytochrome c (cytoC) from the mitochondrial intermembrane space into the cytosol[22]. Release of cytoC induces oligomerization of Apaf-1 in complex with the apical caspase of intrinsic apoptosis, caspase-9, to form a complex termed the 'apoptosome'[17,23]. Caspase-9 then activates executioner caspases -3 and -7, triggering cell destruction. Notably, this mitochondrial pathway can also be engaged by extrinsic apoptosis through caspase-8-mediated activating cleavage of pro-apoptotic Bcl-2 family member Bid.

The morphology of extrinsic or intrinsic apoptotic death is essentially the same[15], as apoptotic cells undergo chromatin condensation and DNA cleavage accompanied by cellular shrinkage. The cell dissociates into membrane-bound vesicles termed apoptotic bodies, which neatly package intracellular contents and dying cell organelles away from the extracellular space. These apoptotic bodies, coated in 'eat-me' signals such as phosphatidylserine (PS) and calreticulin (CRT), are rapidly cleared by phagocytes through a process known as efferocytosis[24,25]. Notably, because apoptosis is employed under homeostatic conditions for cellular turnover and renewal, efferocytosis is typically viewed as non-inflammatory. (**Figure**

**2A**). Indeed, mutations in genes associated with the proper packaging, recognition, and breakdown of apoptotic cells in the absence of any other infection or damage signals are associated with a break in immunological tolerance and manifestation of auto-immune disorders including systemic lupus erythematosus[26-28].

*Necroptotic Signaling*

In contrast to apoptosis, necroptosis is a more recently defined lytic form of PCD. While apoptosis depends on caspase activation, necroptosis requires activation of receptor-interacting protein kinases RIPK1 and RIPK3 **(Figure 1)**. Interestingly, RIPK1 is one of the adaptor proteins recruited to activated DR leading to NF-κB-dependent gene expression[29]. As noted previously, NF-κB signaling leads to formation of inhibitory cFLIP/caspase-8 heterodimers that prevent caspase-8 activation and subsequent extrinsic apoptosis. Notably, this heterodimer also suppresses necroptosis by inhibiting formation of RIPK1/RIPK3 heterodimers, which interact via RIP homotypic interaction motif (RHIM) domains present on both RIPK1 and RIPK3[5,30,31]. Thus, necroptosis downstream of DR ligation requires inhibition of caspase-8 through either viral effector proteins (such as the vICA protein encoded by MCMV)[32], pharmacological inhibitors (such as pan-caspase inhibitors zVAD-fmk or QVD-OPh), or possibly by loss of caspase-8 (observed in neuroendocrine cancers and others)[33]. In addition to DR signaling, evidence suggests RIPK3 can be activated downstream of viral sensing by the receptor DAI[32,34], viral nucleic acids detected by TLR3[35,36], or bacterial lipopolysaccharide sensed via TLR4[37].

Once RIPK3 is activated it engages in pleiotropic signaling that appears to be highly cell type- and context-specific[38]. Classically, RIPK1-RIPK3 interaction through RHIM domains aggregates into a multiprotein signaling complex variously termed the ‘necrosome’ or

'ripoptosome'. RIPK3 then phosphorylates the necroptosis executioner molecule mixed lineage kinase-like (MLKL)[39]. Phosphorylated MLKL forms homoheptameric pore-forming complexes which insert into cell membranes allowing cation entry and subsequent influx of extracellular fluid due to differences in osmolarity[40]. This influx is rapidly followed by catastrophic rupture of the plasma membrane and release of intracellular contents. Thus, necroptosis is a lytic form of PCD in sharp contrast to apoptosis: there is limited compartmentalization of organelles, and no ordered packaging of cell-associated debris for clearance by professional phagocytes. Necroptotic lysis releases several known immunogenic molecules, termed damage-associated molecular patterns (DAMPs), which can stimulate innate immune pattern recognition receptors (PRRs). Such DAMPs include self-nucleic acids that interact with PRRs typically associated with detecting viral DNA such as cGAS/STING[41], polymerized actin which can be recognized by Clec9a/DNGR1[42,43], HMGB1 which activates RAGE[44,45], ATP which activates P2X7[46,47], and calreticulin which activates CD91[48,49].

Originally, immune stimulation by necroptosis was primarily attributed to this release of DAMPs and subsequent activation of PRRs. However, the pattern of DAMPs released is virtually indistinguishable from other lytic forms of cell death including unprogrammed necrosis, or cell rupture following caspase-1-dependent pyroptosis[50]. Growing evidence indicates that necroptosis drives immune responses independent of — or in addition to — lytic MLKL-mediated death through other ripoptosome signaling[10-12,37,51,52]. Mice lacking caspase-8 are embryonic lethal due to RIP kinase induced necroptosis; additional loss of MLKL or RIPK3 results in viable offspring but subsequent development of autoimmune disorders, with earlier onset in MLKL deficient mice implicating MLKL-independent effects of RIPK3[51]. In a vaccination model, the ability of necroptotic cells to cross-prime antigen-specific cytotoxic $CD8^+$

T cells (CTL) required RIPK1-mediated NF-κB activation for production of pro-inflammatory cytokines and chemokines[10]. In this system, necroptotic cells incapable of signaling via RIPK1 due to disrupted RHIM binding still died following RIPK3/MLKL activation, and showed lytic DAMP release, but failed to cross-prime. During West Nile virus infection in the brain, RIPK3 activation produced pro-inflammatory chemokines that mediated leukocyte recruitment which was required for viral control[11]. Notably, this therapeutic effect of RIPK3 activation occurs independently of necroptotic death, as infected neurons are resistant to RIPK3-dependent lytic cell death.

Although the mechanisms whereby RIPK1 and/or RIPK3 upregulate pro-inflammatory gene expression remain to be elucidated, it has become apparent that this regulation contributes to necroptotic cell immunogenicity independent of lytic cell death and DAMP release. Because necroptosis appears to have evolved as an anti-viral form of cellular suicide, the current model is that necroptosis both eliminates a pathogen's replicative niche through deletion of infected cells while simultaneously providing a burst of *de novo* inflammatory signaling for recruitment and activation of leukocytes to the site of necroptotic cell death[6,53] (**Figure 2A**).

### 1.3 Endogenous mechanisms of cell death in the tumor microenvironment

Cancer represents a particular challenge when considering the impact of cellular death, as various environmental pressures have been placed on cancer cells to suppress one or more death pathways as they undergo continuous rounds of proliferation driven by dysregulated signaling and extensive mutation. This section summarizes what is known about endogenous engagement or activation of PCD, and how these processes impact oncogenesis.

*Apoptosis is commonly engaged, and evaded, during oncogenesis*

As the first PCD pathway described, apoptosis is well studied in cancer; accordingly, evasion of apoptosis is considered one of cancer's defining hallmarks[54]. Cancer cells can downregulate or block apoptotic signaling through regulation of protein expression, protein-protein interactions, or metabolic regulation[55-57]. Major targets of this regulation include: loss or inhibition of transcription factor p53 which normally drives pro-apoptotic gene expression following cellular stress or damage[58]; over-expression of antagonists to either extrinsic or intrinsic apoptotic pathways including increased expression of cFLIP and pro-survival BCL-2 protein family members[56,57]; and induction of the transcription factor hypoxia inducible factor-1 (HIF-1) contributing to pro-survival metabolism, increased angiogenesis, and immune suppression[55,59,60]. This anti-apoptotic regulation is not necessarily a direct cause of cancer but instead contributes to therapeutic resistance and disease progression in many cancer types.

The immune system also contributes selective pressure toward evasion of apoptosis. This process has been defined as 'immunoediting' and encompasses the concepts of elimination (early immune clearance of abnormal cells), equilibrium (a balance of immune resistance and immune stimulation), and escape (eventual outgrowth of tumors due to successful immune evasive or

immunosuppression)[56,61]. Early during oncogenesis, abnormal cells expressing mutated or modified proteins can stimulate immune responses by CTL, while over-expression of stress-related surface proteins or down-regulation of HLA can stimulate NK cells. CTL and NK cells use similar methods to induce cancer cell death; they release perforin and granzyme B into target cells to stimulate intrinsic apoptosis, or engage FasL-Fas to trigger extrinsic apoptosis. However, as described earlier, cancer cells have multiple mechanisms to subvert these apoptotic pathways and can thereby become resistant to immune attack[62,63]. Additionally, inflammatory events following immune recognition and activation, particularly production of interferon gamma (IFNγ), contribute to increased expression of PD-L1 on cancer cells[64]. PD-L1 is the ligand for PD-1, a negative regulatory receptor expressed on T cells including CTL. Engagement of PD-1 leads to suppressed T cell function and even T cell apoptosis[64]. Thus, cancer clones may be selected that are resistant to immune-mediated apoptosis, while simultaneously inducing apoptotic death in responding lymphocytes.

Despite early pressures to lose pro-apoptotic signaling, new work highlights the contribution of apoptosis to cancer progression[16,65,66] (**Figure 2B**). Tumors with high rates of spontaneous apoptotic death exhibit increased angiogenesis, increased risk of metastasis, and reduced patient survival, though these effects may be tumor type-specific[16,65]. Apoptosis downstream of DNA damaging agents has been implicated in lymphomagenesis due to the forced cycling of progenitor cells[67,68]. Engulfment of apoptotic debris by macrophages, as well as signaling by the caspase-3-dependent prostaglandin E2, increases macrophage production of vascular endothelial growth factor (VEGF) and matrix-metallo-proteinases responsible for extracellular matrix remodeling and implicated in metastatic progression[16]. Furthermore, apoptotic cell-derived prostaglandin E2 has also been implicated in promoting proliferation of

surviving tumor cells following radiotherapy[65]. Phosphatidylserine (PS) on the surface of apoptotic bodies allows binding of clotting factors to induce the coagulation cascade, which further contributes to a tumorigenic 'wound healing' program in macrophages. Additional 'find me' signals expressed during apoptosis such as CX3CL1 and lactoferrin have been associated with angiogenesis and promoting oncogenic receptor signaling[65,66]. Expression of 'don't eat me' molecules such as surface protein CD47 on cancer cells can inhibit phagocytosis by signaling through SIRPα, a receptor of the immunoglobulin superfamily, on myeloid cells[66], reducing uptake of tumor associated antigens for priming CTLs. While CD47 is over-expressed on many cancer cells, it is unclear how cancer cell death might regulate CD47 expression and function[66]. Thus, a complicated relationship exists between initial selective pressures to lose apoptotic sensitivity, followed by later pro-tumor benefits provided by immune suppressive or modulatory effects of excessive apoptotic death.

*Non-programmed cell death in the tumor environment*

Apoptosis is not the only form of cell death commonly associated with tumors, as solid tumors often harbor regions of necrotic tissue. However, it is difficult to determine signaling events preceding apparent necrosis - necrotic regions may result from PCD, such as secondary necrosis following apoptotic death, or from non-programmed cell death following physical loss of membrane integrity due to factors such as metabolic by-products or high interstitial pressure. There are no good markers to distinguish between residual debris generated by non-programmed necrotic death and late-stage debris generated by PCD discussed in this review. The distinction largely relies on morphological assessment to rule out apoptosis through the lack of apoptotic bodies, chromatin condensation, blebbing, or cytoplasmic vacuolization[1].

Tumor necrosis aligns closely with areas of hypoxia, suggesting this is a primary driver of necrosis[69]. As noted earlier, hypoxia would normally trigger apoptosis, but in some cancer cells, disruption of apoptotic signaling prevents normal cell death progression, resulting in cytoC release without activation of caspases and eventual necrosis[70]. The extent of tumor necrosis typically associates with negative prognoses across a variety of tumor types, as necrosis correlates with tumor size and grade, lymph node metastasis, and angiogenesis, suggesting that the presence of necrotic tissue is detrimental to anti-tumor responses[69]. Some of these effects may be attributable to the over-expression of HIF1 often detected surrounding these regions[71,72].

*Roles for necroptosis during oncogenesis*

In contrast to apoptosis, there is less evidence supporting engagement of endogenous necroptotic signaling within tumor cells. Necroptosis is a more recently described form of PCD typically studied in the context of viral infection; as such, cancer biology researchers may not be aware of the vagaries of defining necroptosis within the tumor microenvironment. This is further complicated by the fact that necroptotic cells can be difficult to detect *in vivo*[73-75]. The only necroptosis-specific readouts are phosphorylation of RIPK3 and/or MLKL, both of which are transient events only detectable in a narrow time window between initial engagement of necroptotic signaling and breakdown of necroptotic cells. More thorough characterization of necroptotic signaling proteins within human or murine tumors will be needed to determine whether endogenous necroptosis is engaged across different tumor models.

Despite obstacles to detection, there is promising evidence that engagement of immunogenic RIPK3 signaling within tumor cells could benefit anti-tumor immunity. In a recent screen of over 60 murine cancer cell lines, the majority of non-hematopoietic lines lacked RIPK3

protein expression; mechanistically, this silencing was attributed to inhibitory methylation of the *Ripk3* promoter[76]. Indeed, RIPK3 protein expression was similarly silenced in samples from human AML and breast cancer patients[76]. Additionally, *RIPK3* mRNA is decreased in human colorectal cancer (CRC) tissues compared to healthy colon controls[77], and loss of *RIPK*3 is associated with tumor progression in CRC[78]. Conversely, increased expression of *RIPK3* positively correlates with favorable outcomes in a variety of human tumors, including $HPV^+$ cervical cancer[79] and AML[80]. Consistent with the idea that RIPK3 expression promotes anti-tumor responses, the locus of the *RIPK3* gene (chromosome 14q11.2)[81] is frequently mutated in several types of neoplasia, including nasopharyngeal carcinoma[82] and acute lymphoblastic leukemia[83], although it remains to be determined whether these mutations are specifically within the *RIPK3* gene. Notably, complete loss of necroptotic components such as RIPK3 and MLKL does not result in spontaneous carcinogenesis[39,84,85], although combined loss of both necroptotic and apoptotic machinery results in lymphoproliferative disorders[30,31,51].

Collectively, these findings indicate that necroptotic signaling may exert a selective pressure during oncogenesis, whereby necroptosis-resistant clones are selected during immunoediting and subsequent immunoevasion. This offers a conceptually parallel selection mechanism as defined for the preferential outgrowth of apoptosis-resistant tumor cells[54,57,86]. Clones that lack signaling components required for multiple forms of PCD would have a considerable survival advantage over their apoptosis- or necroptosis-competent counterparts. In light of this, it is intriguing to consider therapeutic strategies for reconstituting tumor cells with PCD signaling components lost during selection to restore their ability to undergo immunogenic cell death programs. These findings also raise the question of which aspects of oncogenic

transformation, tumor formation, and metastasis may engage necroptotic signaling to account for the apparent pressure against this pathway in tumor evolution.

Conversely, other groups have shown a pro-tumorigenic role of RIPK3 signaling within tumors. In human pancreatic ductal adenocarcinoma (PDAC) samples, *RIPK1*, *RIPK3*, and *CXCL1* were highly expressed compared to healthy pancreatic tissue[87]. Interestingly, *Ripk3*$^{-/-}$ mice were protected from PDAC tumor progression, which was associated with decreased CXCL1-dependent intratumoral infiltration of immunosuppressive MDSCs and macrophages in conjunction with increased activation of tumor-infiltrating CTLs[88]. Furthermore, RIPK1 activation in murine B16.F10 primary melanoma tumors was associated with increased vascular permeability through p38/HSP27 activation, which enables tumor cell extravasation and dissemination throughout the vasculature, promoting metastasis[89].

Beyond direct evidence of pro-tumorigenic RIPK1/RIPK3 signaling, others have reported adverse prognoses associated with DAMPs released by lytic death. STING activation and type I IFN production promote oncogenesis in some settings[90], and even induction of immunological tolerance of tumor cells through downstream production of suppressive immune modulators including IDO, IL-10, and TGF-β[91,92]. Lastly, elevated extracellular potassium ion concentrations in areas of melanoma tumor necrosis suppress Akt-mTOR signaling and disable the function of intratumoral CTL[93], identifying an additional mechanism by which tumor necrosis promotes tumor survival by actively inhibiting CTL. Together, these papers identify a variety of mechanisms in which necroptotic signaling and its downstream byproducts may potentiate tumor subversion of the immune system.

Clearly, this second set of findings highlights the heterogeneous effects of RIPK1/RIPK3 signaling and its variability between immune, stromal, and tumor cell types, and how this affects

the tumor microenvironment (**Figure 2B**). It further stresses the paradoxical role of inflammation in the context of tumor immunity: although the established tumor microenvironment is typically viewed as immunosuppressive, pro-inflammatory signals are strongly implicated at various points during tumorigenesis and metastasis[94]. Therefore, it is likely that the specific combination of inflammatory signals derived from necroptotic cells, and the role they play in either promoting or suppressing anti-tumor immune responses, will prove to be context-specific[95-99]. We stress an outstanding need for thorough characterization of downstream RIPK3 signaling effects across different cell types, and across diverse categories of neoplasia, in consideration of whether immunogenic PCD such as necroptosis could confer an overall therapeutic benefit to the patient.

## 1.4 Established strategies for targeting programmed cell death in tumors

The primary goal of most cancer therapies is induction of tumor cell death to the point of tumor elimination and cure. With increasing awareness of therapy-induced immune responses, it is important to ask whether the specific form of induced PCD affects the longevity of tumor clearance following therapy-induced tumor debulking. This section will review methods of inducing specific forms of PCD and known immunogenic outcomes. These therapeutic approaches are also summarized in Table 1.

*Specific inducers of apoptosis*

Therapeutic agents have been developed to specifically trigger apoptosis by targeting the regulatory pathways that limit apoptotic death in cancer cells, primarily targeting BCL-2 proteins and IAPs. Structural mimetics of the BH3 domains of BCL-2 proteins have been developed to antagonize the anti-apoptotic BCL-2 family members[100-103]. While highly promising, their efficacy has been restricted by the inability to target them to specific cell types (i.e. cancer cells) without inducing apoptosis in healthy bystanders. Indeed, the ability of BH3-only proteins to induce death of immune cells has led to their proposed use as immune modulators during transplantation, graft versus host disease, and autoimmunity[103]. SMAC mimetics target cIAP family members and the endogenous inhibitor of caspases, XIAP[104]. SMAC mimetics bind to cIAPs and prevent their ability to inhibit caspases, but also stimulate cIAP auto-ubiquitination and degradation, thereby sensitizing cells to apoptotic death downstream of DR signaling[104]. Thus, combining SMAC mimetics with other death agonists improves the induction of cancer cell death. SMAC mimetics may also be capable of inducing necroptosis when coupled with caspase inhibition, potentially enhancing the immunogenicity of this therapy. However, as with

BH3 mimetics, a lack of tumor cell specificity, and ancillary effects within the non-canonical NF-κB pathway, have limited their clinical success.

*Induction of immunogenic apoptosis*

Most standard of care anti-cancer therapies appear to induce apoptosis, however a select few do so in an 'immunogenic' way. This includes traditional chemotherapies such as anthracyclines[105], the protease inhibitor bortezomib[106], the platinum derivative oxaliplatin[107], as well as gamma-irradiation[108] and hypericin-photodynamic therapy[109]. While demonstrating caspase activation and apoptotic morphology, such therapies also trigger the release of DAMPs not normally associated with apoptosis such as calreticulin, HMGB1, ATP, type I IFN, nucleic acids, and annexin A1[1]. Additionally, certain chemotherapies increase the expression of tumor-associated antigens, while upregulating expression of HLA and requisite processing machinery[110]. The exact signaling events determining immunogenic versus non-immunogenic apoptosis are still under investigation, but potentially rely on elements of the ER stress response and intact exocytosis pathways[1].

Irradiation is of particular interest in triggering cancer death, as it benefits from combination therapies with the immune checkpoint blocking antibody, anti-CTLA-4, contributing to abscopal tumor control[110-111]. However, irradiation induces both apoptotic and necrotic death, and there may be an important distinction between the immunologic outcomes depending on which form of death dominates. Lowering the overall radiation dose as well as delivering this radiation in smaller fractions rather than as a single dose can increase the proportion of apoptotic death induced, and better correlates with immune-mediated protection[110]. The exact signaling pathway whereby irradiation triggers apoptosis, necrosis, or other PCD is not clear based on clinical evidence; however, the form of death may also depend on the p53 status

of tumor cells at the time of therapy. Abnormal p53 expression/function disrupts the ability of cells to respond appropriately to irradiation induced DNA damage (by undergoing rapid apoptosis) and instead cells may proceed through the cell cycle unchecked, potentially resulting in delayed apoptosis, cellular senescence, or even activation of the necroptotic pathway[112].

Recent work has highlighted strategies to render apoptosis immunogenic by blocking aspects of its execution that silence the immune response to apoptotic cells. Genetic ablation of the executioner caspases was found to arrest rapid apoptosis, instead leading to engagement of STING-dependent IFN signaling due to release of mitochondrial DNA[113,114]. Given this finding, subsequent efforts combined intrinsic apoptosis inducing BH3 mimetics with pharmacologic caspase inhibition. This combination induced MOMP but arrested apoptosis execution, instead engaging immunogenic STING signaling[115]. Importantly, this inhibition of executioner caspases does not rescue cell viability, as MOMP represents a cellular "point of no return". Rather, this strategy re-directs apoptosis from a rapid immunosuppressive program to a slow, potentially immunogenic form of cell death. Clinical evidence is needed to show whether apoptosis-targeting therapies augment the immunogenicity of cell death in tumors, but the possible synergy between these strategies and immune checkpoint inhibitors is an exciting future research avenue.

*Specific targeting of necroptosis*

As discussed previously, extrinsic necroptosis requires DR engagement in the presence of caspase inhibition; accordingly, it is difficult to induce necroptosis in tumor cells without off-target toxicity associated with global caspase inhibition[116-118]. Furthermore, therapies targeting endogenous necroptotic signaling operate under the assumption that tumor cells have intact necroptotic signaling components. However, as discussed above, there is evidence for RIPK3

silencing or loss in many different tumor types. Nevertheless, pharmacological compounds that stimulate necroptosis represent an alternative strategy for killing tumor cells resistant to apoptotic stimuli[119]. Examples of such compounds are highlighted in Table 1.

Several compounds have been shown to induce necroptosis in cancer cell lines *in vitro*. This includes the antimicrobial peptide HPA3P[120], the natural product Shikonin[92,121-123], and several strategies using SMAC mimetics combined with IFNγ[124], pan-caspase inhibitor zVAD[125], or demethylating agents and zVAD[126]. Cell culture models have also provided evidence of RIPK3 and/or MLKL activation following chemotherapy such as cisplatin[127,128] or oxaliplatin[129].

The advantage of studying necroptosis in cell lines is the ability to confirm the specific activation of necroptotic signaling components; however, these studies do not account for off-target toxicity, or questions concerning pharmacokinetics and drug availability within the tumor microenvironment. A limited number of *in vivo* studies are beginning to show promising results using these therapies. In a model of multiple myeloma, LCL161 triggered inflammatory cytokine secretion and activation of anti-tumor immune responses independent of direct tumor toxicity, which supported observations of durable anti-myeloma responses in LCL161-treated patients[130]. Treatment of caspase-8-deficient murine CRC tumors via intratumoral injection of the SMAC mimetic LCL161 led to tumor regression; notably, these effects were seen both in hereditary murine ApcMin/+ tumors as well as a xenograft model of human HT-29 tumor cells[131]. Furthermore, tumor control by LCL161 required both caspase-8 deficiency and RIPK3 expression in tumor cells, implying that these tumors were genetically sensitized to undergo necroptosis downstream of SMAC mimetic administration[131]. Another group showed that Shikonin treatment of preclinical osteosarcoma cells induced RIPK1-dependent cell death *in vitro*, and that administration of Shikonin to intratibial osteosarcoma-bearing mice reduced both

the size of the primary tumor as well as the number of lung metastases, prolonging animal survival[121]. As the mechanisms underlying Shikonin-induced necroptosis remain relatively poorly characterized, future investigation into the mechanism of action of Shikonin should include evaluation of caspase-8 and cIAP expression within the targeted tumor cells.

Overall, these results highlight the need to either screen patient tumors to confirm the presence of intact necroptotic signaling pathways and/or caspase deficiency prior to administration of pro-necroptotic stimuli. Alternatively, exploring possible strategies to reinstate expression of necroptotic signaling components within tumor cells could represent another therapeutic target. Historically, work in the tumor gene therapy field has focused on using viral vectors to transduce tumor cells *in situ* to enforce expression of a wide variety of anti-tumor effectors, including inflammatory cytokines[132-134], Flt3L[135-137], CD40L[138-139], HLA re-expression[140], tumor suppressors[141], as well as suicide genes[142,143]. Considering this evidence, one can envision future gene therapy strategies aimed at transducing tumor cells *in situ* to enforce expression of immunogenic cell death signaling components. Tumor cells could be rendered susceptible once again to apoptosis- or necroptosis-inducing stimuli to which they were previously refractory. Indeed, tumor cells reconstituted with activatable caspase-9[144] or caspase-3[145] via adenoviral gene delivery became sensitized to apoptosis *in vivo*, demonstrating that this approach could be successful in tumor immunotherapy.

### 1.5 Stimulation of innate immunity as a tumor immunotherapy target

Currently, the study of PCD signaling modalities and their downstream effects on immune responses have primarily focused on the effects of PCD in the context of host-pathogen interactions. Notably, modulation of PCD and its subsequent effects on innate immune signaling pathways in the context of tumor immunity has remained relatively unexplored. Indeed, the field of tumor immunotherapy has classically focused primarily upon the manipulation of antigen specificity, activation status, and overall phenotype of tumor-reactive $CD4^+$ or $CD8^+$ T cells, obviously with great success in a variety of cancer models[146-149]. Given the extensive characterization of innate immunity in the context of host-pathogen interactions, several groups have sought to apply these concepts in characterizing the beneficial effects of activating specific innate immune signaling pathways specifically within tumors[150-154]. Indeed, innate immune signaling can serve as an upstream event in the generation of an anti-tumor immune response, which is distinct from any therapeutic strategies that target T cell function within the tumor microenvironment. Therefore, any attempts at therapeutically manipulating innate immunity within a tumor could function as promising orthogonal treatment modalities administered in conjunction with currently successful T cell-targeted therapeutics[155-157]. Considering how certain forms of PCD (such as necroptosis) result in the release of DAMPs that can stimulate innate immune pattern recognition receptors (PRRs), consideration of immunogenic PCD in the tumor context must take into account the innate immune response.

Strategies to stimulate activation signals through innate immune pathways include agonism of nucleic sensing via cGAS/STING[158-161], RNA sensing via MDA5[162], or TLR pathways[163]. Furthermore, inhibition of regulatory signals on myeloid cells, including the TYRO3, AXL, and MERTK (TAM) innate immune inhibitory receptors, provides another

promising target for tumor immunotherapy by eliminating repression of inflammatory responses[164-166]. Inhibition of TAMs on tumor-associated myeloid cells may support polarization of tumor macrophages from a pro-tumorigenic tissue repair phenotype to a classical, pro-inflammatory profile; indeed, inhibition of AXL[167] or MERTK[168] have yielded promising results in pre-clinical tumor models. Collectively, these studies highlight the therapeutic benefits of manipulating innate immune signaling targets within the tumor microenvironment to preferentially skew polarization and/or activation of tumor-associated myeloid cells, effectively promoting tumor-reactive CTL responses.

Clearly, modulation of innate immune responses that have been classically associated with pro-inflammatory signaling initiated through DAMP/PRR or PAMP/PRR interactions can function to effectively promote beneficial inflammatory signaling within the classically immunosuppressive tumor microenvironment. However, the ways in which DAMPs derived from tumor cells dying via distinct forms of PCD could potentially yield similarly beneficial signals remains poorly defined. It is interesting to consider that certain forms of programmed lytic cell death, such as necroptosis, might function in a combinatorial fashion by delivering a bolus of multiple DAMPs that can simultaneously stimulate multiple innate immune signaling pathways in the presence of tumor antigens, potentially functioning as a potent immunogenic payload **(Figure 2)**.

## 1.6 Concluding Remarks

The tumor immunology field lacks a comprehensive understanding of how distinct PCD within tumors differentially modulates downstream immune responses. Considering advances in the cell death field in defining specific PCD signaling programs, in conjunction with recent efforts to stimulate innate immune pathways as targets of tumor immunotherapy, it would appear that the field is ready for more extensive interrogation of different forms of PCD. This is no trivial undertaking, as the complex signaling programs regulating PCD are likely to have considerable variation not only across healthy tissue and cell subsets, but also across different types of cancers, and exhibit further heterogeneity amongst patients due to genetic diversity and environmental factors[169].

In summary, specific modulation of PCD within the tumor microenvironment represents a relatively poorly explored immunotherapeutic target. In considering the current immunotherapy landscape **(Figure 3**), tumor cell death constitutes the most proximal event in the generation of an immune response against dying cell-derived antigens. Optimized combinations of PCD targeting and immunotherapy will likely act upon different stages of anti-tumor immune responses[156,170]. One can envision future combination therapies whereby induction of (a) maximally immunogenic tumor cell death is coupled with (b) modulation of tumor-associated antigen presenting cells in conjunction with (c) immune checkpoint blockade to maximize CTL killing of remaining tumor cells. Of course, co-administration of multiple anti-tumor drugs will need to be carefully balanced with the need to suppress systemic inflammation and attack of non-tumor targets, as highlighted by recent issues with neurotoxicity and cytokine release syndrome observed in some patients[171-173]. Nevertheless, the complex processes underlying tumor cell heterogeneity necessitate the expansion of treatments which can kill transformed cells that have

escaped the selection pressures exerted by singular therapies to acquire immunotherapy resistance[174]. It is therefore an attractive hypothesis that targeting specific forms of immunogenic cell death may constitute a relatively unexplored orthogonal treatment modality in the future repertoire of tumor immunotherapies.

## 1.7 Figures

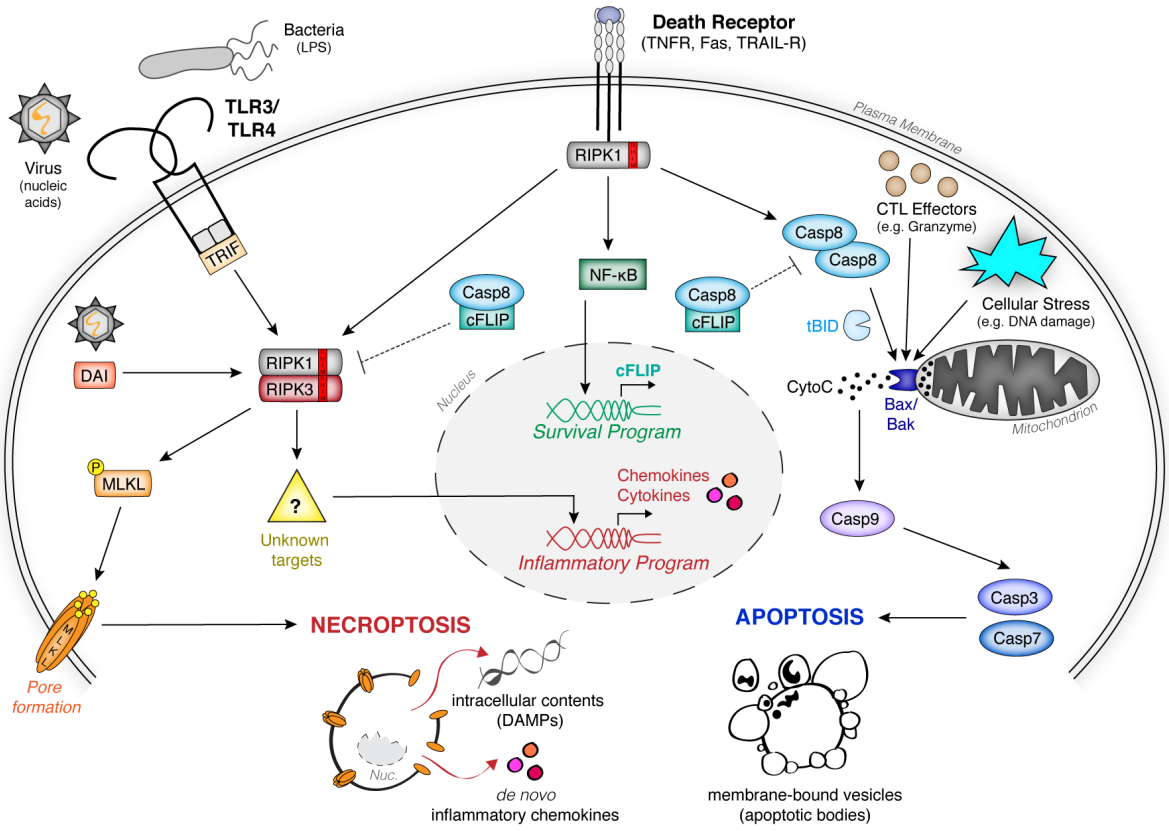


**Figure 1. Signaling pathways governing apoptosis and necroptosis.** Binding of death receptor family members by their cognate ligands leads to pleiotropic signaling that can promote either survival, extrinsic apoptosis, or necroptosis, depending on the inhibition of the pro-apoptotic caspase-8 homodimer complex and/or pro-necroptotic RIPK1-RIPK3 hetero-oligomer. Upon inhibition of pro-survival NF-κB signaling, the apoptotic caspase-8 complex dominates signaling, leading to downstream activation of the executioner caspases -3 and -7 and subsequent induction of apoptosis. Intrinsic apoptosis occurs following mitochondrial perturbation leading to cytochrome C release and subsequent caspase-9 apoptosome complex formation, which converges upon the activation of the executioner caspases -3 and -7. Cytotoxic T lymphocytes

(CTL) also trigger intrinsic apoptosis by perforin-mediated delivery of granzyme B. In the presence of caspase inhibition, the RHIM-RHIM domain interactions allow for assembly of the RIPK1-RIPK3 hetero-oligomer, and necrosome signaling dominates. This leads to (1) phosphorylation and activation of the pore-forming executioner MLKL, and (2) de novo inflammatory gene expression by necroptotic cells through poorly-defined mechanisms. Aside from extrinsic death receptor signaling, the RIPK1-RIPK3 necrosome complex can also be activated through virus- or bacteria-induced TLR3/4 signaling in conjunction with the adaptor molecule TRIF, or upon activation of the intracellular sensor DAI during certain viral infections.

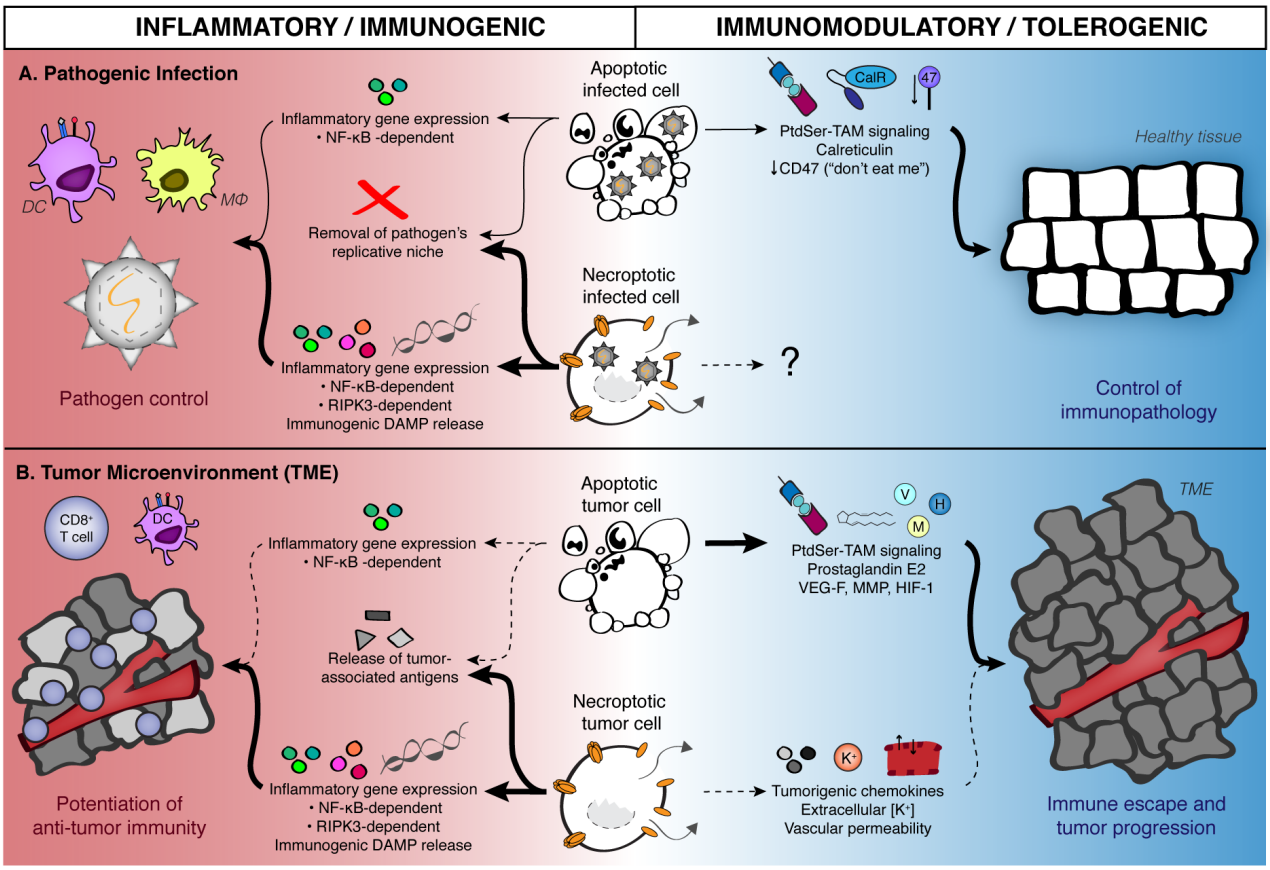


**Figure 2. Contribution of apoptosis and necroptosis to inflammation and immunogenicity during infection and tumorigenesis.** (**A**) During pathogenic infection, stimulation of apoptosis or necroptosis in infected cells leads to the production of a variety of inflammatory mediators in conjunction with removal of the pathogen's intracellular replicative niche, enabling pathogen control and promoting clearance. Additional inflammatory signals derived from RIPK3 activation and release of damage-associated molecular patterns (DAMPs) due to necroptotic cell lysis lead us to believe that necroptosis is a more potently immunogenic form of PCD during pathogen infection. Signals derived from apoptotic cells can also promote the resolution of inflammation, allowing for infected tissues to return to homeostatic conditions. Note that no known role has been defined for necroptosis in promoting the control of tissue immunopathology in the context of infection. (**B**) Apoptosis and necroptosis may function similarly to promote

analogous responses in the tumor microenvironment, although this has been examined less extensively within the cell death signaling field. Both apoptotic and necroptotic tumor cells can serve as a source of tumor-associated antigens, as well as inducing NF-κB signaling. As with pathogenic infection, necroptotic cells can also serve as a source of RIPK3-dependent inflammatory genes (such as chemokines and cytokines), as well as cell-associated immunostimulatory DAMPs; all of these factors may contribute to necroptotic cells providing predominantly immunogenic signals within the tumor microenvironment. Conversely, there is evidence for pro-tumorigenic roles of signals derived from both apoptotic as well as necroptotic (or necrotic) tumor cells.

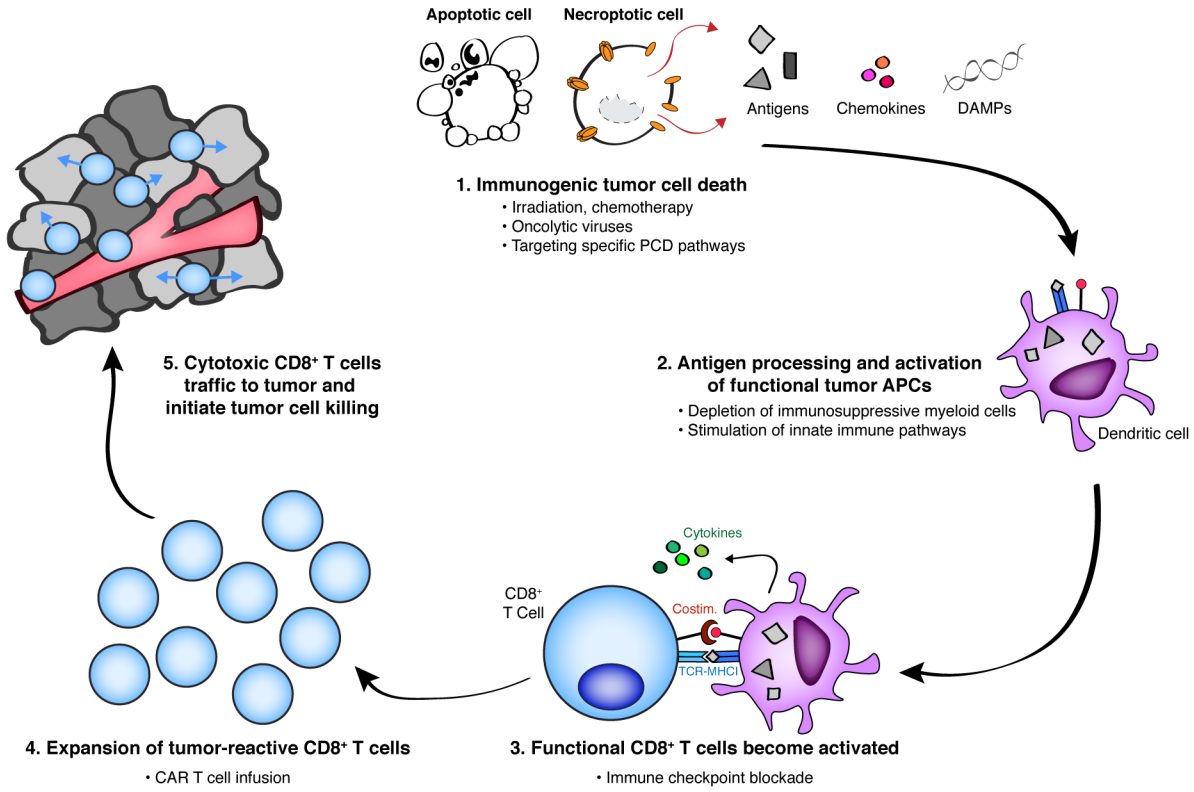


**Figure 3. Immunogenic cell death serves as proximal target within the current repertoire of tumor immunotherapy.** Generation of cytotoxic $CD8^+$ T cell (CTL) immunity against living tumor cell targets can be broadly separated into 5 steps: (**1**) Tumor cell death releases cell-associated antigens in the presence or absence of various immunogenic signals derived from dying cells; (**2**) Tumor-associated antigen-presenting cells (tuAPCs) phagocytose, process, and cross-present antigen from dying cells; (**3**) Tumor-reactive CTLs recognize tumor antigen and become activated (priming in the tumor-draining lymph node) or re-activated (re-stimulation of existing CTLs) in the presence of functional tuAPCs; (**4**) Activated CTL proliferate and expand; (**5**) Activated and functionally-capable CTLs traffic to the tumor microenvironment, where they recognize live tumor cell targets and exert their cytolytic effector function to promote tumor cell killing. Therapies with known mechanisms of action at each of these steps are listed below each step. Although different modalities of both programmed and unprogrammed cell death can be

induced by a variety of chemotherapeutic agents, it remains to be determined which of these initial treatments maximizes the immunogenicity of dying cells within the tumor microenvironment. Strategy-driven selection of combination therapy regimens will likely necessitate inclusion of immunotherapy agents that best potentiate anti-tumor immunity at separate steps within this cycle.

## 1.8 Tables

Table 1. Death-inducing cancer therapies

| Therapy | Mechanism | Primary PCD induced | Cancers tested | Status | Ref. |
|---|---|---|---|---|---|
| BH3 mimetics | Antagonize antiapoptotic BCL-2 proteins, sensitizing cells to proapoptotic signals | Apoptosis | Lymphomas, CLL, AML, ALL, MM, SCLC | Clinical and preclinical trials | [96] |
| SMAC mimetics | Bind to cIAPs and XIAP, blocking endogenous inhibitors of caspases. Also relieves repression of RIPK1/RIPK3 | Apoptosis | HNSCC, solid tumors | Phase I/II clinical trials | [97] |
| Anthracyclines (doxorubicin) | Intercalates DNA/RNA strands leading to irreparable DNA damage | Immunogenic apoptosis | Solid tumors, MM, leukemias and lymphomas | Commonly prescribed | [98] |
| Bortezomib | Protease inhibitor, induction dependent on BH3 proteins | Immunogenic apoptosis | MM, MCL | Commonly prescribed | [99] |
| Platinum derivatives (cisplatin, oxaliplatin) | Cross-links DNA inhibiting synthesis and transcription | Immunogenic apoptosis, necroptosis | Solid tumors | Commonly prescribed | [100] |
| Gamma-irradiation | Direct and indirect DNA damage | Immunogenic apoptosis, necrosis, other? | Solid tumors | Commonly prescribed | [101] |
| Hypericin-photodynamic therapy | Cellular sensitization to light and ROS production leading to cellular damage | Immunogenic apoptosis | Solid tumors | Phase I/II clinical trials | [102] |
| HPA3P | Increased levels of RIPK3 expression | Necroptosis | CRC (HT-29, SW480 HCT116 p53+/+) | Preclinical | [113] |
| Shikonin | Downregulation of procaspase-8 | Necroptosis | BRC (MCF-7), APML (HL60) | Preclinical | [85, 114-116] |
| SMAC mimetics + IFNγ | Relieved repression of RIPK1/RIPK3; IRF1-dependent downstream of IFNγ | Necroptosis | CRC (HT-29), BRC (EFM-192A), AML (MV4-11, Molm-13) | Preclinical | [117] |
| SMAC mimetics + caspase inhibition | Relieved repression of RIPK1/RIPK3; caspase inhibition allows for ripoptosome formation | Necroptosis | OVC (OVCAR3) | Preclinical | [118] |
| SMAC mimetics + demethylating agents + caspase inhibition | Relieved repression of RIPK1/RIPK3 + demethylation to inhibit prosurvival NF-κB signaling + inhibit caspase to skew from apoptotic to necroptotic death | Necroptosis | AML (MV4-11, NB4) | Preclinical | [119] |

Cancer types: ALL acute lymphocytic leukemia, AML acute monocytic leukemia, APML acute promyelocytic leukemia, BRC breast cancer, CRC colorectal cancer, HNSCC head and neck squamous cell carcinoma, MM multiple myeloma, MCL mantle cell lymphoma, OVC ovarian cancer, SCLC small cell lung cancer. Specific cell lines listed in parentheses.

# Chapter 2

Ectopic introduction of RIPK1/RIPK3 activation in the tumor microenvironment stimulates anti-tumor immune responses

This chapter is adapted from the following publication:

Snyder AG, Hubbard NH, Messmer MN, Kofman SB, Hagan CE, Orozco SL, Chiang K, Daniels BP, Baker D, Oberst A. Intratumoral activation of the necroptotic pathway components RIPK1 and RIPK3 potentiates antitumor immunity. *Sci Immunol*. 2019; **4**: eaaw2004 (In Press).

## 2.1 Introduction

Tumor immunotherapy, which boosts the ability of the body's own immune system to recognize and kill transformed cells, constitutes an immensely promising advance in the modern treatment of cancer. Notably, the efficacy of existing T cell-targeted therapies such as immune checkpoint blockade (ICB) can often be boosted upon co-administration of cytotoxic treatments such as irradiation[111,175]. However, the specific forms of programmed cell death (PCD) initiated upon administration of cytotoxic therapies to tumor cells are often not rigorously defined[176]. Considering the growing body of evidence supporting differential immune activation or suppression in response to distinct PCD modalities[3], strategies to maximize the immunogenicity of dying tumor cells could potentially function to boost the effects of co-administered treatments including ICB.

Cells can undergo distinct forms of PCD in response to cellular stress, pathogen infection, and organismal development[5,6]. Apoptosis occurs following activation of a family of proteases termed caspases, and the clearance of apoptotic debris is often associated with tolerogenic signaling[24]. These immunomodulatory processes include the caspase-directed inactivation of immunostimulatory damage-associated molecular patterns (DAMPs) such as high-mobility group box-1 protein (HMGB1)[177], as well as immunosuppressive functions of the Tyro3/Axl/Mertk receptor tyrosine kinases (TAM RTKs) in promoting tissue repair phenotypes in phagocytes that have engulfed apoptotic debris[164]. As apoptotic cells may exhibit competing immunosuppressive and immunogenic signals within the tumor microenvironment (TME), their immunostimulatory capacity will likely prove to be highly tumor cell- and context-specific. Notably, apoptosis is believed to be the mechanism of PCD in tumor cells following administration of a wide variety of anti-cancer drugs, including chemotherapeutic agents[105,107],

and specific inducers of apoptosis[100,102,104]. Induction of immune tolerance by apoptotic cells may therefore limit synergistic effects when combining these anti-cancer compounds with ICB or other immunotherapy regimens.

Necroptosis is a form of PCD that occurs downstream of the receptor-interacting protein kinases RIPK1 and RIPK3, which assemble into an oligomeric complex termed the 'necrosome'[16,38]. A growing body of evidence supports the idea that necroptosis is a more potently immunogenic form of PCD than apoptosis in certain contexts[3]. Necroptotic cells undergo rapid membrane permeabilization via the executioner protein mixed-lineage kinase-like (MLKL), leading to the release of intracellular contents including immunogenic DAMPs that can activate innate immune pattern recognition receptors[44,46,178]. Furthermore, death-independent functions of RIPK3 have also been recently defined, including inflammatory chemokine and cytokine production that can promote cross-priming of $CD8^+$ T cell vaccination responses[10] and confer protection during viral infection[11]. Therefore, a model emerges in which necroptosis can function as an alternative PCD modality that can eliminate caspase-compromised cells in the event of infection, while simultaneously releasing a payload of inflammatory signals to recruit and activate immune cells[179]. Notably, these findings have not yet been comprehensively applied to the field of tumor immunology, in part due to technical limitations related to the manipulation of PCD programs *in vivo*. Indeed, specific targeting of necroptosis using endogenous signaling components is difficult, as there is extensive regulatory cross-talk between extrinsic apoptotic and necroptotic signaling pathways[4]. This is further complicated by the fact that many tumors have mutated or silenced either caspases[57] or the RIP kinases[76]. Given these obstacles, the specific differential effects of enforced RIPK3 activation versus caspase-8 or -9 activation within the TME have not been described.

Here, we describe a beneficial role for activation of the necroptotic pathway components RIPK1 and RIPK3 within the TME. Using engineered versions of pro-death enzymes, we present a reductionist system that circumvents endogenous pro-death signaling pathways within tumor cells. Importantly, ectopic activation of RIPK3 promotes tumor antigen loading by tumor APCs associated with enhanced $CD8^+$ leukocyte-mediated anti-tumor responses, which leads to systemic tumor control that synergizes robustly with ICB co-administration. These beneficial effects occur specifically following administration of necroptotic cells within solid tumors, but not following exposure to apoptotic cells or cells dying via lytic necrosis, indicating that these protective effects are due to signals specifically derived from the RIPK1/RIPK3 necrosome complex. Collectively, these findings demonstrate a promising proof-of-concept that RIPK1/RIPK3 activation in established solid tumors promotes robust anti-tumor immunity.

## 2.2 Results

### Necroptotic cells confer tumor control across multiple syngeneic flank tumor models

To assess the impact of necroptotic tumor cell death on gross tumor outgrowth responses, we utilized a model of intratumoral dying cell administration that allowed us to precisely control the timing and number of cells undergoing various cell death pathways within the TME. We employed constructs encoding chimeric versions of pro-death proteins fused to activatable ("ac") $FKBP^{F36V}$ domains, which we have previously shown allow activation of the chimeric protein following incubation with a synthetic bivalent homologue of rapamycin that functions as a nontoxic ligand[180]. Tumor cells transduced with activatable versions of either pro-apoptotic caspase-8 (acCASP8), pro-apoptotic caspase-9 (acCASP9), or pro-necroptotic RIPK3 (acRIPK3) (Figure 1A) were pulsed with ligand drug *in vitro* to enforce oligomerization of these pro-death enzymes, and then injected intratumorally into pre-established syngeneic flank tumors. In this system, ectopically administered cells are alive at the time of injection, but are fated to undergo respective forms of PCD within the TME, accompanied by any signaling activity induced downstream of acCASP8, acCASP9, or acRIPK3. Transduction with pro-apoptotic acCASP9 was better tolerated in tumor cell lines, while acCASP8 was better tolerated in fibroblast cell lines. Using this model, we observed that administration of autologous necroptotic (acRIPK3), but not apoptotic (acCASP9), tumor cells into cell type-matched tumors conferred control of tumor outgrowth and extended survival of animals bearing either B16.F10-OVA melanoma flank tumors (Figure 1B, Figure S1B) or Lewis Lung (LL/2)-OVA adenocarcinoma flank tumors (Figure 1C, Figure S1C).

Unexpectedly, the tumor control effects of necroptosis did not require that necroptotic cells themselves carry tumor antigen, as injection of an unrelated fibroblast line, NIH-3T3,

similarly led to tumor control and extension of animal survival following necroptotic, but not apoptotic (acCASP8) fibroblast administration in B16.F10-OVA (Figure 1D, Figure S1D), LL/2-OVA (Figure 1E, Figure S1E), and E.G7-OVA thymoma[181] (Figure 1F, Figure S1F) flank tumors. These tumor control effects were not an artifact of the immunodominant OVA epitope expressed by tumor cells, as administration of necroptotic fibroblasts also conferred tumor outgrowth and survival extension in mice implanted with non-OVA-expressing B16.F10 (Figure 1G, Figure S1G) or LL/2 (Figure 1H, Figure S1H) flank tumors. These data indicate that necroptotic cells delay tumor outgrowth and even confer complete tumor clearance in a small percentage of animals across multiple syngeneic flank tumor models.

Considering these findings, we next tested if this treatment could act systemically in a bilateral flank tumor model, where a single mouse is implanted with separate B16.F10-OVA tumors on either flank. Following injection of necroptotic fibroblasts into a treated (ipsilateral) tumor, we observed control of flank tumor outgrowth in both the ipsilateral as well as the untreated (contralateral) tumor (Figure 1I), leading to an extension of animal survival and increase in median survival time (Figure 1I). Control of both tumors in this bilateral tumor model indicates an abscopal effect, whereby application of a therapeutic agent to a primary tumor can lead to the control and even elimination of distal, untreated metastases. Notably, this effect required tumor antigen matching between the ipsilateral and contralateral tumors, as mice implanted with a B16.F10-OVA ipsilateral tumor and an antigenically disparate LL/2 contralateral tumor failed to exhibit abscopal tumor control following administration of necroptotic fibroblasts (Figure S1I). These data suggest that the introduction of necroptotic cells to the TME initiates a systemic immune response to tumor-derived antigens, irrespective of antigen matching between necroptotic cells and the tumor cells themselves.

**Tumor control by necroptotic cells requires BATF3$^+$ cDC1 and CD8$^+$ leukocytes**

Given the unexpected finding that introduction of necroptotic cells to the TME promoted systemic tumor control irrespective of antigen matching, we sought to establish that the control we observed was immune-mediated. BATF3 is a transcription factor required for the development of cDC1 dendritic cells, which are critical for cross-presentation of exogenous antigens to stimulate CD8-mediated immunity, and are required for endogenous anti-tumor immune responses[182]. We found that the tumor control effects of necroptotic fibroblasts required BATF3$^+$ cDC1, as *Batf3*$^{-/-}$ mice failed to restrict B16.F10-OVA (Figure 2A) or LL/2-OVA (Figure S2A) tumor growth compared to controls. Consistent with the critical role for cDC1 in mediating anti-tumor immunity, we also observed that depletion of CD8$^+$ leukocytes (including both CD8$\alpha^+$ cytotoxic T cells and CD8$\alpha^+$ dendritic cells) completely abrogated the therapeutic effect of necroptotic fibroblast administration, while depletion of CD4$^+$ leukocytes did not affect tumor control responses (Figure 2B); depletion of each leukocyte population was confirmed via flow cytometry (Figure S2B). These data indicate that control of tumors following introduction of necroptotic cells is immune mediated, and proceeds via activation of CD8$^+$ leukocytes.

**Immune-mediated tumor control by necroptotic cells requires NF-κB activation within dying cells, but not DAMP release**

We next investigated the signals emanating from necroptotic cells within the TME that promoted immune activation and tumor control. As necroptosis is a lytic form of cell death, necroptotic cells might initiate immune responses through the release of DAMP molecules within the TME. To assess this possibility, we first tested the ability of necroptotic fibroblasts to

recapitulate tumor control effects in several knockout mouse strains, whose tumor-infiltrating immune cells lack expression of pattern recognition receptors (PRRs) capable of recognizing DAMPs, or their downstream signaling components. We found that mice deficient in signaling components involved in cytosolic DNA sensing (*Tmem173*$^{-/-}$, *Mb21d1*$^{-/-}$, *Aim2*$^{-/-}$), cytosolic RNA sensing (*Mavs*$^{-/-}$), TLR signaling (*Myd88*$^{-/-}$, *Ticam1*$^{-/-}$, *Irf3*$^{-/-}$) or general inflammation (*Tnf*$^{-/-}$) all retained the ability to control tumor outgrowth following administration of necroptotic fibroblasts into either B16.F10-OVA (Figure 3A) or LL/2-OVA (Figure S3A, left panel) tumors, indicating that the therapeutic effects of necroptotic cells are not strictly mediated through the singular activity of these innate immune signaling components within tumor-infiltrating leukocytes. Interestingly, *Ifnar1*$^{-/-}$ mice were resistant to tumor outgrowth restriction by necroptotic cells in both B16.F10-OVA (Figure 3A) and LL/2-OVA tumors (Figure S3A, left panel), indicating that sensing of Type I IFN on host immune cells was required for therapeutic efficacy. Interestingly, enumeration of leukocyte subsets isolated from B16.F10-OVA tumors on day 6 post-tumor injection revealed significant decreases across many immune cell populations in *Ifnar1*$^{-/-}$ mice compared to B6/J controls (Figure S3A, right panel), indicating that failure to control tumors may be at least partially attributed to defective leukocyte recruitment to the TME at baseline, before therapy application. Furthermore, antibody-mediated blockade of the necrotic cell sensor CLEC9A[43] did not affect tumor restriction or animal survival extension by necroptotic fibroblasts (Figure 3B); effective blockade of CLEC9A expression was confirmed on dendritic cell (DC) subsets in both spleen and tumor (Figure S3B). Taken together, these results indicate that tumor control by necroptotic cells is not mediated solely through the activation of any of these individual innate immune signaling pathways.

Our previous findings indicate that RIPK3 activation induces NF-κB-mediated transcriptional responses in addition to lytic cell death[10]. We therefore sought to separate these two potentially immunostimulatory processes to understand the contribution of each to necroptosis-mediated tumor control. To do this, we first administered fibroblasts dying via either necroptosis or lytic necrosis into established B16.F10-OVA tumors, using 3 different forms of lytic necrotic fibroblasts (Figure S1A): (1) cells expressing a mutated version of activatable RIPK3 lacking the RIP Homotypic Interaction Motif (RHIM) domain (acRIPK3ΔC), which cannot recruit and activate RIPK1 to induce downstream NF-κB-mediated inflammatory gene transcription, yet maintains the ability to activate MLKL to induce pore formation and lytic cell death[10]; (2) cells expressing an activatable version of MLKL (acMLKL) to induce pore formation and lytic cell death in the absence of upstream RIPK3 activation[183]; and (3) cells that were mechanically lysed via repeated freeze/thaw cycles immediately prior to injection. All 3 forms of lytic necrotic cells similarly release cell-associated DAMPs due to loss of plasma membrane integrity, but lack activation of the RIPK1/NF-κB signaling axis that is otherwise observed upon activation of full-length RIPK3 in necroptotic NIH-3T3s[10].

We observed that all 3 treatments of lytic necrotic fibroblasts failed to confer tumor control and extend animal survival compared to fibroblasts dying via acRIPK3-mediated necroptosis, both in single B16.F10-OVA tumors (Figure 3C) and using acRIPK3ΔC fibroblasts in single LL/2-OVA (Figure S3C, left panels) or E.G7-OVA tumors (Figure S3C, right panels). Consistent with this, administration of acRIPKΔC fibroblasts failed to confer tumor control (Figure 3D) and extension of survival (Figure S3D) in bilateral B16.F10-OVA tumor-bearing mice. These results revealed that DAMP release is not sufficient for the tumor control effects of

necroptotic fibroblasts within the TME, suggesting instead that signaling activities downstream of RIPK1/RIPK3 necrosome complex formation and activation may play a role.

To more directly test if the immunogenicity of necroptotic fibroblasts in our tumor model depended on intact NF-κB activation in the dying cells, we pre-incubated NIH-3T3 cells +acRIPK3 with an irreversible IκBα phosphorylation inhibitor, BAY-117085, prior to pulsing with activator drug and injection into B16.F10-OVA tumors. Notably, inhibition of NF-κB activation via BAY-117085 significantly reduced both the tumor control effects (Figure 3E) and survival advantage (Figure S3E) conferred by necroptotic cells compared to vehicle-treated controls, indicating that NF-κB activity in necroptotic fibroblasts is required for their anti-tumor effects. To test if the acRIPK3-NF-κB axis was sufficient to drive the tumor control response in the absence of lytic cell death by these cells, we next generated NIH-3T3 cells +acRIPK3 that lacked expression of the necroptosis executioner MLKL (Figure S3F, left panel). These cells failed to undergo cell death upon exposure to activator drug *in vitro*, unless expression of the pro-survival protein cFLIP was concurrently knocked down (Figure S3F, right panel), consistent with reverse-signaling by the RIPK3 complex to induce apoptosis[184,185]. Notably, injection of $MLKL^{-/-}$ NIH-3T3 +acRIPK3 cells into B16.F10-OVA tumors conferred similar tumor control (Figure 3F, left panel) and survival extension (Figure 3F, right panel) responses as seen in mice that received MLKL-sufficient necroptotic fibroblasts. Taken together, these results indicate that transcriptional signaling downstream of RIPK1/RIPK3/NF-κB activation are responsible for the immunogenicity of necroptotic fibroblasts in the TME, and that this occurs independently of DAMP release by dying cells.

Our data point to the production of NF-kB-dependent cytokines as key to tumor control by necroptotic cells. As these cytokines can act both locally and systemically, we next tested

whether the introduction of necroptotic cells to the TME might drive systemic inflammatory or immune responses. To do this, we measured levels of inflammatory mediators in sera harvested from B16.F10-OVA tumor-bearing mice following necroptotic cell administration. Notably, there were no differences between treatment groups with respect to systemic levels of inflammatory chemokines and cytokines relevant for anti-tumor responses, including IFN-γ, TNF-α, CCL5, and CXCL10 (Figure 3G), or chemokines and cytokines known to be produced by necroptotic NIH-3T3 fibroblasts, including IL-6, CXCL1, and CCL2[10] (Figure S3G). Consistent with this, injection of necroptotic fibroblasts into spatially distinct locations distal from the tumor site, including intraperitoneally, intravenously, or subcutaneously on the opposite flank to the tumor, all failed to confer tumor outgrowth control (Figure 3H) or extend animal survival (Figure S3H) compared to intratumoral injection of necroptotic fibroblasts. These data indicate that administration of necroptotic fibroblasts does not lead to tumor control through nonspecific systemic inflammation, suggesting that the therapeutic effect of this treatment is due to local mechanisms exerted specifically within the TME.

**Necroptosis promotes anti-tumor $CD8^+$ T cell responses and synergizes with immune checkpoint blockade**

We next sought to understand the nature of the immune response instigated by introduction of necroptotic cells to the TME. To do this, we first assessed the effects of dying cell administration on cytotoxic $CD8^+$ T cells, a critical mediator of anti-tumor immunity. Using flow cytometric analysis to identify subsets of OVA-specific (SIINFEKL-$H2K^{b+}$) $CD8^+$ T cells isolated from B16.F10-OVA tumors (Figure S4A), we observed increased numbers of OVA-specific T cells expressing markers of proliferation ($Ki67^+$), effector function ($GranzymeB^+$), and general activation ($CD44^{hi}$) following necroptotic (acRIPK3), but not apoptotic (acCASP8) or

lytic necrotic (acRIPK3ΔC) fibroblast administration (Figure 4A). OVA-specific $CD8^+$ T cells isolated from necroptotic cell-exposed tumor tissue displayed similarly elevated percentages of both $CD44^{hi}$ and PD-$1^+$ cells (Figure S4B, left and center panels), indicating that necroptosis correlated with an overall more activated surface phenotype of intratumoral $CD8^+$ T cells, though these $CD8^+$ T cells did not express higher levels of PD-1 on a per cell basis compared to cells exposed to apoptotic or lytic necrotic fibroblasts (Figure S4B, right panel). Furthermore, we observed significant increases in the ratios of both activated ($CD44^{hi}$) or tumor-specific (SIINFEKL-$H2k^{b+}$) $CD8^+$ T cells to $CD25^+Foxp3^+$ $T_{REG}$ (Figure 4B) specifically within tumors that received necroptotic fibroblasts, indicating that the profile of tumor-infiltrating T cells was skewed towards more favorable cytotoxic $CD8^+$ T cells, rather than an immunosuppressive profile dominated by $T_{REG}$. These data indicate that exposure to necroptotic cells within the TME is associated with increased numbers of tumor-specific $CD8^+$ T cells present in the tumor tissue.

In order to characterize the effects of necroptotic cell administration on lymph node priming, we concurrently examined the abundance and quality of $CD8^+$ T cell responses in the tumor-draining lymph node (tdLN) of these mice (Figure S4C). We observed an increased frequency (Figure 4C) and number (Figure S4D) of overall activated (defined as $CD44^{hi}$ $CD62L^{lo}$) $CD8^+$ T cells in the tdLN of mice that received intratumoral necroptotic fibroblasts. These were accompanied by increases in the numbers of bulk $CD8^+$ and single-positive $CD44^{hi}$ $CD8^+$ T cells, but not $CD69^+$ $CD8^+$ T cells (Figure S4D). We also observed similar increases in the frequency (Figure 4D) and number (Figure S4D) of activated, tumor-specific (defined as $CD44^{hi}$ SIINFEKL-$H2k^{b+}$) $CD8^+$ T cells in the tdLN of necroptotic cell-treated mice. Therefore, in addition to an expansion of favorable $CD8^+$ T cell phenotypes locally within the TME,

necroptotic fibroblast injection also resulted in lymph node priming of tumor-reactive cytotoxic $CD8^+$ T cells.

To test whether recruitment of these newly-primed $CD8^+$ T cells into the TME was required for necroptotic cells to exert tumor control, we co-administered necroptotic fibroblasts with the sphingosine-1-phosphate receptor modulator FTY-720 to inhibit egress of lymphocytes from the tdLN. Interestingly, blockade of lymphocyte trafficking did not affect B16.F10-OVA tumor control by necroptotic fibroblasts, as FTY-720-treated animals still exhibited effective control over tumor outgrowth and extension of animal survival compared to vehicle-treated controls (Figure 4E). Consistent with a lack of influx of newly-primed lymphocytes, enumeration of various tumor-associated lymphocyte populations isolated from B16.F10-OVA tumors 48 hours post-dying cell administration revealed similar total numbers of $CD19^+$ B cells, $CD4^+$ T cells, and $CD8^+$ T cells within the TME among tumors that received apoptotic (acCASP8), necroptotic (acRIPK3), or lytic necrotic (acRIPK3ΔC) cell injections (Figure S4E).

Notably, inhibition of lymph node egress by primed leukocytes also did not alter abscopal tumor control in bilateral B16.F10-OVA tumors (Figure 4F, S4F), suggesting that untreated contralateral tumor control could be mediated by re-circulating leukocytes in the periphery. These results show that rapid recruitment of tumor-reactive lymphocytes from the tumor-draining lymph node is not required for growth restriction of treated or distal, untreated tumors responding to necroptotic fibroblast exposure, and further implicate local effects of necroptotic cells within the TME.

The efficacy of ICB is often boosted upon co-administration with cytotoxic therapies, including irradiation[111]. Because stimuli from necroptotic cells boosted activation of tumor-specific $CD8^+$ T cells both in tumor and in tumor-draining lymph node, we hypothesized that the

presence of necroptotic cells within the TME that would synergize with ICB, specifically α-PD-1. To test this, we interleaved injections of necroptotic fibroblasts into B16.F10-OVA flank tumors with administration of α-PD-1, and observed that mice exhibited significantly improved survival outcomes (Figure 4G) and improved tumor growth restriction (Figure S4G, left panel), as 71.4% of mice successfully cleared their tumors (Figure S4G, right panel) following this co-administration regimen. To determine whether this successful combination therapy conferred protective immune memory, we re-challenged mice ~2 months after they successfully cleared their tumors, injecting identical tumor cells into the same flank that bore the initial B16.F10-OVA tumor (Figure 4H, left panel). Notably, 100% of mice were protected from tumor re-challenge (Figure S4H) and failed to succumb to tumor outgrowth compared to naïve B6/J controls (Figure 4H, right panel). Altogether, these data indicate that necroptosis in the TME can potently synergize with ICB co-administration to promote durable tumor rejection.

**Exposure to necroptosis in the TME promotes antigen uptake and activation of tumor-associated APCs**

Our data indicate that necroptosis potentiates anti-tumor $CD8^+$ T cell responses even when necroptotic cells do not contain tumor antigen, implicating broad activation of tumor-associated antigen-presenting cells as the key effect of necroptotic cells within the TME. We therefore aimed to define necroptosis-induced changes to tumor-associated myeloid cell populations that could function to initiate adaptive immunity. Using a previously published gating strategy to identify subsets of tumor-associated innate immune cells (Figure S5C)[186], we enumerated various innate immune cells isolated from B16.F10-OVA tumor tissue following administration of apoptotic (acCASP8), lytic necrotic (acRIPK3ΔC), or necroptotic (acRIPK3)

fibroblasts. Notably, we observed a significant increase in the number of $CD24^+$ $CD103^+$ DC1 (Figure 5A), although there were no significant differences in the number of $Ly6C^{hi}$ monocytes, $NK1.1^+$ NK cells, bulk $MHCII^+$ antigen-presenting cells (APCs), $F4/80^+$ macrophages, or $CD24^+$ $CD11b^+$ DC2 (Figure 5A, Figure S5A). This was promising, given that $CD103^+$ DC1 are often viewed as the most functional tumor APC subset with respect to stimulating $CD8^+$ T cell-mediated anti-tumor immunity[182,186-187]. Consistent with this increase in intratumoral $CD103^+$ DC1, we measured significantly elevated levels of the DC chemoattractants CCL3, CCL4, and CCL5 in tumor homogenates following exposure to necroptotic fibroblasts (Figure 5B). Considering that $CD103^+$ DC1 can be recruited to the TME via NK cell-derived chemokines[188], we tested whether depletion of NK cells (Figure S5B, right panel) abrogated the therapeutic effect of necroptotic fibroblasts. Interestingly, NK cell depletion had no effect on tumor control and survival extension (Figure S5B, left panel) by necroptotic fibroblasts.

We next evaluated the phenotype of phagocytic tumor APCs with respect to tumor antigen loading and their activation status. To do this, we implanted mice with B16.F10-OVA cells that also express the bright and stable fluorophore zsGreen, then gated on $zsGreen^+$ tumor-associated phagocytes to identify tumor APCs that have ingested tumor-derived material (Figure 5C, Figure S5C). Using this gating strategy, we identified $zsGreen^+$ subsets of 6 primary tumor APC populations: bulk $CD24^+$ DCs, $CD103^+$ DC1, $CD11b^+$ DC2, bulk $F4/80^+$ tumor-associated macrophages (TAM), $CD11b^+$ TAM1, and $CD11c^+$ TAM2. Intriguingly, the proportion of $zsGreen^+$ cells was significantly increased across all tumor APC subsets following administration of non-zsGreen-labeled necroptotic fibroblasts; this increase was particularly pronounced in the DC subsets examined (Figure 5D). Accordingly, the absolute number of $zsGreen^+$ cells among tumor DC subsets was increased following necroptotic cell exposure (Figure S5D). As zsGreen

expression was restricted to B16.F10-OVA tumor cells in this model, these results show that signals derived from necroptotic fibroblasts act *in trans* to increase either the rate of phagocytosis or the retention of tumor-associated antigen within tumor APC populations.

To further characterize the phenotype of tumor APCs in our model, we evaluated expression of the necrotic cell uptake marker CLEC9A on DCs, and inhibitory PD-L1 on tumor cells and across different APC subsets. Exposure to necroptotic fibroblasts changed neither cell surface expression of either CLEC9A (Figure 5E) or PD-L1 (Figure 5F), nor the percentage of $CLEC9A^+$ (Figure S5E) or $PD\text{-}L1^+$ (Figure S5F) populations from each cell subset. We also assessed the activation status of $zsGreen^+$ tumor APCs following exposure to dying fibroblasts within the TME. We first observed that $zsGreen^+$ tumor APCs expressed higher levels of the costimulatory marker CD80 on a per cell basis following administration of necroptotic fibroblasts; this increase was consistent across all 6 tumor APC subsets examined (Figure 5G). Notably, we also observed a significant increase in the gMFI of CD80 following exposure to necroptotic cells when gating on $zsGreen^-$ (non-tumor antigen-loaded) populations of each tumor APC subset (Figure S5G), revealing that stimuli derived from necroptotic fibroblasts increased CD80 expression across all tumor APCs, regardless of tumor antigen uptake status. Importantly, this increase in activation marker expression correlated with an improved functional capacity of $zsGreen^+$ tumor APCs following exposure to necroptotic cells in the TME, as $zsGreen^+$ tumor APCs sorted *ex vivo* were capable of more robustly stimulating proliferation of previously-activated transgenic OVA-specific (OT-I) $CD8^+$ T cells in an *in vitro* co-culture system (Figure 5H). This stimulatory effect was limited to $CD8^+$ T cells with TCR specificity for tumor antigen, as *ex vivo* co-culture of $zsGreen^+$ tumor APCs did not induce proliferation of T cells expressing an irrelevant LCMV GP33 TCR (P14 transgenic TCR, Figure S5H). Therefore, exposure to

necroptotic cells in the TME increases not only the abundance, but also the immunostimulatory quality of tumor antigen-loaded tumor APCs.

Consistent with this, we found that necroptotic cells appear to enhance antigen uptake by phagocytes in a tumor-independent setting, as co-culturing bone marrow-derived macrophages (BMDMs) with necroptotic B16.F10 tumor cells *in vitro* resulted in increased uptake of an inert dextran-fluorophore substrate included in the co-culture, compared to BMDMs cultured with live B16.F10 cells (Figure 5I, left panel). Notably, uptake of this bystander substrate was also associated with an increase in CD80 expression on both dextran$^+$ and zsGreen$^+$ BMDMs only following co-culture with necroptotic B16.F10 cells (Figure 5I, center and right panels), while expression of the immunomodulatory markers CD206 and VCAM-1 was decreased on zsGreen$^+$ BMDMs co-cultured with necroptotic tumor cells compared to live tumor cell controls (Figure S5I). Collectively, these data indicate that stimuli derived from necroptotic cells increase antigen loading by phagocytic cell subsets, and that this effect may constitute a conserved response to necroptotic cell-derived stimuli rather than a tissue-specific effect restricted to the TME.

## 2.3 Discussion

Distinct forms of PCD can differentially instruct subsequent immune responses mounted against antigens derived from dying cells. Here, we describe a role for RIPK1/RIPK3 activation in which necroptotic fibroblasts within the TME drive increased antigen uptake and activation of tumor APCs to potentiate tumor-specific $CD8^+$ T cell immunity, which synergizes with α-PD-1 co-administration to confer durable tumor rejection (Figure 6). Importantly, our data indicate that tumor control by necroptotic cells is primarily mediated via the activation of a RIPK1/RIPK3/NF-κB signaling axis independently of cell lysis, as MLKL deficiency in necroptotic fibroblasts does not abrogate tumor control (Figure 3F), while NF-κB inhibition or use of a mutant form of RIPK3 that triggers cell lysis without engaging RIPK1-dependent transcription eliminates the therapeutic efficacy of these cells (Figure 3E). Thus, while in most experiments reported here we are engaging necroptotic cell death (as defined by activation of MLKL by RIPK3), activation of transcription that parallels cell death is likely the cause of the beneficial immune stimulation we observe. This conclusion is further supported by the fact that singular deficiency of a variety of innate immune signaling molecules involved in cytosolic nucleic acid sensing, TLR signaling, or TNF-mediated inflammation in tumor-infiltrating leukocytes does not affect tumor control following immune stimulation via necroptosis. Although any of these pathways could provide a partial contribution to tumor control, none of the candidates tested were absolutely required for the therapeutic effect of necroptotic cells.

These findings are consistent with reports of RIPK1- and NF-κB-dependent gene expression mediating the immunogenic effects of necroptotic cells, both with respect to dendritic cell maturation and priming of protective $CD8^+$ T cells in vaccination models[10]. A growing body of evidence has revealed death-independent functions of RIPK1/RIPK3 signaling that function

independently of cell lysis via MLKL-mediated pore formation, including the production of protective inflammatory chemokines during neuroinvasive viral infection[11], or cytokines following TLR4 stimulation via LPS treatment or infection with avirulent strains of Gram-negative bacteria[37,38]. Future work will need to define the specific signals derived from necroptotic cells that are responsible for mediating our observed anti-tumor immune responses. Using an intratumoral dying cell injection model, it appears that the therapeutic effects of necroptotic cells occur independently of MLKL activation, cell lysis, and subsequent DAMP release, and suggest that NF-κB transcriptional signaling downstream of the RIPK1/RIPK3 necrosome complex is required for therapeutic efficacy of necroptosis in the TME. Interestingly, our observation of increased tumor-derived antigen within tumor APCs exposed to necroptotic cells is consistent with a previous report of necrotic debris being ingested alongside extracellular contents via macropinocytosis[190]. However, the specific signals derived from necroptotic cells that are responsible for driving macropinocytosis to increase sampling of the local extracellular microenvironment remain unknown; our data imply that these signals are defined by cytokines, rather than DAMPs, produced by dying cells. Defining the mechanistic targets of RIPK1/RIPK3 activation and how these targets interact with tumor APCs to drive either increased macropinocytosis or improved retention of tumor antigen in order to better stimulate cytotoxic $CD8^+$ T cells remains an important area for future study.

Despite mounting evidence that inflammatory necroptosis promotes immune responses in the context of vaccination and viral infection, it is important to note that inflammation plays a paradoxical role in the field of tumor immunity. Although inflammatory signals within the TME may be beneficial in some cases, tumorigenic functions of inflammation are still strongly implicated during transformation and metastasis[39]. DAMPs released via lytic cell death, such as

nucleic acid species that activate STING, can promote oncogenesis[90], and can even promote immunological tolerance of tumor cells via local production of immunomodulatory molecules such as IDO and TGF-β[91]. Interestingly, recent work has shown that apoptotic or necroptotic cell death at the onset of hepatocyte transformation can differentially direct lineage commitment in liver cancer[191], highlighting the influence of distinct PCD modalities within a given microenvironment during tumorigenesis. Furthermore, recent findings in pancreatic ductal adenocarcinoma implicate tumorigenic functions of necroptotic signaling via RIPK1, RIPK3, and CXCL1[87]. Taken together, these findings stress the likelihood that the specific signals derived from necroptotic cells, and their role in either promoting or suppressing anti-tumor immunity, are likely to be highly cell type- and cancer context-specific.

The overarching goal of tumor immunotherapy is to engage cytotoxic $CD8^+$ T cells to kill tumor cells. This branch of the immune response evolved to combat intracellular pathogens such as viruses; treatments that activate innate immune pathways associated with viral sensing within tumors have therefore proven effective at provoking cytotoxic anti-tumor immunity. Such strategies include agonism of nucleic acid sensing via cGAS/STING[45,160] and TLR pathways[163], as well as inhibition of regulatory signals such as TAM RTKs on tumor-associated myeloid cells to eliminate repression of inflammatory responses[167,168]. These studies highlight the therapeutic benefit of manipulating innate immune signaling targets within the tumor microenvironment to preferentially skew the polarization or activation of tumor APCs to more effectively promote tumor-reactive T cell responses. Here, we show that necroptosis induction within the TME can similarly function to beneficially stimulate the activation of tumor APCs and subsequent $CD8^+$ T cell-mediated immunity, which successfully synergizes with ICB to promote durable tumor rejection. The necroptotic pathway likely evolved to combat viral infection via elimination of

the replicative niche, and is also promotes cross-priming of the $CD8^+$ T cell responses required for viral elimination[10]. Activation of this pathway within tumors can therefore be considered an additional strategy to direct anti-viral immunity toward tumor elimination. The dynamic nature of tumor-immune interactions necessitates the identification of novel therapeutic targets to add to the existing arsenal of tumor immunotherapy[156,174]. Tumor cell death represents a proximal event in the generation of tumor immunity, and specific modulation of PCD to maximize its immunogenicity may constitute an important orthogonal target to complement existing innate- and T cell-based forms of immunotherapy for optimal stimulation of anti-tumor immune responses. While much work remains to validate these findings in clinically relevant models, our data suggest that RIPK1/RIPK3 activation within the TME warrants further development as a component of tumor immunotherapy.

## 2.4 Materials and Methods

### *Study design*

Pilot studies were used to estimate mean differences in tumor growth between treatment groups. Using the Sample Size Calculator resource (Boston University), we calculated biological replicate numbers needed to avoid experimental underpowering by using the percent difference in group means from pilot studies, with 0.80 power level and $\alpha$ level = 0.05. Age-matched mice were randomly assigned to treatment groups, and tumor measurements were conducted by a researcher blinded to treatment groups for at least 1 experimental replicate.

### *Cell culture*

B16.F10-OVA, LL/2-OVA, NIH-3T3, and HEK-293T cells were maintained in Dulbecco's modification of Eagle medium (DMEM) supplemented with 10% (vol/vol) FBS, 2mM L-glutamine, 10mM HEPES, and 1mM sodium pyruvate (complete DMEM). E.G7-OVA cells were maintained in RPMI 1640 supplemented with 10% FBS, 2mM L-glutamine, 10mM HEPES, 1mM sodium pyruvate, 0.05mM beta-mercapthoethanol, 0.4mg/mL geneticin (G418), and 4.5g/L D-glucose. B16.F10 and LL/2 cell lines were transduced with a plasmid (pSLIK) encoding activatable versions of caspase-9 or RIPK3 under TRE control; thus, these cells were cultured in 1μg/mL doxycycline (Sigma) for 18h to induce construct expression prior to harvesting as described below for dying cell injections. Bone marrow-derived macrophages (BMDMs) were cultured in complete DMEM + penicillin/streptomycin + 20ng/mL rM-CSF and differentiated for 7 days prior to plating for experiments. All cells were cultured at 37°C with 5% $CO_2$.

***Mice***

C57BL6/J (B6/J) mice were purchased (Jackson) and allowed to acclimate up to one week prior to experiment initiation. All other genotypes were bred and housed under specific-pathogen-free conditions at the University of Washington. All animals were maintained according to protocols approved by the University of Washington Institutional Animal Care and Use Committee (IACUC).

***Tumor models***

6-10 week old female (B16.F10-OVA, E.G7-OVA) or male (LL/2-OVA) mice were injected subcutaneously on the right flank with 1 x $10^5$ (B16.F10-OVA, E.G7-OVA) or 2 x $10^5$ (LL/2-OVA) tumor cells, mixed in a 1:1 volumetric ratio with the basement membrane matrix Matrigel HC (Corning) for a final injection volume of 100μL. For bilateral tumor experiments, mice were equivalently implanted with tumor cells on the left flank on the same day (d.0) of right flank tumor injection. As previously described[160], tumor volume was calculated using the following formula: Volume = Short axis$^2$ x Long axis x 0.523. Mice were euthanized once tumor burden reached a volume ≥2000mm$^3$. Mice that developed skin ulceration over the tumor site were excluded from experimental analyses. Complete tumor clearance was determined by the absence of a palpable tumor mass at the site of tumor injection.

***Intratumoral dying cell injections***

NIH-3T3, B16.F10, or LL/2 cells stably transduced with pro-death constructs were harvested activated as previously described[10]. Briefly, 5 x $10^6$ cells/mL were incubated in complete DMEM + 1mM of B/B homodimerizer (Clontech) for 15min at 37°C. Cells were then washed with cold

PBS, resuspended at 20 x $10^6$ cells/mL, and kept on ice prior to injection. 1 x $10^6$ dying cells were administered intratumorally in 50μL. Remaining cells were re-plated and cultured at 37°C overnight to ensure <95% of treated cells underwent PCD. Dying cells were administered on days 6, 8, and 10 post-initial tumor challenge. For experiments involving IκBα inhibition, NIH-3T3 cells were pre-treated with 10μM BAY 11-7085 (Cayman Chemical) for 45min prior to harvesting for B/B homodimerizer incubation, as described[10].

***In vivo antibody administration***

200μg of α-CD8 (clone 2.43, BioXCell), α-CD4 (clone GK1.5, BioXCell), α-PD-1 (clone RMP1-14, BioXCell), or respective isotype controls were administered to mice via intraperitoneal injection on days 5, 7, 9, and 11 post-initial tumor challenge. NK cell depletion experiments followed the same dosing protocol, using 250μg of α-NK1.1 (clone PK136, BioXCell). CLEC9A blocking experiments followed the same dosing protocol, using 400μg of α-CLEC9A (clone 7H11, BioXCell) or isotype control, as described[43].

***Flow cytometry and cell sorting***

Leukocytes were isolated from either tumor-adjacent inguinal lymph node (iLN) or spleen by mashing over a 70μM strainer, or from tumor tissue by digesting minced tumors in 1X PBS + 2.6mg/mL Collagenase A (Sigma) + 23U/mL DNase I (Sigma) at 37°C with agitation for 45min prior to mashing tissue over a 70μM strainer. 1-3 x $10^6$ cells were blocked with anti-CD16/32 (BD Biosciences) and stained with Zombie viability dye (BioLegend) at room temperature for 30min. Cells were then incubated with appropriate fluorochrome-conjugated antibodies in 1X PBS + 0.5% FBS + 2mM EDTA at for 4°C for 1h. Permeabilization and intranuclear staining

were performed using a Foxp3 Intranuclear Transcription Factor Staining Kit (eBiosciences). Data were collected using an LSRII flow cytometer (BD) and analyzed using FlowJo software (Treestar). For sorting of zsGreen$^{+}$ tumor APC populations, B16.F10-OVA-zsGreen tumors were harvested 48h post-intratumoral dying cell injection, leukocytes were processed and stained as described above, and subsets were sorted using a FACSAria II (BD). Flow antibody information is provided in Table S1.

***OT-I/P14 proliferation assay***

Lymph nodes and spleens from OT-I or P14 TCR transgenic mice were processed and enriched for CD8$^{+}$ T cells via negative selection using biotinylated antibodies against B220, CD4, CD11b, CD11c, and Ter119 (eBioscience) followed by magnetic separation. Purified transgenic T cells were activated via 6 day co-culture with irradiated splenocytes pulsed with 100ng/mL SL8 (for OT-I) or GP33 (for P14) peptides (Invivogen). 20,000 previously-activated transgenic T cells were labeled with 5μM CellTrace Violet (Thermo Fisher) and plated with 4,000 sorted zsGreen$^{+}$ tumor APC subsets in 96 well U-bottom plates for 72h prior to analysis of proliferation dye dilution via flow cytometry.

***Murine cytokine assessment***

To evaluate serum cytokine levels, sera were harvested from mice receiving indicated intratumoral treatments 48h post-dying cell administration and stored for <2 weeks at -80°C. As a positive control for systemic inflammation, B6/J mice were injected intraperitoneally with 40mg/kg of the STING agonist DMXAA (ApexBio), and sera were harvested 5h post-injection, then frozen at -80°C. To evaluate intratumoral cytokine levels, tumors were harvested 48h post-

dying cell administration. Tumors were then minced and homogenized using metal beads with vigorous shaking in tubes, then frozen at -80°C. Thawed samples were analyzed using a Th1/Th2 ProcartaPlex$^{TM}$ Panel 1 Luminex kit (Thermo Fisher).

***CRISPR/Cas9 gene targeting***

The following guide RNA (gRNA) sequences were cloned into a pRRL-Cas9-T2A-puromycin CRISPR/Cas9 lentiviral vector (a gift from Dr. Daniel Stetson[192]): murine non-targeting gRNA (5'- GCGAGGTATTCGGCTCCGCG -3')[193]; murine *Mlkl* gRNA (5'- GCACACGGTTTCCTAGACGC -3'). Constructs were transduced into NIH-3T3 +acRIPK3 cells using standard lentiviral transduction protocols, and selected in 1μg/mL puromycin.

***siRNA knockdown***

2 x $10^5$ MLKL$^{-/-}$ NIH-3T3 cells +acRIPK3 were transfected with SiGenome SMARTpool siRNAs (Dharmacon) targeting murine RIPK1 (M-040150-01), murine caspase-8 (M-043044-01), murine cFLIP (M-041091-01), or non-targeted "scramble" pool (D-001206-14), using Lipofectamine siRNA Max (Life Technologies). 48h post-transfection, cells were re-plated, treated with 100nM B/B homodimerizer (Clontech), and cell death kinetics were characterized as described above.

***Western blot***

Cell lysates were harvested and quantitated using a BCA Protein Assay (Thermo). 30μg total protein/sample were separated using SDS-PAGE gels (Invitrogen) and detected using traditional protocols. The following antibodies were used for protein detection: rat α-MLKL clone 3H1

(EMD Millipore), rabbit α-FKBP12 (Thermo), mouse α-actin C4 (EMD Millipore), goat α-rat IgG-HRP (Santa Cruz), donkey α-rabbit IgG-HRP (Santa Cruz), and goat α-mouse IgG-HRP (Santa Cruz).

***In vitro dextran uptake assay***

BMDMs were plated in a 1:5 ratio with either live or acRIPK3-expressing B16.F10-zsGreen tumor cells. acRIPK3 cells were induced to die upon 18h incubation with 1μg/mL doxycycline prior to co-culture with BMDMs, then incubated with 100nM B/B homodimerizer (Clontech) for 24h before adding 1mg/mL Dextran-PE.TexasRed (10,000 MW, Thermo Scientific). Dextran incubations were performed in triplicate at either 4°C or 37°C for 30min, and plates were tapped every 10min to mix. Cells were washed 3x, stained with fluorochrome-conjugated antibodies, and immediately analyzed on a flow cytometer. Dextran uptake was calculated as follows[186]: ΔgMFI = (gMFI dextran binding at 37°C - gMFI dextran binding at 4°C).

***Statistics***

Unless otherwise noted in figure legend, data represent mean +/- SEM. Survival curves were analyzed via Mantel-Cox log-rank test. All other experiments were compared using parametric 2-tailed student's t-test, chi-square test, or 1-way or 2-way ANOVA, with appropriate corrections for repeated measures of tumor growth curves. All statistical analyses were performed using GraphPad Prism software unless noted otherwise.

**2.5 Acknowledgements**

We thank P. Ralli-Jain for technical assistance. We thank D. Stetson (U. Washington) for *Tmem173*$^{-/-}$, *Mb21d*$^{-/-}$, and *Mavs*$^{-/-}$ mice, M. Gale Jr. (U. Washington) for *Irf3*$^{-/-}$, *Myd88*$^{-/-}$, *Ticam1*$^{-/-}$, and P14 TCR transgenic mice, and M. Gerner (U. Washington) for OT-I TCR transgenic mice. We thank N. Subramanian (Institute for Systems Biology) for the pSLIK plasmid.

**Funding**: This work was supported by NIH grant R01CA228098 and by a Wade F.B. Thompson CLIP award from the Cancer Research Institute, both to AO. AGS was supported by PHS NRSA T32GM007270 and NSF GRFP (DGE-1256082); NWH by T32AI106677-05; MNM by T32CA080416; BPD by F32 AI129254.

**Author contributions**: AGS and AO conceived the study and designed experiments. AGS, NWH, MNM, BPD, SBK, CEH, SLO, and KC performed experiments. AGS and BPD analyzed data. AGS and AO wrote the manuscript.

## 2.6 Figures

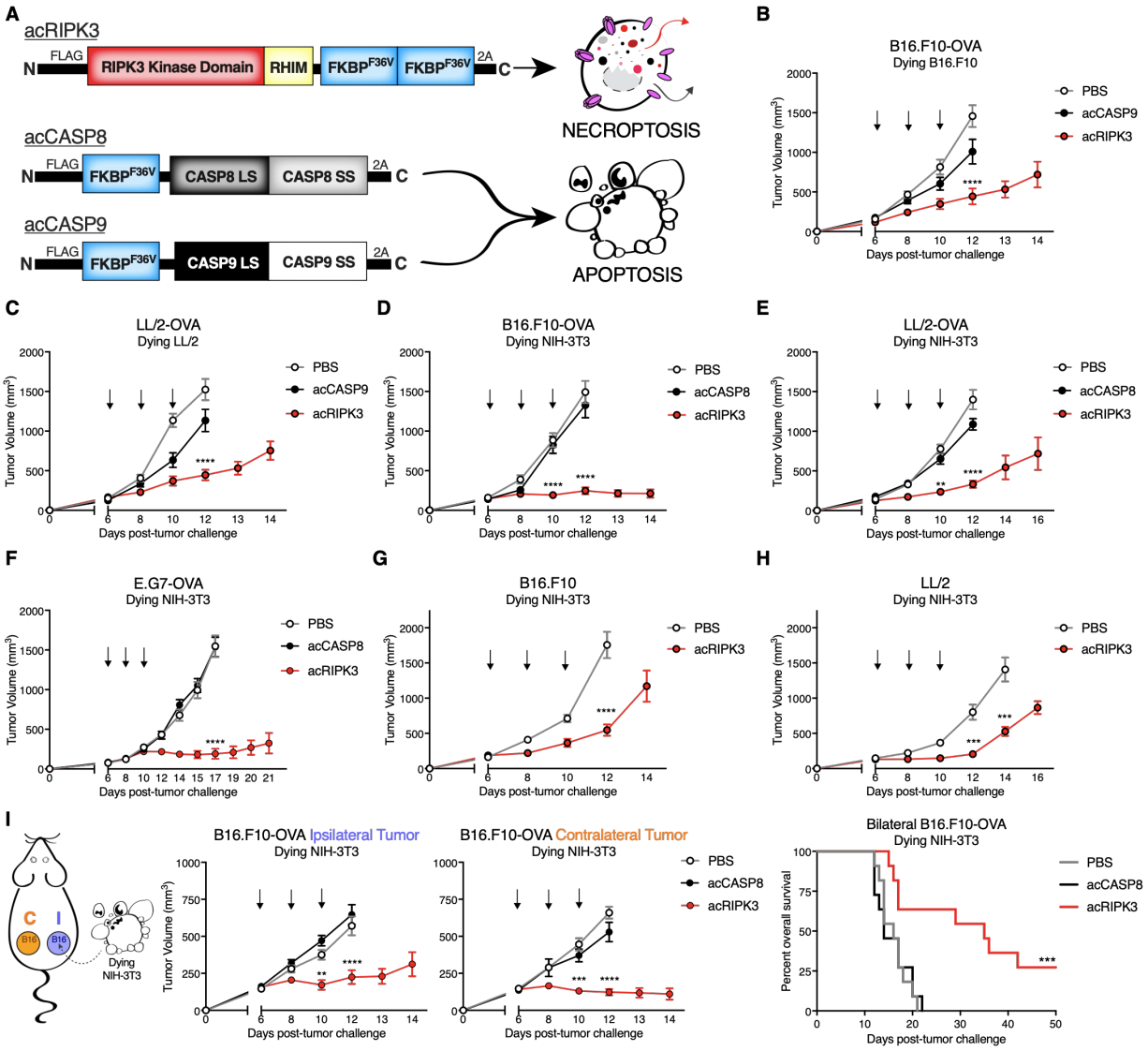


**Figure 1: Necroptotic cells confer tumor control across multiple syngeneic flank tumor models.** (**A**) Schematic of pro-death enzyme constructs and respective types of PCD induced downstream following enzyme activation with B/B homodimerizer. (**B-F**) Tumor growth of B6/J mice bearing (**B,D**) B16.F10-OVA, (**C,E**) LL/2-OVA, or (**F**) E.G7-OVA flank tumors following administration of apoptotic or necroptotic (**B,C**) autologous or (**D-F**) unmatched NIH-3T3 fibroblast cells. N=10-16 mice per group. (**G,H**) Tumor growth of B6/J mice bearing (**G**)

B16.F10 or (**H**) LL/2 flank tumors following administration of necroptotic NIH-3T3 cells. N=9-14 mice per group. (**I**) Tumor growth of ipsilateral ("I", treated) and contralateral ("C", untreated) B16.F10-OVA tumors following administration of either apoptotic or necroptotic NIH-3T3 cells (left, center panels), and survival curve of mice from the same experiment (right panel). N=9-11 mice per group. **p<0.01, ***p<0.001, ****p<0.0001. Black arrows indicate intratumoral dying cell injections. Error bars represent SEM. Data are pooled from 3-5 independent experiments.

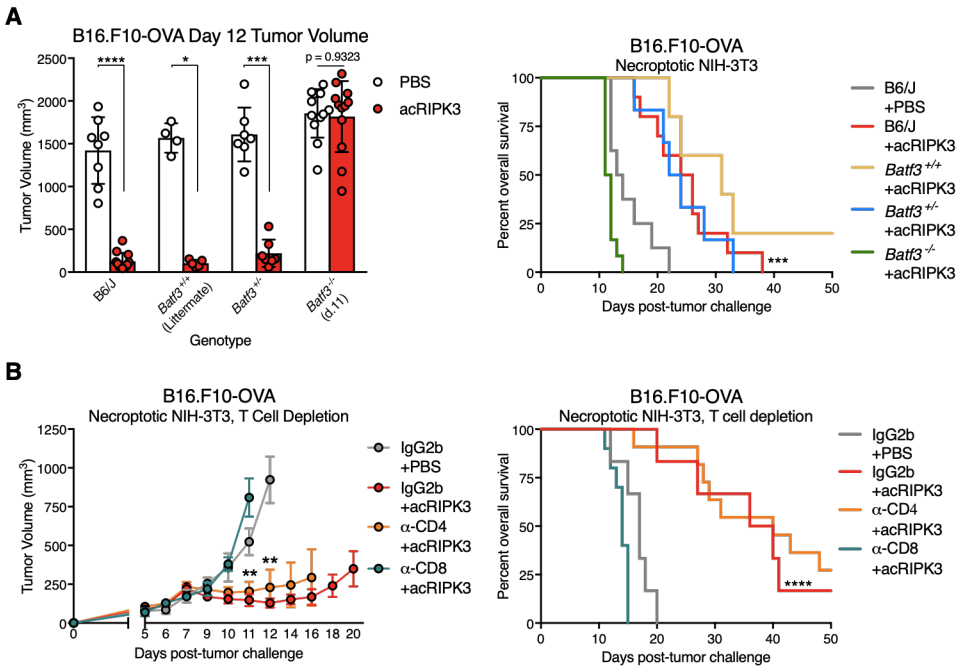


**Figure 2: Tumor control by necroptotic cells requires BATF3$^+$ cDC1 and CD8$^+$ leukocytes.** (**A**) Day 12 B16.F10-OVA tumor volumes (left panel) and animal survival (right panel) of mice with varying *Batf3* genotypes following necroptotic fibroblast injections. N=4-12 mice per group. (**B**) B16.F10-OVA tumor growth (left panel) and animal survival (right panel) upon co-administration of necroptotic fibroblasts with depleting antibodies against either CD4$^+$ or CD8$^+$ leukocytes. N=6-11 mice per group. *p<0.05, **p<0.01, ***p<0.001, ****p<0.0001. Black arrows indicate intratumoral dying cell injections. Error bars represent SEM. Data are pooled from 2-4 independent experiments.

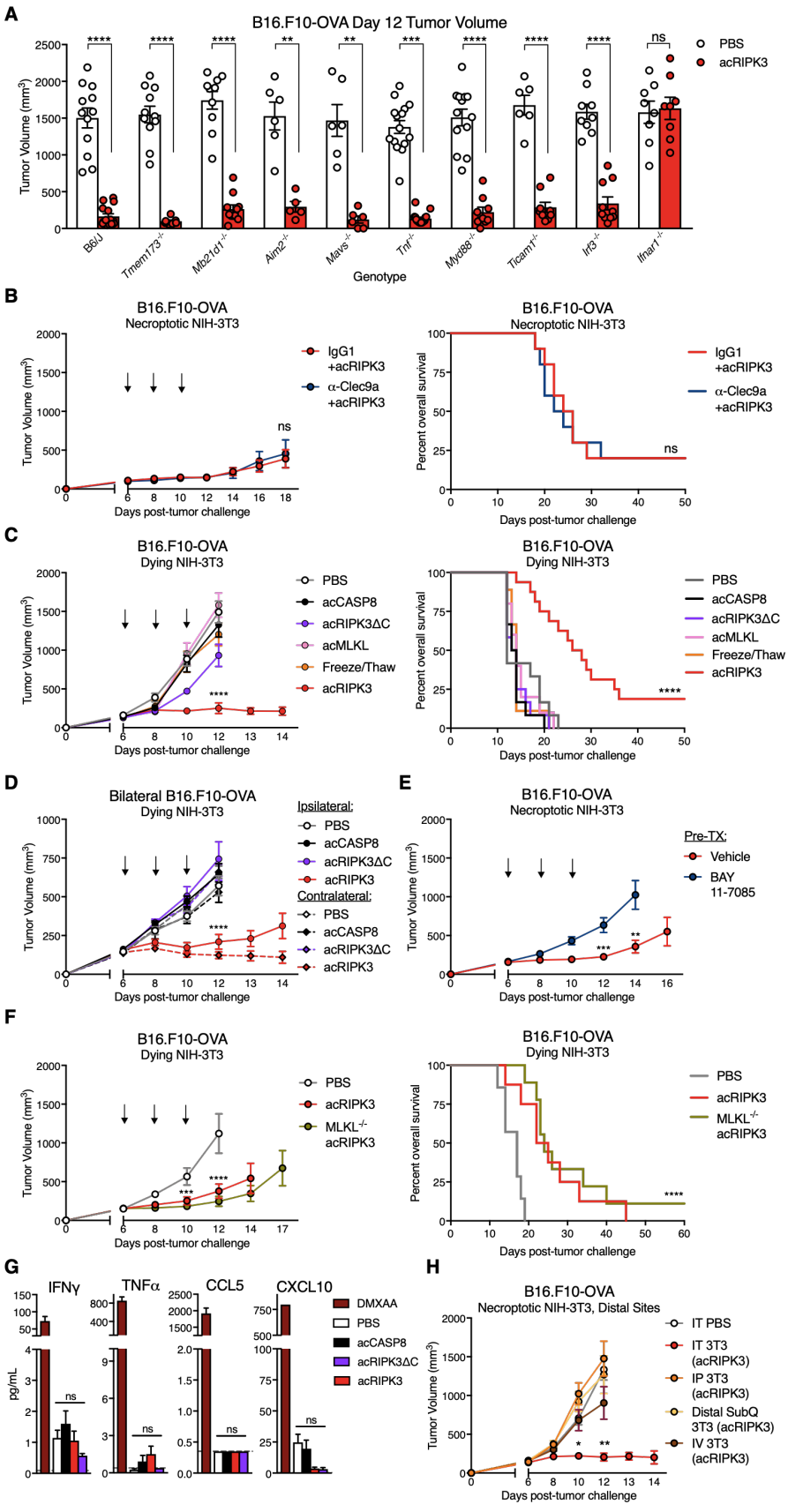
A
B16.F10-OVA Day 12 Tumor Volume
Tumor Volume (mm3)
PBS
acRIPK3
B6/J
Tmem173-/-
Mb21d1-/-
Aim2-/-
Mavs-/-
Tnf-/-
Myd88-/-
Ticam1-/-
Irf3-/-
Ifnar1-/-
Genotype
B
B16.F10-OVA
Necroptotic NIH-3T3
IgG1 +acRIPK3
α-Clec9a +acRIPK3
Days post-tumor challenge
Percent overall survival
C
B16.F10-OVA
Dying NIH-3T3
PBS
acCASP8
acRIPK3ΔC
acMLKL
Freeze/Thaw
acRIPK3
D
Bilateral B16.F10-OVA
Dying NIH-3T3
Ipsilateral:
Contralateral:
E
Pre-TX:
Vehicle
BAY 11-7085
F
MLKL-/- acRIPK3
G
IFNγ
TNFα
CCL5
CXCL10
pg/mL
DMXAA
H
B16.F10-OVA
Necroptotic NIH-3T3, Distal Sites
IT PBS
IT 3T3 (acRIPK3)
IP 3T3 (acRIPK3)
Distal SubQ 3T3 (acRIPK3)
IV 3T3 (acRIPK3)

**Figure 3: Immune-mediated tumor control by necroptotic cells requires NF-κB activation within dying cells, but not MLKL-mediated cell lysis and DAMP release.** (**A**) Day 12 volumes of B16.F10-OVA tumors in various innate immune knockout mice following necroptotic fibroblast injections on days 6, 8, and 10. N=5-15 mice per group. (**B**) B16.F10-OVA tumor growth (left panel) and animal survival (right panel) upon co-administration of necroptotic fibroblasts with blocking α-CLEC9A antibody. N=10 mice per group. (**C-D**) Tumor growth and overall survival following administration of lytic necrotic fibroblasts in (**C**) single, or (**D**) contralateral B16.F10-OVA flank tumors. Tumor growth and survival curves for PBS, acCASP8, and acRIPK3 as presented in Figure 1 are also graphed for comparison. (**E**) B16.F10-OVA tumor growth curves following injection of necroptotic NIH-3T3 fibroblasts pre-incubated with the IκBα phosphorylation inhibitor BAY-117085, which prevents NF-κB activation in treated cells. N=10 mice per group. (**F**) B16.F10-OVA tumor growth (left panel) and animal survival (right panel) following IT injection of PBS, necroptotic fibroblasts, or $MLKL^{-/-}$ necroptotic fibroblasts. N=7-9 mice per group. (**G**) Assessment of systemic inflammation via Luminex assay for inflammatory serum cytokines and chemokines 48h post-intratumoral dying NIH-3T3 injection. DMXAA-injected mice were included as a positive control for systemic inflammatory cytokine production. Gray dotted line represents limit of detection. N=3-5 mice per group. (**H**) B16.F10-OVA tumor growth curves following intratumoral (IT), intraperitoneal (IP), distal subcutaneous (distal subQ), or intravenous (IV) injection of necroptotic fibroblasts. N=7-9 mice per group. *p<0.05, **p<0.01, ***p<0.001, ****p<0.0001. Black arrows indicate intratumoral dying cell injections. Error bars represent SEM. Data are pooled from 2-5 independent experiments.

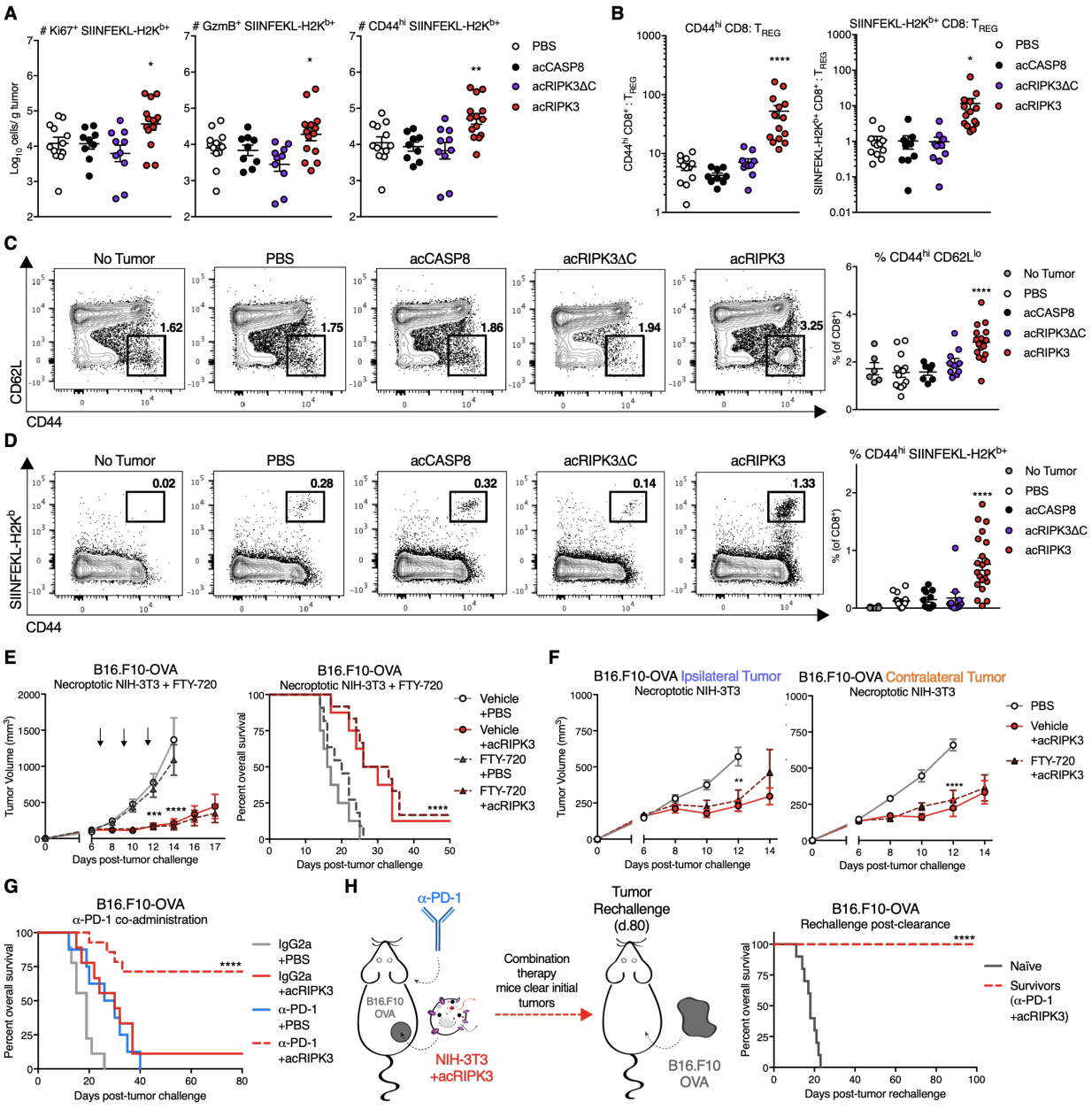


**Figure 4: Necroptosis promotes anti-tumor CD8$^+$ T responses and synergizes with immune checkpoint blockade.** (**A**) Absolute numbers of intratumoral CD8$^+$ T cells with various phenotyping markers for proliferation (Ki67), effector function (GranzymeB, GzmB), and activation (CD44), normalized per gram of tumor tissue. (**B**) Quantification of the ratio of intratumoral activated (CD44$^{hi}$, left panel) or tumor antigen-specific (SIINFEKL-H2K$^{b+}$, right panel) CD8$^+$ T cells to immunosuppressive Foxp3$^+$ CD25$^+$ $T_{REG}$, normalized per gram of tumor

tissue. (**C**) Sample flow plots (left panel) and percentages (right panel) of overall activated $CD8^+$ T cells in the tumor-draining (inguinal) lymph node. (**D**) Sample flow plots (left panel) and percentages (right panel) of OVA-specific and activated $CD8^+$ T cells in the tumor-draining (inguinal) lymph node. (**E**) B16.F10-OVA tumor growth (left panel) and animal survival (right panel) following co-administration of necroptotic fibroblasts with the lymphocyte trafficking inhibitor FTY-720. N=8-12 mice per group. (**F**) Tumor growth of ipsilateral (treated, left panel) and contralateral (untreated, right panel) B16.F10-OVA tumors following administration of necroptotic NIH-3T3 cells with FTY-720. N=9-10 mice per group. (**G**) Survival curves of B16.F10-OVA tumor-bearing mice following co-administration of necroptotic fibroblasts with the immune checkpoint blockade reagent α-PD-1 or IgG2a isotype. N=8-14 mice per group. (**H**, left panel) Schematic of tumor re-challenge experiments in mice from (**G**) that successfully clear B16.F10-OVA tumors. (**H**, right panel) Survival of mice re-challenged with B16.F10-OVA cells on the same flank as initial tumor location. N=10 mice per group. *$p<0.05$, **$p<0.01$, ***$p<0.001$, ****$p<0.0001$. All flow harvests performed 48h post-dying cell injection. Error bars represent SEM. Data are pooled from 2-4 independent experiments.

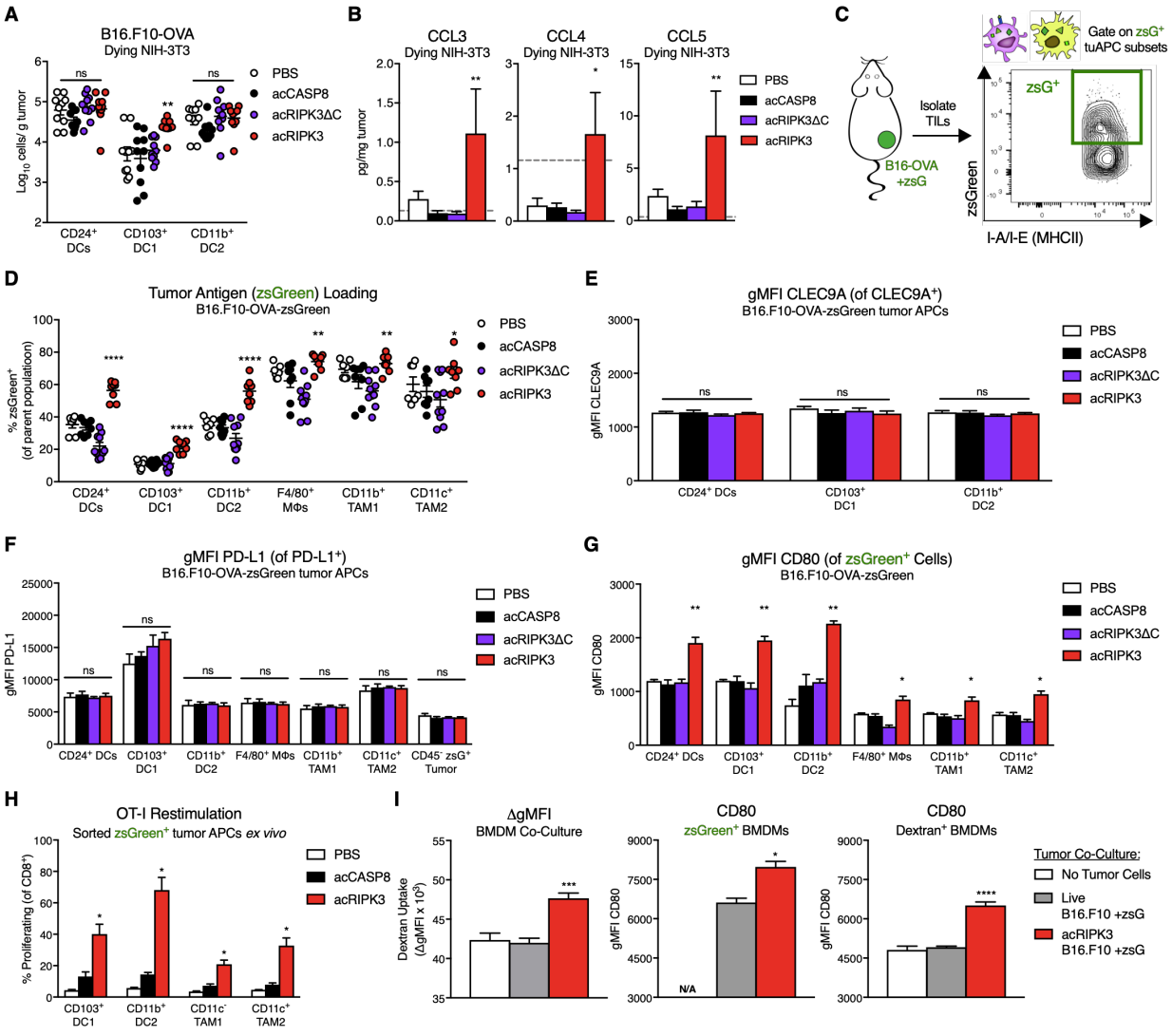


**Figure 5: Exposure to necroptosis in the TME promotes antigen uptake and activation of tumor-associated APCs.** (**A**) Absolute numbers of tumor-associated dendritic cell (DC) subsets 48h following intratumoral dying cell administration, normalized per gram of tumor tissue. (**B**) Intratumoral concentrations of DC-recruiting chemokines 24h post-dying NIH-3T3 injection. Gray dotted line represents limit of detection. N=3-5 mice per group. (**C**) Experimental schematic of B16.F10-OVA tumor cells expressing zsGreen as a surrogate tumor antigen, allowing for gating on tumor APCs that have phagocytosed tumor antigen. (**D**) Percent of zsGreen$^{+}$ tumor APCs following dying cell administration. (**E**) Geometric mean fluorescence

intensity (gMFI) of CLEC9A receptor on subsets of tumor DC populations. N=4-6 mice per group. (**F**) gMFI of PD-L1 on subsets of tumor APC populations and $CD45^-$ $zsGreen^+$ tumor cells. N=4-6 mice per group. (**G**) gMFI of the costimulatory marker CD80 on $zsGreen^+$ subsets of tumor APC populations. N=3-4 mice per group. (**H**) Quantification of previously activated OT-I T cell proliferation upon co-culture with $zsGreen^+$ tumor APC subsets sorted *ex vivo* from B16.F10-OVA-zsGreen tumors following dying cell injection. N=3 technical replicates per group, using pooled cells from 5 mice per treatment group. (**I**) *In vitro* characterization of bone-marrow derived macrophages (BMDMs) co-cultured with live or necroptotic B16.F10-zsGreen tumor cells and dextran-fluorophore beads, assessed for phagocytosis via dextran uptake (left panel), and expression of costimulatory marker CD80 gMFI in $zsGreen^+$ BMDMs (middle panel) or $dextran^+$ beads (right panel). N=3 technical replicates per group. *$p<0.05$, **$p<0.01$, ***$p<0.001$, ****$p<0.0001$. All flow harvests performed 48h post-dying cell injection. Error bars represent SEM. Data are representative plots from 1-3 independent experiments (**E-I**), or pooled from 2-3 independent experiments (**A,B,D**).

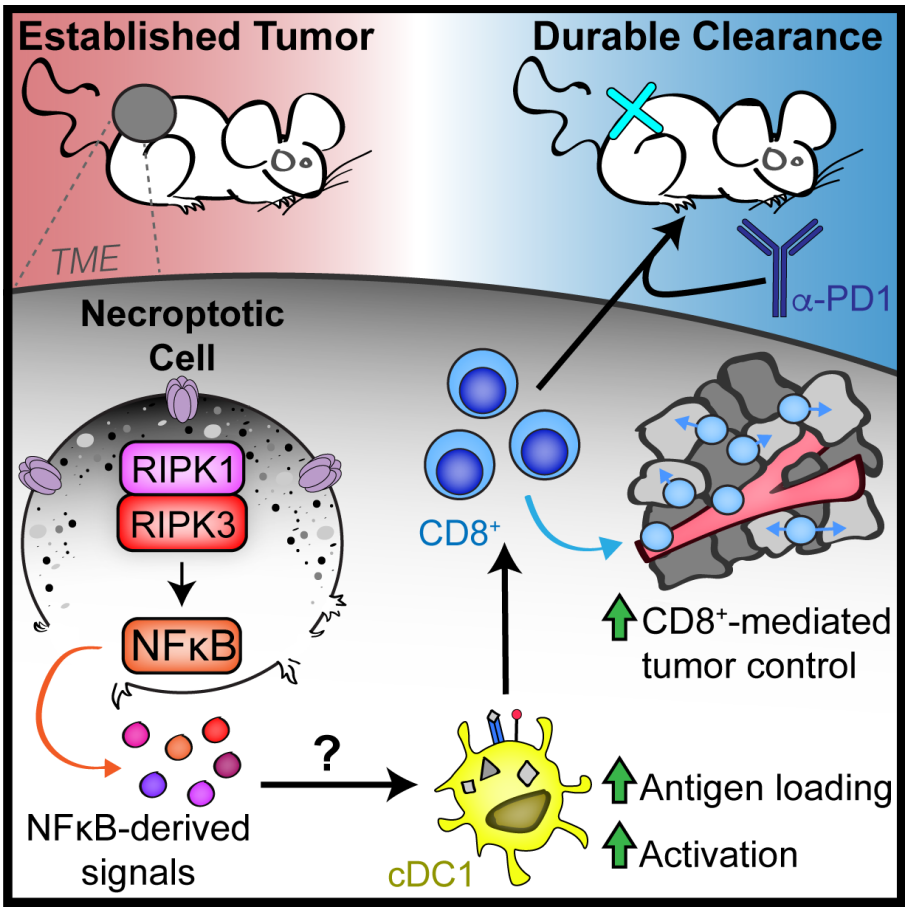


**Figure 6: Proposed model by which necroptotic cell death within the tumor microenvironment promotes anti-tumor immunity.** RIPK1/RIPK3 activation in necroptotic cells produces NF-κB-dependent signals that promote $CD103^+$ cDC1 and $CD8^+$ leukocyte-mediated anti-tumor immunity, which synergizes with α-PD1 to promote durable tumor clearance.

## 2.7 Supplemental Figures

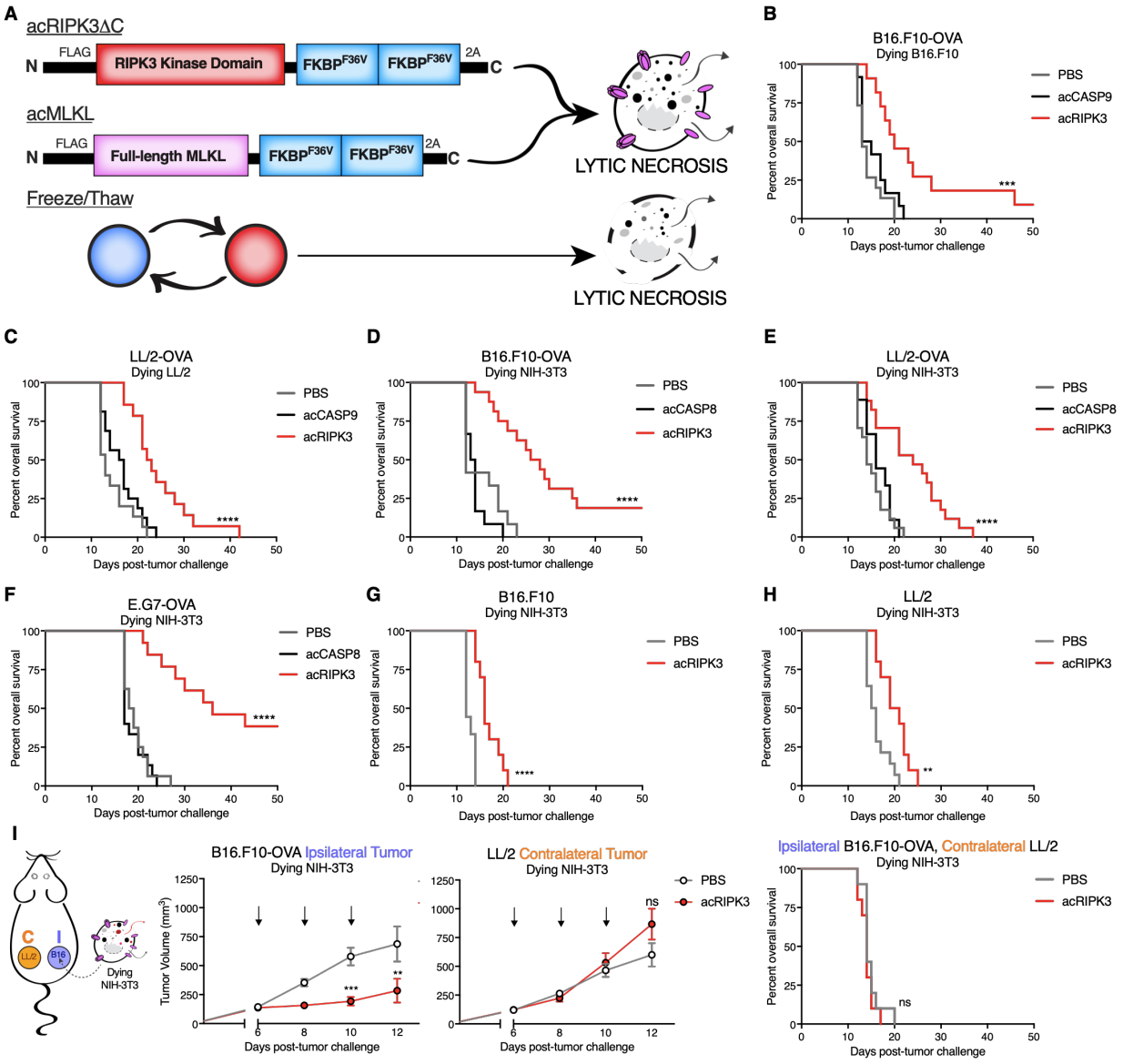


**Figure S1 (Related to Figure 1): Necroptotic cells extend the survival of tumor-bearing mice.** (**A**) Schematic of pro-death enzyme constructs or freeze/thaw cycles that lead to induction of lytic necrosis. (**B-F**) Overall survival of B6/J mice bearing (**B,D**) B16.F10-OVA, (**C,E**) LL/2-OVA, or (**F**) E.G7-OVA flank tumors following administration of apoptotic or necroptotic (**B,C**) autologous or (**D-F**) unmatched NIH-3T3 fibroblast cells. N=10-16 mice per group. (**G,H**) Overall survival of B6/J mice bearing (**G**) B16.F10 or (**H**) LL/2 flank tumors following

administration of necroptotic NIH-3T3 cells. N=9-14 mice per group. (**I**) Tumor growth of B16.F10-OVA ipsilateral ("I", treated) and LL/2 contralateral ("C", untreated) tumors following administration of either apoptotic or necroptotic NIH-3T3 cells (left, center panels), and survival curve of mice from the same experiment (right panel). N=10 mice per group. **$p<0.01$, ***$p<0.001$, ****$p<0.0001$. Black arrows indicate intratumoral dying cell injections. Error bars represent SEM. Data are pooled from 1-5 independent experiments.

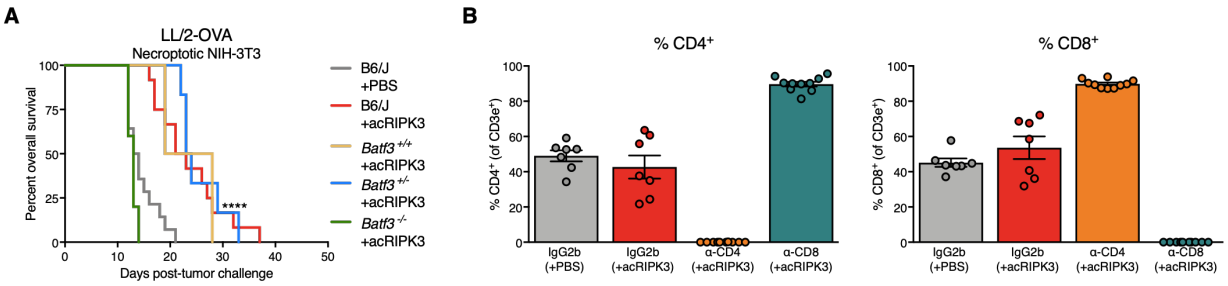


**Figure S2 (Related to Figure 2): BATF3$^+$ and CD8$^+$ leukocyte requirements for tumor control by necroptotic cells.** (**A**) Survival of LL/2-OVA tumor-bearing mice with varying *Batf3* genotypes following necroptotic fibroblast injections on days 6, 8, and 10. N=2-14 mice per group. (**B**) Confirmation of CD4$^+$ or CD8$^+$ leukocyte depletion in peripheral blood following depletion antibody administration. Blood leukocytes were collected and analyzed day 8 post-initial tumor challenge. T cells were gated on CD45$^+$ > CD19$^-$ CD3$^+$> either CD4$^+$ or CD8$^+$ cells, using α-CD4 or α-CD8 antibody clones distinct from those targeted by depletion antibodies. ****p<0.0001. Black arrows indicate intratumoral dying cell injections. Error bars represent SEM. Data are pooled from 2-5 independent experiments.

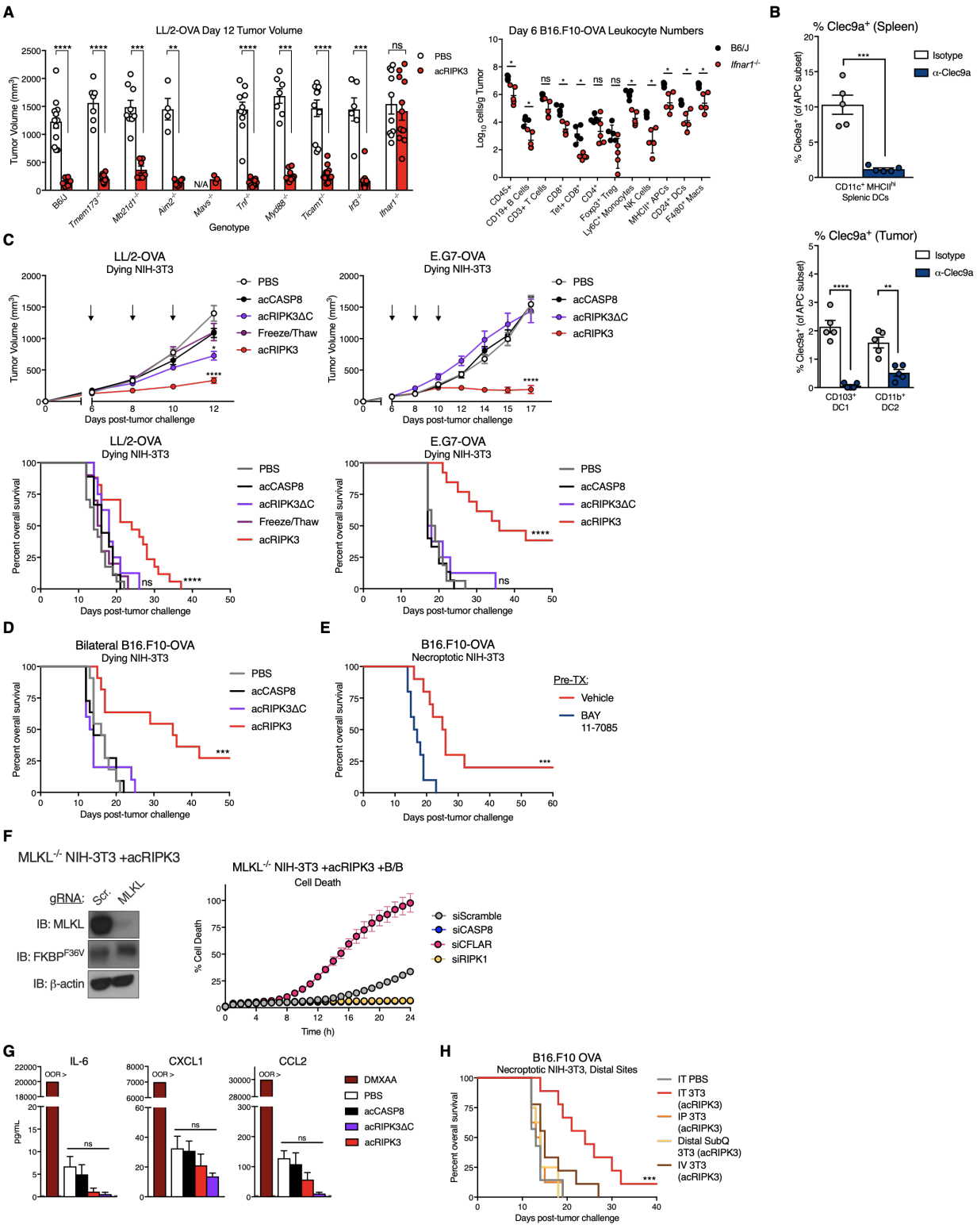


**Figure S3 (Related to Figure 3): DAMP-independent tumor control by necroptotic fibroblasts is recapitulated in multiple syngeneic tumor models.** (**A**) (Left panel) Day 12

volumes of LL/2-OVA tumors in various innate immune knockout mice following necroptotic fibroblast injections on days 6, 8, and 10 (left panel). N=4-10 mice per group. (Right panel) Total numbers of leukocyte subsets harvested on day 6 from B16.F10-OVA tumors implanted on B6/J or *Ifnar1*$^{-/-}$ mice. (**B**) Confirmation of CLEC9A receptor blockade on spleen and tumor-associated dendritic cell (DC) populations following α-CLEC9A administration. Organs were harvested on day 8 post-initial tumor challenge. CLEC9A$^{+}$ cells were gated based on DC subsets as described in Figure S5C in tumor tissue, and CD45$^{+}$ > CD19$^{-}$ CD3$^{-}$ > CD11b$^{+}$ Ly6C$^{-}$ > F4/80$^{-}$ > CD11c$^{+}$ MHCII$^{hi}$ cells in spleen. (**C**) Growth curves of (upper left panel) LL/2-OVA or (upper right panel) E.G7-OVA flank tumors receiving intratumoral lytic necrotic (RIPK3ΔC) fibroblasts. Corresponding survival curves of (lower left panel) LL/2-OVA or (lower right panel) E.G7-OVA flank tumor-bearing mice. N=8-17 mice per group. (**D**) Survival of bilateral B16.F10-OVA tumor-bearing mice following treatment with intratumoral lytic necrotic (RIPK3ΔC) fibroblasts. N=10-11 mice per group. (**E**) Survival of B16.F10-OVA tumor-bearing mice following injection of necroptotic NIH-3T3 fibroblasts pre-incubated with the IκBα phosphorylation inhibitor BAY-117085. N=10 mice per group. (**F**) Confirmation of MLKL protein expression deletion in NIH-3T3 cells transduced with MLKL-targeting CRISPR/Cas9 construct (left panel). Percent cell death in MLKL$^{-/-}$ NIH-3T3 +acRIPK3 cells treated with 100nM B/B homodimerizer (activator drug) following siRNA-mediated knockdown of CASP8, RIPK1, or CFLAR (cFLIP) expression. N=3 technical replicates per group. (**G**) Assessment of systemic inflammation via Luminex assay for inflammatory serum cytokines and chemokines typically associated with necroptotic NIH-3T3 cells, 48 hours post-intratumoral dying NIH-3T3 injection. DMXAA-injected mice were included as a positive control for systemic inflammatory cytokine production. Gray dotted line represents limit of detection. N=3-5 mice per group. (**H**)

Survival of B16.F10-OVA tumor-bearing mice following intratumoral (IT), intraperitoneal (IP), distal subcutaneous (distal subQ), or intravenous (IV) injection of necroptotic fibroblasts. N=7-9 mice per group. *p<0.05, **p<0.01, ***p<0.001, ****p<0.0001. OOR> represents out of range detection value; bar represents upper limit of detection. Error bars represent SEM. Data are pooled from 1-5 independent experiments.

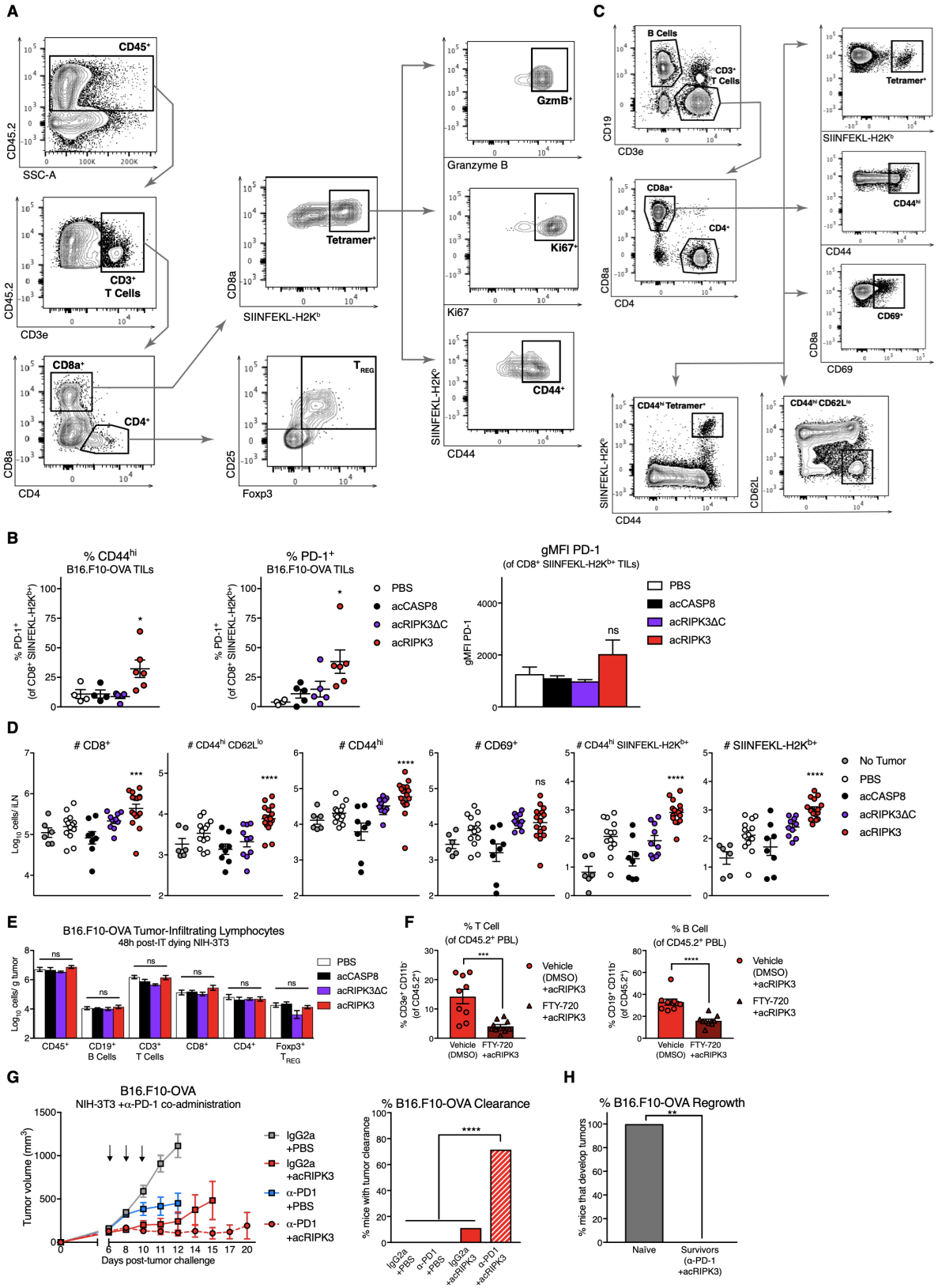
A
CD45⁺
CD45.2
SSC-A
CD3⁺ T Cells
CD3e
CD8a⁺
CD4⁺
CD8a
CD4
Tetramer⁺
SIINFEKL-H2Kᵇ
CD8a
T_REG
CD25
Foxp3
GzmB⁺
Granzyme B
Ki67⁺
Ki67
SIINFEKL-H2Kᵇ
CD44⁺
CD44
C
B Cells
CD3⁺ T Cells
CD19
CD3e
CD8a⁺
CD4⁺
CD8a
CD4
Tetramer⁺
SIINFEKL-H2Kᵇ
CD44ʰⁱ
CD44
CD69⁺
CD8a
CD69
CD44ʰⁱ Tetramer⁺
SIINFEKL-H2Kᵇ
CD44
CD44ʰⁱ CD62Lˡᵒ
CD62L
B
% CD44hi
B16.F10-OVA TILs
% PD-1⁺ (of CD8⁺ SIINFEKL-H2Kᵇ⁺)
% PD-1+
B16.F10-OVA TILs
gMFI PD-1
(of CD8⁺ SIINFEKL-H2Kᵇ⁺ TILs)
gMFI PD-1
ns
PBS
acCASP8
acRIPK3ΔC
acRIPK3
D
# CD8⁺
# CD44hi CD62Llo
# CD44hi
# CD69⁺
# CD44hi SIINFEKL-H2Kb+
# SIINFEKL-H2Kb+
Log10 cells/ LN
No Tumor
PBS
acCASP8
acRIPK3ΔC
acRIPK3
E
B16.F10-OVA Tumor-Infiltrating Lymphocytes
48h post-IT dying NIH-3T3
Log10 cells/ g tumor
CD45⁺
CD19⁺ B Cells
CD3⁺ T Cells
CD8⁺
CD4⁺
Foxp3⁺ T_REG
F
% T Cell
(of CD45.2⁺ PBL)
% CD3e⁺ CD11b⁻ (of CD45.2⁺)
Vehicle (DMSO) +acRIPK3
FTY-720 +acRIPK3
% B Cell
(of CD45.2⁺ PBL)
% CD19⁺ CD11b⁻ (of CD45.2⁺)
G
B16.F10-OVA
NIH-3T3 +α-PD-1 co-administration
Tumor volume (mm³)
Days post-tumor challenge
IgG2a +PBS
IgG2a +acRIPK3
α-PD1 +PBS
α-PD1 +acRIPK3
% B16.F10-OVA Clearance
% mice with tumor clearance
H
% B16.F10-OVA Regrowth
% mice that develop tumors
Naïve
Survivors (α-PD-1 +acRIPK3)

**Figure S4 (Related to Figure 4): Gating strategies and quantification of T cell subsets in tumor and tumor-draining lymph node following dying cell administration.** (**A**) Gating strategy for identification of $T_{REG}$ and $CD8^+$ T cells exhibiting various phenotype markers, from leukocytes isolated from tumor tissue. (**B**) Percentages of $CD44^{hi}$ (left panel) or PD-$1^+$ (center panel) $CD8^+$ T cells isolated from tumor tissue; geometric mean fluorescence intensity (gMFI) of PD-1 expression on OVA-specific (SIINFEKL-$H2K^{b+}$) $CD8^+$ T cells isolated from tumor tissue. (**C**) Gating strategy for identification of $CD8^+$ T cells exhibiting various phenotype markers, from leukocytes isolated from tumor-draining (inguinal) lymph node. (**D**) Absolute numbers of various phenotypes of $CD8^+$ T cells isolated from tumor-draining (inguinal) lymph node. (**E**) Absolute numbers of lymphocyte subsets isolated from B16.F10-OVA tumors 48 hours post-dying NIH-3T3 injection. N=5-10 mice per group. (**F**) Confirmation of circulating $CD19^+$ (B cell) or $CD3e^+$ (pan-T cell) lymphocyte reduction in peripheral blood following FTY-720 administration. Blood leukocytes were collected and analyzed day 8 post-initial tumor challenge. Cells were gated on $CD45^+$ > $CD11b^-$ > either $CD3e^+$ or $CD19^+$ cells. (**G**) B16.F10-OVA tumor growth following co-administration of intratumoral necroptotic NIH-3T3 fibroblasts with the immune checkpoint blockade reagent α-PD-1 or IgG2a isotype (left panel). N=8-14 mice per group. Percent of mice that successfully cleared B16.F10-OVA tumors following co-administration of necroptotic fibroblasts with α-PD-1 (right panel). N=8-14 mice per group. (**H**) Percent of mice in different treatment groups that grew B16.F10-OVA tumors following tumor re-challenge. N=10 mice per group. *<p.0.05, **p<0.01, ***p<0.001, ****p<0.0001. All flow harvests performed 48 hours post-dying cell injection. Error bars represent SEM. Data are pooled from 3-4 independent experiments (**D-F**), or 1 experiment with 4-6 mice per group (**B**).

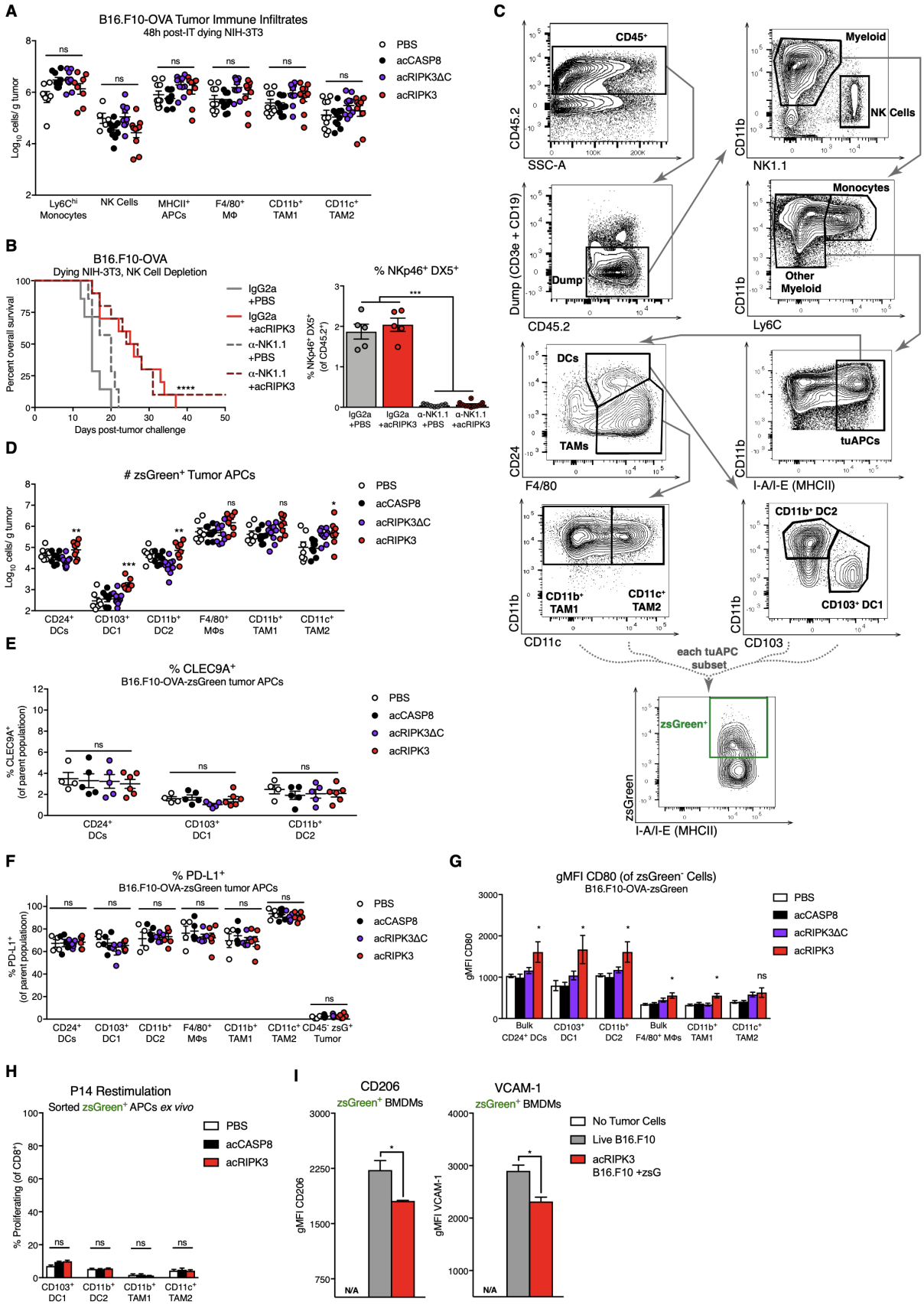
A
B16.F10-OVA Tumor Immune Infiltrates
48h post-IT dying NIH-3T3
Log10 cells/ g tumor
PBS
acCASP8
acRIPK3ΔC
acRIPK3
ns
Ly6Chi Monocytes
NK Cells
MHCII+ APCs
F4/80+ MΦ
CD11b+ TAM1
CD11c+ TAM2
B
B16.F10-OVA
Dying NIH-3T3, NK Cell Depletion
Percent overall survival
Days post-tumor challenge
IgG2a +PBS
IgG2a +acRIPK3
α-NK1.1 +PBS
α-NK1.1 +acRIPK3
****
% NKp46+ DX5+
% NKp46+ DX5+ (of CD45.2+)
***
C
CD45+
CD45.2
SSC-A
Myeloid
NK Cells
CD11b
NK1.1
Dump (CD3e + CD19)
Dump-
Monocytes
Other Myeloid
Ly6C
DCs
TAMs
CD24
F4/80
tuAPCs
I-A/I-E (MHCII)
CD11b+ TAM1
CD11c+ TAM2
CD11c
CD11b+ DC2
CD103+ DC1
CD103
each tuAPC subset
zsGreen+
zsGreen
D
# zsGreen+ Tumor APCs
Log10 cells/ g tumor
CD24+ DCs
CD103+ DC1
CD11b+ DC2
F4/80+ MΦs
CD11b+ TAM1
CD11c+ TAM2
E
% CLEC9A+
B16.F10-OVA-zsGreen tumor APCs
% CLEC9A+ (of parent population)
F
% PD-L1+
B16.F10-OVA-zsGreen tumor APCs
% PD-L1+ (of parent population)
CD45- zsG+ Tumor
G
gMFI CD80 (of zsGreen- Cells)
B16.F10-OVA-zsGreen
gMFI CD80
Bulk CD24+ DCs
Bulk F4/80+ MΦs
H
P14 Restimulation
Sorted zsGreen+ APCs ex vivo
% Proliferating (of CD8+)
I
CD206
zsGreen+ BMDMs
gMFI CD206
N/A
VCAM-1
gMFI VCAM-1
No Tumor Cells
Live B16.F10
acRIPK3 B16.F10 +zsG

**Figure S5 (Related to Figure 5): Gating strategies and effects of dying cell administration on tumor APC subsets.** (**A**) Absolute numbers of tumor-associated myeloid cell subsets following intratumoral dying cell administration, normalized per gram of tumor tissue. N=6-10 mice per group. (**B**) Survival of B16.F10-OVA tumor-bearing mice following co-administration of intratumoral necroptotic NIH-3T3 fibroblasts with depleting antibody against $NK1.1^+$ NK cells (left panel). N=7-10 mice per group. Confirmation of $NK1.1^+$ leukocyte depletion in peripheral blood following depletion antibody administration (right panel). Blood leukocytes were collected and analyzed day 8 post-initial tumor challenge. NK cells were gated on $CD45^+$ > $CD19^-$ $CD3e^-$ > $NKp46^+$ $DX5^+$ cells. (**C**) Gating strategy for identification of myeloid cell populations from leukocytes isolated from tumor tissue. tuAPC = tumor-associated antigen presenting cell; TAM = tumor-associated macrophage; DC = dendritic cell. (**D**) Absolute numbers of $zsGreen^+$ tumor APCs following intratumoral dying cell administration. (**E**) Percentage of $CLEC9A^+$ tumor DC subsets. N=4-6 mice per group. (**F**) Percentage of $PD\text{-}L1^+$ tumor APC populations and $CD45^-$ $zsGreen^+$ tumor cells. N=4-6 mice per group. (**G**) gMFI of the costimulatory marker CD80 on $zsGreen^-$ subsets of tumor APC populations. (**H**) Quantification of previously activated P14 T cell proliferation upon co-culture with $zsGreen^+$ tumor APC subsets sorted *ex vivo* from B16.F10-OVA-zsGreen tumors following dying cell injection. N=3 technical replicates per group, using pooled cells from 5 mice per treatment group. (**I**) *In vitro* assessment of immunosuppressive CD206 (left panel) and VCAM-1 (right panel) expression on bone-marrow derived macrophages (BMDMs) co-cultured with live or necroptotic B16.F10-zsGreen tumor cells and dextran-fluorophore beads. N=3 technical replicates per group. *$p<0.05$, **$p<0.01$, ***$p<0.001$, ****$p<0.0001$. All flow harvests performed 48 hours post-dying cell injection. Error bars represent SEM. Data are pooled from 1-

3 independent experiments (**A,B,D,E,F,H**), or representative plots from 2-3 independent experiments (**C**,**G,I**).

## 2.8 Supplementary Tables

Table S1. Flow antibody information

| Antigen | Clone | Fluorophore | Catalog Number |
|---|---|---|---|
| MHCII | M5/114.15.2 | PerCP-Cy5.5 | BD 562363 |
| CD103 | M290 | APC | BD 562772 |
| CD11b | M1/70 | APC-R700 | BD 564985 |
| Zombie NIR | Live/Dead | APC-Cy7 | BioLegend 423106 |
| CD11c | N418 | BV421 | BD 565451 |
| F4/80 | T45-2342 | BV510 | BD 740159 |
| Ly6C | AL-21 | BV605 | BD 563011 |
| CD24 | M1/69 | BV711 | BD 563450 |
| CD80 | 16-10A1 | BUV737 | BD 564616 |
| CD45.2 | 104 | BUV395 | BD 564616 |
| GranzymeB | NGZB | FITC | BD 118898 |
| CD3e | 145-2C11 | PerCP-Cy5.5 | BD 561108 |
| SIINFEKL-H2K$^{b}$ | OVA Tetramer | PE | FHCRC Tetramer Core |
| CD62L | MEL-14 | APC | BD 553152 |
| CD25 | PC61 | APC-R700 | BD 565134 |
| Zombie NIR | Live/Dead | APC-Cy7 | BioLegend 423106 |
| Foxp3 | MF23 | BV421 | BD 562996 |
| CD8a | 53-6.7 | BV510 | BD 563068 |
| Ki67 | 16A8 | BV605 | BD 652413 |
| CD44 | IM7 | BV650 | BD 103049 |
| CD4 | RM4-5 | BV711 | BD 563726 |
| CD69 | H1.2F3 | BV786 | BD 564683 |
| CD19 | 1D3 | FITC | BD 553785 |
| F4/80 | BM8 | PE-Cy7 | eBioscience 25480182 |
| Ly6C | AL-21 | APC | BD 560595 |
| MHCII | M5/114.15.2 | AF700 | BioLegend 5653180 |
| NK1.1 | PK136 | APC-Cy7 | BD 560518 |
| CD4 | RM4-5 | BV605 | BD 563151 |
| CD11b | M1/70 | BV650 | BioLegend #101239 |
| CD44 | IM7 | PE-Cy7 | BD 560569 |
| Zombie UV | Live/Dead | BUV395 | BioLegend 423108 |
| TCR β chain | H57-597 | APC | BioLegend 109212 |
| PD-1 (CD279) | J43 | BV605 | BD 563059 |
| NKp46 | 29A1.4 | FITC | BioLegend 137605 |
| DX5 (CD49b) | DX5 | APC | BioLegend 108909 |
| CD206 | C068C2 | BV650 | BioLegend141723 |
| PD-L1 (CD274) | 10F.9G2 | PE-Cy7 | BioLegend 124313 |
| VCAM-1 (CD106) | 429 | PE | BioLegend 105713 |
| CLEC9A | 7H11 | PE | BioLegend 143503 |

# Chapter 3

Adeno-associated viruses (AAVs) engineered to target tumor cell necroptosis *in situ* recapitulate tumor control effects of RIPK1/RIPK3 activation

This chapter is adapted from the following publication:

Snyder AG, Hubbard NH, Messmer MN, Kofman SB, Hagan CE, Orozco SL, Chiang K, Daniels BP, Baker D, Oberst A. Intratumoral activation of the necroptotic pathway components RIPK1 and RIPK3 potentiates antitumor immunity. *Sci Immunol*. 2019; **4**: eaaw2004 (In Press).

## 3.1 Introduction

The research presented in Chapter 2 of this dissertation shows that ectopic introduction of necroptotic cells can stimulate anti-tumor immunity. The intratumoral dying cell injections used in these experiments provides a cleanly controlled model for examining how exposure to stimuli derived from necroptotic cells can influence anti-tumor immune responses, allowing us to elucidate some of the immunological mechanisms underlying the observed tumor control responses. However, an obvious caveat of this model is that it fails to assess immune responses to tumor cell necroptosis *in situ*. Given that administration of a bolus of necroptotic cells into tumors is unlikely to be adapted for translational therapy, we turned our attention towards exploring strategies that would specifically induce tumor cell necroptosis *in vivo*.

Recombinant adeno-associated viruses (AAVs) are a commonly used gene therapy vehicle, where administration of viral particles leads to infection and transduction of recipient cells *in situ*, resulting in the expression of a target protein of interest[194]. AAVs are a popular gene therapy vector for translational research, demonstrated by their use in hundreds of clinical trials[194-196]. AAVs exhibit several advantageous qualities that justify their establishment as a leading platform in the gene therapy field. The viral particles lack any synthetic chemical structures or viral genes, minimizing their immunogenicity *in vivo* compared to other gene therapy vehicles[194-196]. In addition to low viral immunogenicity, AAV-derived transgenes fail to integrate into the host genome and instead remain in episomal concatemers in the nucleus of transduced cells[197], further boosting their safety profile. AAVs are also highly potent transducers of target tissues *in vivo*[196]. Ongoing research is focused on additional strategies to maximize the efficiency of transgene delivery to target cells, including optimization of capsid variants[198-199], co-administration of drugs that protect viral particles from intracellular degradation[200-201], or

inclusion of transcriptional or post-transcriptional regulatory elements in the transgene expression cassette[202-204]. Lastly, AAVs can be engineered using a broad array of serotypes that confer specificity across different target tissues, helping to minimize off-target toxicity effects[196,205].

The advantages of AAV-based gene therapy are demonstrated by their success in treating a variety of monogenic disorders in human trials. They have been used for successful therapeutic gene editing in a variety of monogenic disorders in primary human tissues, including restoration of CD40L functionality X-linked hyper-immunoglobulin (Ig)M syndrome[206], introduction of a mutant version of the HIV co-receptor CCR5[207], and expression of wild-type factor IX in hemophilia B patients[208]. Furthermore, AAVs constitute an attractive form of gene therapy that could easily be employed in the treatment of tumors, as they can be produced in bulk and used as an off-the-shelf product with no requirement for autologous cell engineering or transfer.

Considering the benefits of AAVs as gene therapy vectors, we developed a series of AAVs encoding constitutively active forms of various pro-death proteins to target either RIPK1/RIPK3-dependent necroptosis or lytic necrosis via a mutant version of RIPK3 that lacks transcriptional activation downstream of RIPK3 activation (RIPK3ΔC). Using these tractable AAV systems, we show that induction of tumor cell necroptosis *in situ* leads to tumor control that is dependent on $BATF3^+$ cDC1 and $CD8^+$ leukocytes. Furthermore, targeting necroptosis in the tumor microenvironment using this reagent synergizes potently with co-administration of immune checkpoint blockade, conferring durable tumor clearance. These results recapitulate our previous findings using ectopic necroptotic cell administration, strengthening our conclusion that RIPK1/RIPK3 activation in established solid tumors promotes robust anti-tumor immunity.

## 3.2 Results

### Engineered adeno-associated viruses (AAVs) can be used to specifically induce necroptosis of tumor cells *in vitro*

To assess immune responses to tumor cell necroptosis *in situ*, we created reagents that would allow direct induction of necroptosis in tumors *in vivo*. To achieve this, we generated versions of RIPK3 fused to a constitutively-oligomerizing ("co") domain, which consists of a high-affinity 2L6HC3-13 homotrimerizing domain that has been previously synthesized and described[209]. These chimeric forms of RIPK3 undergo oligomerization and activation upon their expression in cells, independent of any upstream signaling or the presence of a ligand. To deliver these reagents to tumor cells, we created AAVs containing genes encoding these constructs under control of a synthetic MND (myeloproliferative sarcoma virus enhancer, negative control region deleted, *d*l587rev primer-binding site substituted) promoter, enabling robust gene expression in target cells (Table S1). Upon transduction of a target cell by these engineered AAVs, the chimeric pro-death protein of interest is expressed, constitutively oligomerizes, and leads to rapid and specific induction of RIPK3-dependent cell death (Figure 1A, Figure S1A).

AAVs are a flexible tool for primary cell transduction, as several serotypes with varying cellular tropisms have been described. We therefore sought to identify an AAV serotype that would selectively deliver construct expression to B16.F10 melanoma cells. Using a hybrid AAV2.5 serotype[210], we observed robust transduction of cultured B16.F10 tumor cells within 24 hours of eGFP-AAV2.5 (eGFP) addition (Figure 1B). Importantly, the AAV2.5 serotype also transduced non-leukocytic $CD45^-$ cells within B16.F10-OVA tumors *in vivo*, exhibiting successful eGFP transduction in a higher percentage of $CD45^-$ cells compared to AAV5, AAV6, AAV8, or AAV9 serotypes (Figure S1B). eGFP-AAV2.5 also had the lowest percentage of off-

target transduction of $CD45^+$ tumor-associated leukocytes *in vivo* (Figure S1B). We therefore concluded that the hybrid AAV2.5 serotype would maximize tumor cell transduction efficiency while limiting off-target transduction of immune cells when adapted for use *in vivo,* potentially limiting off-target toxicity effects.

Next, we characterized the kinetics of death induced by AAV2.5 particles that deliver genes encoding chimeric pro-death proteins *in vitro*. Transduction of B16.F10 tumor cells with necroptosis-targeting AAV2.5 (coRIPK3) or lytic necrosis-targeting AAV2.5 (coRIPK3ΔC) led to 100% cell death within ~15 hours (Figure 1C). Consistent with induction of necroptosis by these reagents, we found that the pan-caspase inhibitor zVAD-fmk did not affect death induction by coRIPK3 or coRIPK3ΔC (Figure S1C, left panel), while addition of the RIPK3 inhibitor GSK-843 eliminated coRIPK3ΔC-induced death while decreasing coRIPK3-induced death; this latter effect was likely due to reverse signaling through the RIPK1/RIPK3 necrosome to induce apoptosis, as previously described (Figure S1C, center panel)[184-185]. Consistent with this, incubation with both zVAD-fmk and GSK-843 eliminated all cell death associated with coRIPK3 treatment (Figure S1C, right panel). This set of experiments shows that either necroptosis or lytic necrosis can be specifically and rapidly induced in B16.F10 tumor cells *in vitro* upon AAV-mediated delivery of coRIPK3 or coRIPK3ΔC, respectively.

As our data using fibroblast injection pointed to activation of NF-κB responses by RIPK3, but not mutant RIPK3ΔC, as a key mediator of anti-tumor immune responses, we next assessed the ability of our AAV constructs to activate inflammatory transcription in dying cells. To do this, we infected B16.F10 tumor cells *in vitro* with AAVs encoding coRIPK3 or coRIPK3ΔC for 10 hours (a time point at which tumor cells have not yet undergone membrane permeabilization, allowing for nucleic acid isolation) and then harvested total RNA for

Nanostring analysis (Table S2). Transduction of tumor cells with coRIPK3 yielded a distinct transcriptional signature compared to cells transduced with coRIPK3ΔC (Figure S1D). Further examination of this signature revealed that necroptotic B16.F10 cells exhibited upregulated expression of numerous NF-κB-dependent gene targets, including *Lta, Ltb, Cd40, Cd86, Mef2a Nod2,* and *Nos2* in comparison to lytic necrotic tumor cells (Figure 1D). Additionally, necroptotic B16.F10 cells also upregulated expression of several inflammatory chemokines and cytokines, including *Cxcl1, Cxcl3, Ccl2, Ccl3, Ccl4, Ccl21a, Ccl22, Il12b, Il22,* and *Ifng* (Figure 1D). Upregulated transcript levels for several of these target genes were independently validated via qRT-PCR (Figure 1E, Table S3). Taken together, these data indicate that the induction of tumor cell death via coRIPK3 transduction *in vitro* leads to an inflammatory transcriptional signature consistent with immunogenic necroptosis[10]. Furthermore, this gene signature depends on the assembly of the RIPK1/RIPK3 necrosome via RHIM-RHIM interactions, as it is absent in tumor cells transduced with coRIPK3ΔC.

**Administration of necroptosis-targeting AAVs in conjunction with α-PD-1 *in vivo* promotes durable tumor clearance**

Following validation of our PCD-targeting AAVs *in vitro*, we applied these tools to study anti-tumor responses *in vivo*. Intratumoral administration of coRIPK3 conferred control of B16.F10-OVA tumor outgrowth (Figure 2A) and extension of animal survival (Figure S2A) in comparison to intratumoral injection of coRIPK3ΔC or control eGFP. Analysis of tumor homogenates revealed increased concentrations of numerous beneficial anti-tumor cytokines and chemokines following coRIPK3 administration, including IFN-γ, CCL3, CCL5, and CXCL10 (Figure 2B), while levels of IL-6, CXCL1, and CXCL2 were unchanged (Figure S2B).

Furthermore, we observed abscopal tumor control effects in a bilateral B16.F10-OVA flank tumor model, as coRIPK3 administration conferred control over tumor outgrowth in both treated (ipsilateral) and untreated (contralateral) tumors (Figure 2C) and significantly extended animal survival (Figure S2C). These results recapitulate the tumor control effects that we observed in a bilateral tumor model using necroptotic fibroblast administration, showing that enforced RIPK3 activation via AAVs can similarly promote tumor control that is associated with increased intratumoral levels of inflammatory chemokines and cytokines.

Next, we tested if necroptosis-targeting AAVs could similarly protect mice from single B16.F10-OVA tumor outgrowth upon co-administration with α-PD-1. Not only did administration of coRIPK3 with isotype controls significantly extend animal survival (Figure 2D) and inhibit tumor growth (Figure S2D) in comparison to eGFP-treated control mice, but the co-administration of coRIPK3 with α-PD-1 led to robust responses, with improved overall survival (Figure 2E) complete tumor clearance in 69.2% of mice (Figure S2E, right panel) and significant control over tumor outgrowth (Figure S2E, left panel). Again, these tumor elimination responses closely paralleled those observed in the intratumoral necroptotic fibroblast injection model.

B16.F10-OVA tumor control following co-administration of coRIPK3 + isotype or α-PD-1 required the presence of $CD8^+$ leukocytes, as depletion of $CD8^+$ cell subsets via antibody injection completely abrogated the protective effects of coRIPK3 + IgG2a or α-PD-1 (Figure 2F, Figure S2F). Additionally, mice lacking $BATF3^+$ cDC1 also failed to control B16.F10-OVA tumors following coRIPK3 + α-PD-1 treatment regimen (Figure 2G, Figure S2G). Considering that tumor control by necroptotic fibroblasts also necessitated the presence of these immune cell compartments, these experiments revealed similar effector cell subset requirements between both

intratumoral dying fibroblast and intratumoral AAV models. With these requirements in mind, we next sought to test if the mice that had successfully cleared their B16.F10-OVA tumors following dual therapy (Figure 2E) had developed protective immune memory. To this end, we re-challenged surviving animals with identical tumor cells on the same flank that initially bore the B16.F10-OVA tumors (Figure 2H, left panel). Strikingly, the majority of these animals were protected from mortality due to tumor outgrowth (Figure 2H, right panel), as only 12.5% of mice regrew tumors (Figure S2H) compared to 100% of naïve controls. Overall, these data demonstrate that intratumoral administration of necroptosis-targeting AAVs in conjunction with α-PD-1 confers durable, immune-mediated tumor rejection similar to that observed upon administration of intratumoral necroptotic NIH-3T3 fibroblasts.

AAV-mediated transduction of tumor cells allows for enforced expression of activated RIPK3, regardless of the expression status of endogenous RIPK3. Considering the beneficial effects of enforced RIPK3 activation that we observed in our murine melanoma model, we asked how endogenous levels of RIPK3 correlated with survival outcomes in human cancer patients. Using tumor biopsy RNAseq data available through The Cancer Genome Atlas (TCGA) database[211], we stratified human skin cutaneous melanoma patients based on upper (High) and lower quartiles (Low) of RIPK3 transcript expression within the tumor tissue. Strikingly, patients with high tumor RIPK3 expression exhibited significantly improved survival outcomes compared to low RIPK3-expressing patients (Figure 2I). Furthermore, multivariate Cox regression modeling revealed a negative coefficient (-0.175), indicating that high expression of RIPK3 is correlated with a better survival outcome (Figure 2I)[212]. Altogether, these results show that higher levels of RIPK3 expression within melanoma tumors are associated with improved survival in a subset of human patients.

### 3.3 Discussion

Distinct PCD modalities can differentially stimulate downstream immune responses. Using recombinant AAV vectors, we show that enforced RIPK3 activation within non-leukocytic cells of the TME promotes tumor control. This control is mediated through $BATF3^+$ cDC1 and $CD8^+$ leukocytes, and synergizes potently with co-administration of immune checkpoint blockade to confer durable tumor clearance. Mechanistically, immunogenic AAV-mediated RIPK3 activation is characterized by an NF-κB-dependent gene signature in B16.F10 melanoma cells *in vitro*, while lytic necrosis following AAV transduction with mutant RIPK3ΔC provides no therapeutic effect. These findings suggest that the immunogenicity of RIPK3 activation in this system is driven by RIPK3-dependent transcriptional targets rather than products released following cell lysis. Collectively, our observations studying the effects of TME-localized necroptosis using AAVs encoding constitutively active form of RIPK3 closely recapitulate our original findings using an intratumoral dying cell injection model.

Existing therapies to target RIPK1/RIPK3 activation *in vivo* exhibit variable efficacy due to off-target effects of global caspase inhibition[116-118] and the differential expression status of endogenous RIPK3 in tumor cells[76-78]. AAV-mediated reconstitution of constitutively active RIPK3 within tumor cells represents a novel strategy to specifically induce this pathway independently of any endogenous signaling requirements. Another group recently reported that intratumoral delivery of mRNA encoding MLKL to promote cell lysis *in situ* conferred protection in murine melanoma and colon carcinoma models[213], and while our findings diverge from theirs with regard to a requirement for NF-κB signaling within dying cells, both studies support the idea that reconstituting expression of necroptotic signaling components can promote anti-tumor immunity. Considering that high levels of RIPK3 expression in human melanoma

tumors correlate with improved patient survival (Figure 2I), it is intriguing to consider how strategies to restore or increase necroptotic signaling in human tumors could serve as a therapeutic target that warrants further exploration.

Cytotoxic therapies such as irradiation can often boost the efficacy of existing T cell-oriented immunotherapies, such as immune checkpoint blockade[111]. However, the development of translationally relevant strategies that maximize the immunogenicity of tumor cell death beyond irradiation or chemotherapy remains an important avenue of future research. AAV-mediated transduction of tumor cells to enforce expression of pro-apoptotic caspases has shown success in rendering previously refractory tumor cells susceptible to apoptotic stimuli[144-145]. Here, we present evidence that enforced activation of pro-necroptotic RIPK3 via AAV administration robustly promotes anti-tumor immune responses. Considering that many patient tumors are refractory to monotherapy with immune checkpoint blockade[214], the tumor immunotherapy field demonstrates a clear need for the development of additional immunostimulatory treatments that stimulate orthogonal immune cell targets relative to T cell-based agents, including cell death. Based on our findings, we propose that AAV-mediated targeting of necroptosis to the TME represents a promising candidate in future translational studies of combinatorial immunotherapy regimens.

## 3.4 Materials and Methods

### *Study design*

Pilot studies were used to estimate mean differences in tumor growth between treatment groups. Using the Sample Size Calculator resource (Boston University), we calculated biological replicate numbers needed to avoid experimental underpowering by using the percent difference in group means from pilot studies, with 0.80 power level and $\alpha$ level = 0.05. Age-matched mice were randomly assigned to treatment groups, and tumor measurements were conducted by a researcher blinded to treatment groups for at least 1 experimental replicate.

### *Cell culture*

B16.F10-OVA and HEK-293T cells were maintained in Dulbecco's modification of Eagle medium (DMEM) supplemented with 10% (vol/vol) FBS, 2mM L-glutamine, 10mM HEPES, and 1mM sodium pyruvate (complete DMEM). All cells were cultured at 37°C with 5% $CO_2$.

### *Mice*

C57BL6/J (B6/J) mice were purchased (Jackson) and allowed to acclimate up to one week prior to experiment initiation. All other genotypes were bred and housed under specific-pathogen-free conditions at the University of Washington. All animals were maintained according to protocols approved by the University of Washington Institutional Animal Care and Use Committee (IACUC).

***Tumor models***

6-10 week old female (B16.F10-OVA) mice were injected subcutaneously on the right flank with 1 x $10^5$ (B16.F10-OVA) tumor cells, mixed in a 1:1 volumetric ratio with the basement membrane matrix Matrigel HC (Corning) for a final injection volume of 100μL. For bilateral tumor experiments, mice were equivalently implanted with tumor cells on the left flank on the same day (d.0) of right flank tumor injection. As previously described[160], tumor volume was calculated using the following formula: Volume = Short axis$^2$ x Long axis x 0.523. Mice were euthanized once tumor burden reached a volume ≥2000mm$^3$. Mice that developed skin ulceration over the tumor site were excluded from experimental analyses. Complete tumor clearance was determined by the absence of a palpable tumor mass at the site of tumor injection.

***In vivo antibody administration***

200μg of α-CD8 (clone 2.43, BioXCell), α-CD4 (clone GK1.5, BioXCell), α-PD-1 (clone RMP1-14, BioXCell), or respective isotype controls were administered to mice via intraperitoneal injection on days 5, 7, 9, and 11 post-initial tumor challenge.

***Recombinant AAV cloning***

Design and sequencing analysis of all plasmids was performed using Geneious software v.7.1[215]. The 2L6HC3-13 trimer homo-oligomer domain was a gift from Dr. David Baker[209]. Trimerizing RIPK3 constructs were directly cloned into a single-stranded AAV (ssAAV) vector using multi-fragment assembly (Infusion HD, Takara Biosciences). AAV backbone was linearized using SnaBI digest as previously described[206]. Primers for amplification of gene fragments were designed to contain 20 base pair 5' and 3' homology to neighboring fusion sequences, and PCR

amplification was carried out using Q5 Polymerase (New England Biosciences). The shortened 3' UTR WPRE and polyA elements were amplified from pAAV-CW3SL-EGFP, a gift from Bong-Kiun Kaang (Addgene #61463). Sense and anti-sense primer sequences were as follows:
Fragment 1 (MND Promoter): (S) CCGCCATGCTACTTATCTACGGAGTCGTGACCTAGGGAACAGAGAAACAGG, (AS) TTCGAGGAAGTCAAAACAGCGTGG;
Fragment 2 (RIPK3 and RIPK3ΔC): (S) CGCTGTTTTGACTTCCTCGAACCATGTCTTCTGTCAAGTTATGG, (full length RIPK3 AS) AGAACCACTCCCTTCTGATCCTTCGGAACCCGTACGCTTGTGGAAGGGCTGCCAGC, (RIPK3ΔC AS) AGAACCACTCCCTTCTGATCCTTCGGAACCCGTACGTCATTGGATTCGGTGGGGTC;
Fragment 3 (2L6HC3-13 homo-trimer domain): (S) GATCAGAAGGGAGTGGTTCTCATATGGGTACGAAATACG, (AS) CAGAGGTTGATTATGCGGCCTTAGTCACTTTTGGCGTTAATTTTC;
Fragment 4 (sWPRE/polyA): (S) GGCCGCATAATCAACCTCTGG, (AS) CCGCCATGCTACTTATCTACAAAAAACCTCCCACATCTCCCCC.
The MND-eGFP self-complementary AAV (scAAV) was a gift from Dr. David Rawlings. The DNA sequence of inserted elements was verified by sequencing, and the integrity of the viral inverted terminal repeat (ITR) within the pAAV backbone confirmed by restriction digest using AhdI, BglI or SmaI, prior to viral production.

***Adeno-associated virus (AAV) production, purification, and quantification***

AAVs were produced as described[207,216]. Briefly, AAV stocks were generated in HEK293T cells via PEI transfection using vector + serotype helper (pLTAAV). Cells were harvested 48h post-transfection, lysed via freeze/thaw cycling, treated with 100U/mL Universal Nuclease (Thermo) at 37°C for 30 minutes, and purified via centrifugation over an iodixanol density step gradient. Titers of viral stocks were determined via qRT-PCR analysis in conjunction with TaqMan reagents and a ViiA 7 Real-Time PCR apparatus (Applied Biosystems). qRT-PCR for viral titer used primers targeting the conserved ITR, using the following sequences: (F) GGAACCCCTAGTGATGGAGTT, (R) CGGCCTCAGTGAGCGA.

***Intratumoral AAV injections***

$1 \times 10^{11}$ infectious units (IFU) of respective AAV were administered intratumorally in 50μL. Virus aliquots used for *in vivo* experiments were thawed once following initial freezing post-purification. AAV injections were administered on days 6, 8, and 10 post-initial tumor challenge.

***Murine cytokine assessment***

To evaluate intratumoral cytokine levels, tumors were harvested 72h post-AAV administration. Tumors were then minced and homogenized using metal beads with vigorous shaking in tubes, then frozen at -80°C. To evaluate cytokine levels *in vitro*, $3 \times 10^5$ B16.F10 cells were infected with $1 \times 10^{11}$ IFU of AAV for 18h, and supernatants were frozen at -80°C. Thawed samples were analyzed using a Th1/Th2 ProcartaPlex™ Panel 1 Luminex kit (Thermo Fisher).

***Nanostring RNA analysis and qRT-PCR***

2 x $10^6$ B16.F10 cells were infected with 1 x $10^{11}$ IFU of respective AAV for 10h. Total RNA was isolated using a Nucleospin RNA Kit (Macherey-Nagel) and run on an nCounter Sprint in conjunction with an nCounter Mouse Inflammation V2 Panel (Nanostring). Data were normalized and analyzed using nSolver software (Nanostring). For target gene validation, oligo(dT) random hexamers and SuperScript III Reverse Transcriptase (Life Technologies) were used to synthesize cDNA from the same total RNA samples used for Nanostring analysis. Fluorogenic quantitative reverse transcriptase PCR (qRT-PCR) analysis was performed using previously published oligonucleotide primer sequences using SYBR Green reagents and a ViiA 7 Real-Time PCR apparatus (Applied Biosystems). Cycle threshold (CT) values for target genes were normalized to CT values of the housekeeping gene *Gapdh* ($\Delta CT = CT_{Target} - CT_{Gapdh}$), and subsequently normalized to baseline control values ($\Delta\Delta CT = \Delta CT_{Experimental} - \Delta CT_{Control}$). Primers used for qRT-PCR are listed in Table S1.

***In vitro cell death assay***

1 x $10^5$ B16.F10-OVA cells were infected with 1 x $10^{11}$ IFU of respective AAV in 24 well plates for 24h. Cell viability was evaluated via incorporation of cell viability dye Sytox Green (Molecular Probes) or Yoyo-3 (200nM, Life Technologies) and quantified using a 2-color Incucyte Zoom bioimaging platform (Essen Biosciences), as described[217]. Where indicated, 50μM zVAD-fmk (SM Biochemicals) or 100nM GSK-873 (GlaxoSmithKline) were added to inhibit pan-caspase activation or RIPK3 activation, respectively.

### *TCGA analysis*

The OncoLnc package[212] was used to analyze RNASeqV2 and overall survival data generated by The Cancer Genome Atlas Research Network database[211]. OncoLnc was used to conduct survival analyses using multivariate Cox regression modeling, assign logrank p values and Cox coefficients to assess significance, and generate Kaplan-Meier survival curves.

### *Statistics*

Unless otherwise noted in figure legend, data represent mean +/- SEM. Survival curves were analyzed via Mantel-Cox log-rank test unless noted otherwise. All other experiments were compared using parametric 2-tailed student's t-test, chi-square test, or 1-way or 2-way ANOVA, with appropriate corrections for repeated measures of tumor growth curves. All statistical analyses were performed using GraphPad Prism software unless noted otherwise.

### 3.5 Acknowledgements

We thank P. Ralli-Jain for technical assistance. We thank D. Baker (U. Washington) and D. Rawlings (Seattle Children's Research Institute) for AAV-related constructs.

**Funding**: This work was supported by NIH grant R01CA228098 and by a Wade F.B. Thompson CLIP award from the Cancer Research Institute, both to AO. AGS was supported by PHS NRSA T32GM007270 and NSF GRFP (DGE-1256082); NWH by T32AI106677-05; MNM by T32CA080416; BPD by F32 AI129254.

**Author contributions**: AGS and AO conceived the study and designed experiments. NWH designed AAV plasmid constructs. DB provided oligomerization domain constructs used in AAV experiments. AGS, NWH, MNM, BPD, SBK, CEH, SLO, and KC performed experiments. AGS and BPD analyzed data. AGS and AO wrote the manuscript.

**Competing interests**: The testing of necroptosis-inducing AAVs was supported in part by funds received from FivePrime Therapeutics as part of a sponsored research agreement; AO has acted as a paid consultant for FivePrime Therapeutics. AGS, NWH, and AO are inventors on a pending patent held by the University of Washington (U.S. patent number 62/622,049) for the constitutively-oligomerizing cell death enzymes described in this manuscript. These materials are available for research use under an MTA from the University of Washington.

## 3.6 Figures

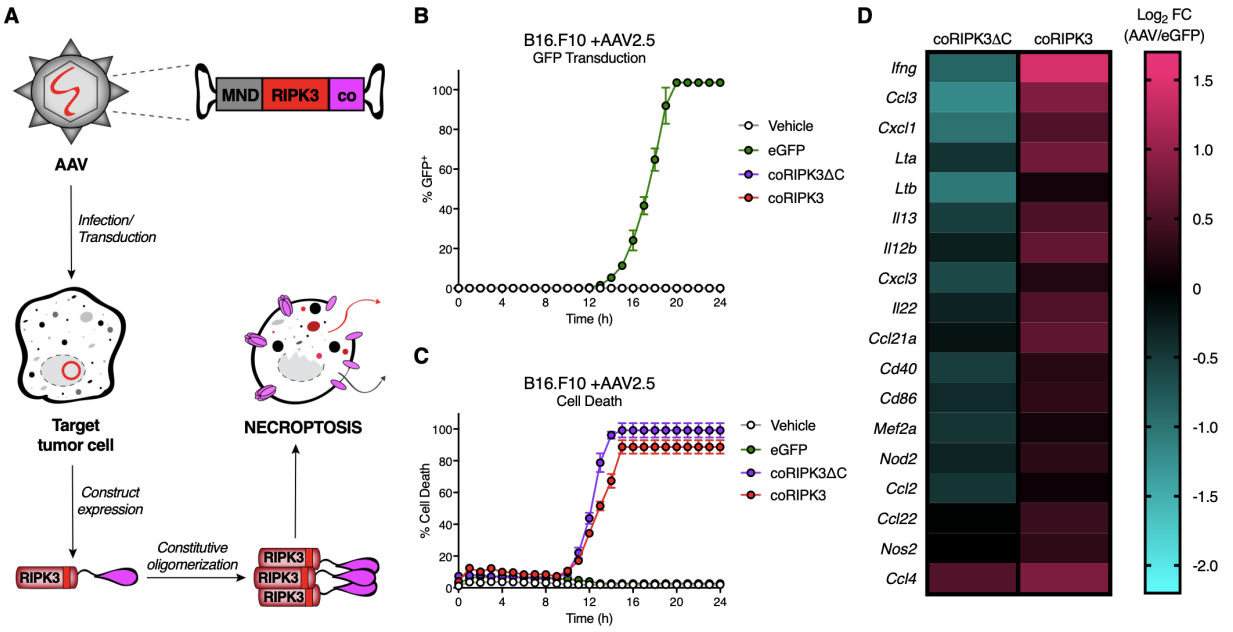


**Figure 1: Engineered adeno-associated viruses (AAVs) can be used to specifically induce necroptosis of tumor cells *in vitro*.** (**A**) Schematic of AAVs used to transduce tumor cells to express engineered pro-death enzymes fused to a constitutively-oligomerizing ("co") recruitment domain under the control of a synthetic MND promoter, leading to subsequent induction of a corresponding PCD modality. (**B,C**) Validation and kinetics of AAV2.5 serotype transduction efficiency in B16.F10 cells *in vitro*. (**B**) Percent of $GFP^+$ cells transduced with AAV2.5-eGFP control, (**C**) Percent cell death in cells transduced with various death-inducing constructs. N=3 technical replicates per group. (**D**) Heat map depicting relative expression values of NF-κB-dependent gene targets, chemokines, and cytokines via Nanostring analysis of B16.F10 tumor cells compared to eGFP-transduced controls 10h following AAV2.5 transduction (1 x $10^{11}$ IFU). Data are representative plots from 2 independent experiments (**B,C**), or mean of 3 technical replicates from 1 experiment (**D**).

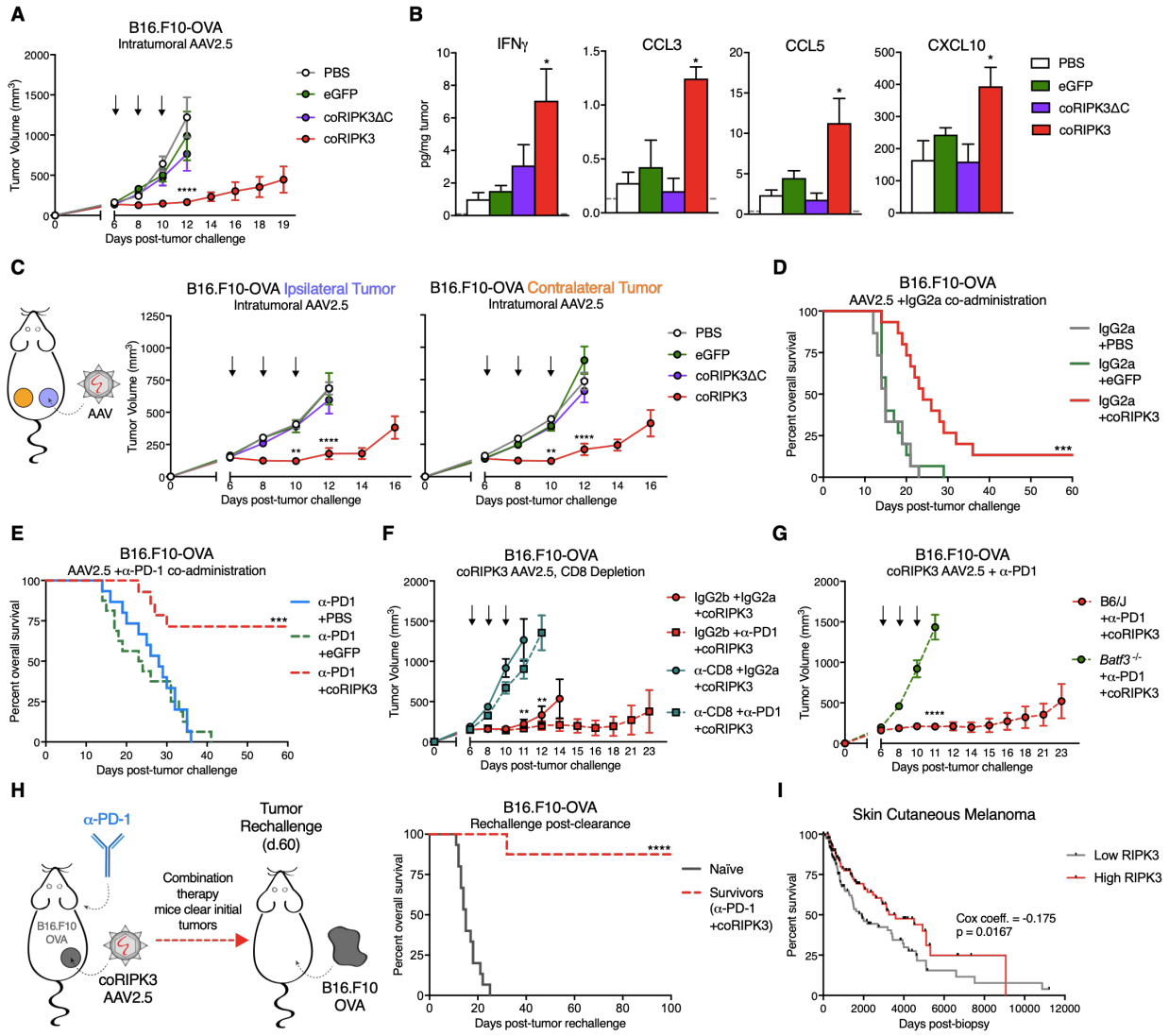


**Figure 2: Administration of necroptosis-targeting AAVs in conjunction with α-PD-1 *in vivo* promotes durable tumor clearance.** (**A**) B16.F10-OVA tumor growth curves following intratumoral administration of 1 x $10^{11}$ IFU death-inducing AAVs or eGFP control AAV. N=8-14 mice per group. (**B**) Intratumoral concentrations of inflammatory cytokines and chemokines 48h post-intratumoral AAV injection. Gray dotted line represents limit of detection. N=3-4 mice per group. (**C**) Tumor growth of ipsilateral ("I", treated) and contralateral ("C", untreated) B16.F10-OVA tumors following AAV administration. N=10-12 mice per group. (**D**) Survival

curves of B16.F10-OVA tumor-bearing mice following co-administration of AAVs with isotype control antibody. N=14-15 mice per group. (**E**) Survival curves of B16.F10-OVA tumor-bearing mice following co-administration of AAVs with α-PD-1. N=13-16 mice per group. (**F**) B16.F10-OVA tumor growth upon co-administration of necroptosis-inducing coRIPK3 AAV with α-$CD8^+$ depletion antibody. N=8-10 mice per group. (**G**) B16.F10-OVA tumor growth in *Batf3* $^{-/-}$ or wild-type control mice following necroptosis-inducing AAV administration. N=10-13 mice per group. (**H**, left panel) Schematic of tumor re-challenge experiments in mice from (**E**) that successfully clear B16.F10-OVA tumors. (**H**, right panel) Survival of mice re-challenged with B16.F10-OVA cells on the same flank as initial tumor location. N=8-10 mice per group. (**I**) Kaplan-Meier plot for overall survival of skin cutaneous melanoma patients in TCGA data set. Data are parsed on upper and lower quartiles (25%ile) of RIPK3 mRNA expression. N=114 patients per group. *p<0.05, **p<0.01, ***p<0.001, ****p<0.0001. Black arrows indicate intratumoral AAV injections. Error bars represent SEM. Data are pooled from 2-4 independent experiments (**A-H**).

## 3.7 Supplemental Figures

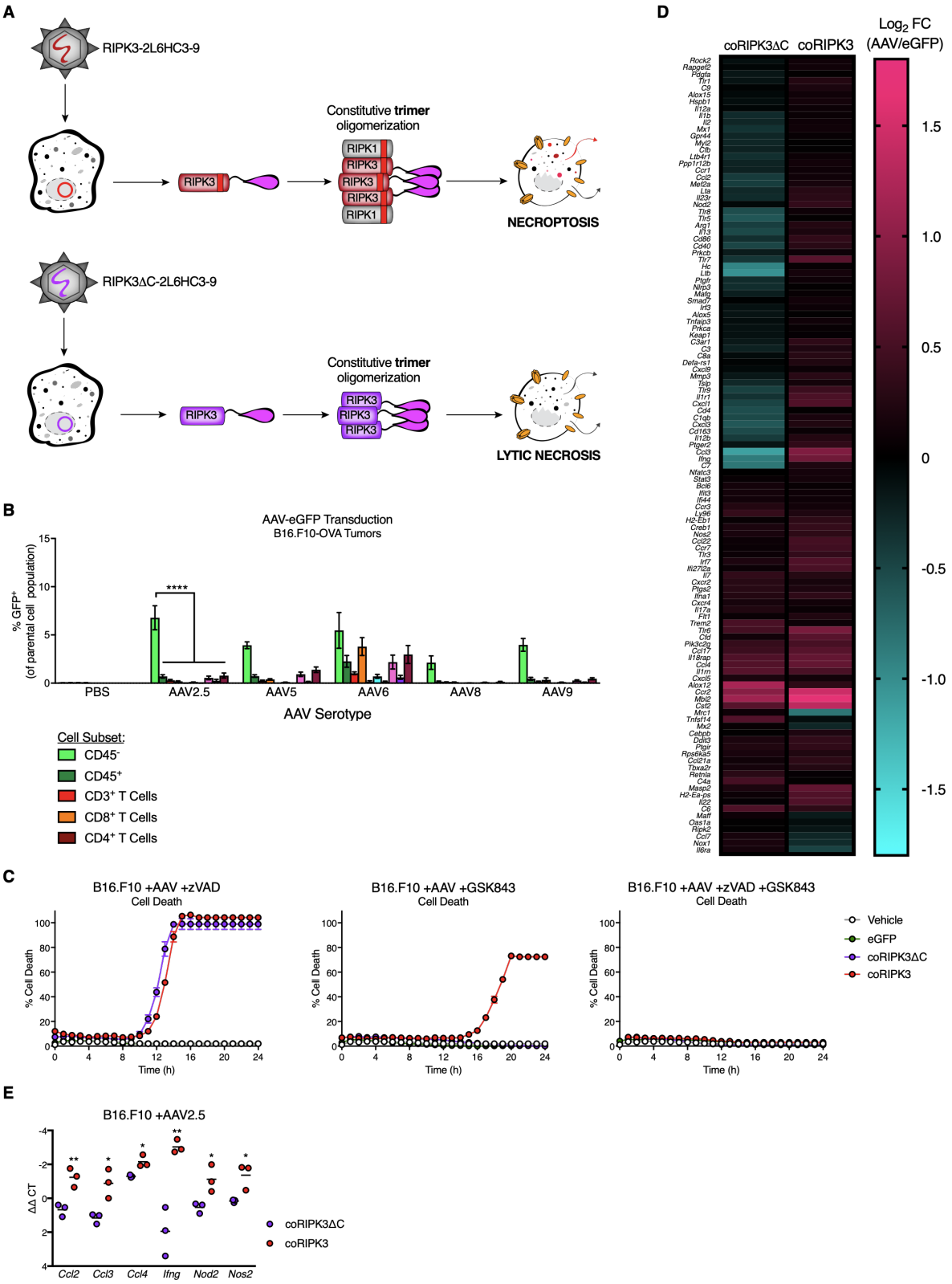

**Figure S1 (Related to Figure 1): Characterization of transduction efficiency and cell death induction by engineered AAVs.** (**A**) Summary of AAVs tested. coRIPK3 and coRIPKΔC denote target protein fusion to a 2L6HC3-9 trimerization ("co") domain that is sufficient for necroptosis or lytic necrosis induction, respectively. (**B**) Percentage of GFP transduction in non-leukocytic ($CD45^-$) and various immune cell populations isolated from B16.F10-OVA tumors 48 hours following intratumoral injection of $1x10^{11}$ IFU of different AAV serotypes encoding eGFP. N=5-10 mice per group. (**C**) Confirmation of PCD modality dependence upon expected signaling components in B16.F10 cells. zVAD = pan-caspase inhibitor zVAD-fmk, which inhibits caspase-dependent apoptosis (left panel). GSK843 = murine RIPK3 inhibitor, which inhibits RIPK3-mediated necroptosis and RIPK3ΔC-mediated lytic necrosis. Cells transduced with coRIPK3 undergo caspase-8 dependent apoptosis in the presence of GSK843 alone (center panel), which is eliminated upon co-administration of GSK843 +zVAD (right panel). N=3 technical replicates per group. (**D**) Heat map depicting relative expression values of genes via Nanostring analysis of B16.F10 tumor cells compared to eGFP-transduced controls 10 hours following AAV2.5 transduction ($1 \times 10^{11}$ IFU). (**E**) qRT-PCR analysis of target gene mRNA expression in B16.F10 tumor cells 10 hours following AAV2.5 transduction ($1 \times 10^{11}$ IFU). Error bars represent SEM. Data are representative plots from 2 independent experiments (**B,C**), mean of 3 technical replicates from 1 experiment (**D**), or biological replicates from 1 experiment (**E**).

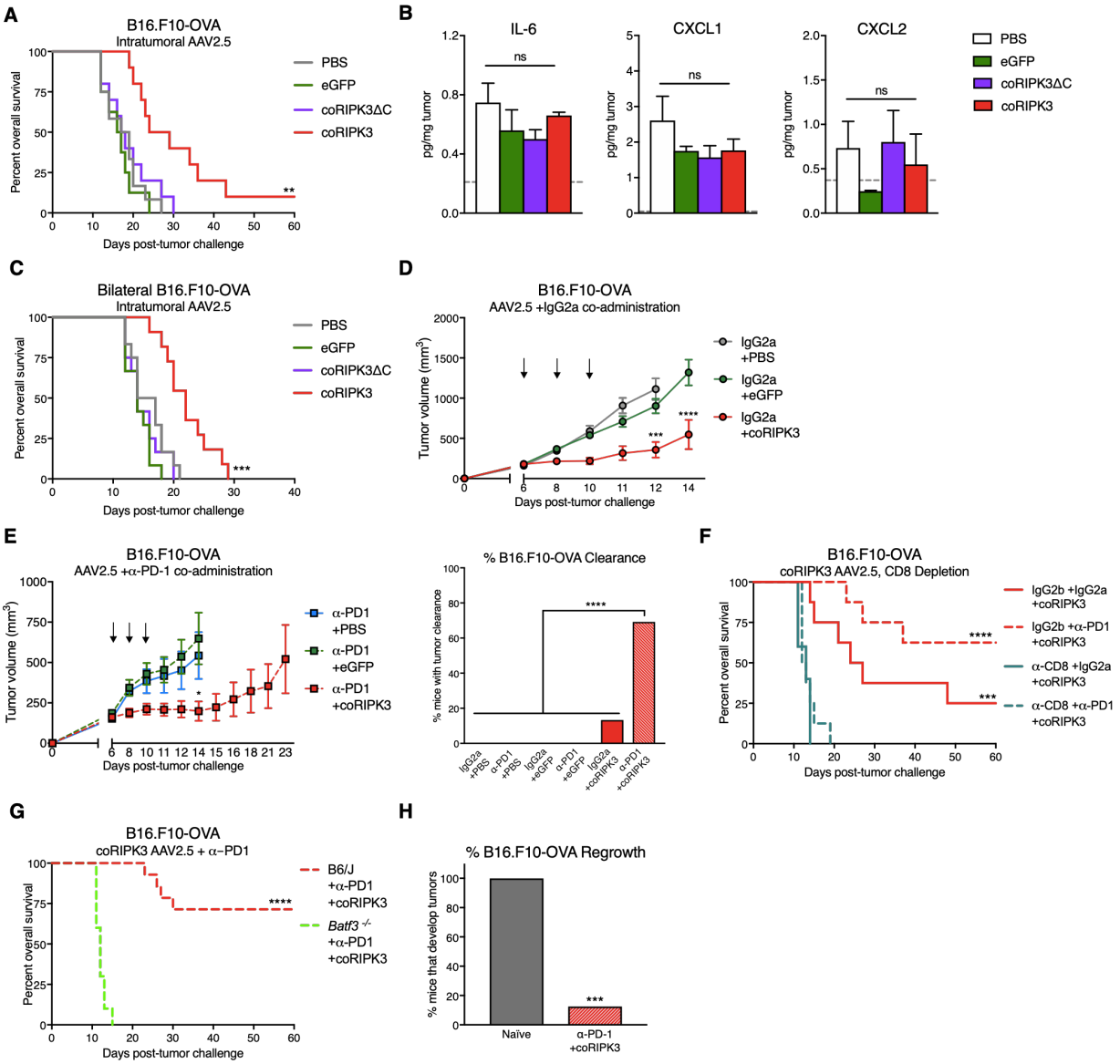


**Figure S2 (Related to Figure 2): Tumor growth restriction and survival extension following administration of AAVs targeting tumor cell necroptosis *in situ*.** (**A**) Survival curves of B16.F10-OVA tumor-bearing mice following intratumoral administration of 1 x $10^{11}$ IFU death-inducing AAVs or control eGFP AAV. N=8-14 mice per group. (**B**) Intratumoral concentrations of potentially tumorigenic cytokines and chemokines 48h post-intratumoral AAV injection. Gray dotted line represents limit of detection. N=3-4 mice per group. (**C**) Survival curves of mice bearing bilateral B16.F10-OVA tumors following administration of various death-inducing

AAV2.5 constructs. N=10-12 mice per group. (**D**) B16.F10-OVA tumor growth curves following co-administration of intratumoral AAVs with IgG2a isotype control antibody. N=14-15 mice per group. (**E**) B16.F10-OVA tumor growth curves following co-administration of intratumoral AAVs with the immune checkpoint blockade reagent α-PD-1 (left panel). Percent of mice that successfully cleared B16.F10-OVA tumors following co-administration of coRIPK3 AAV2.5 with α-PD-1 (right panel). N=13-16 mice per group. (**F**) Survival curves of B16.F10-OVA tumor-bearing mice following co-administration of necroptosis-inducing coRIPK3 AAV2.5 with α-PD-1 in addition to $CD8^+$ leukocyte depletion via antibody injection. Asterisks denote significant differences between corresponding IgG2b and α-CD8 treatment groups. N=8-10 mice per group. (**G**) Survival curves B16.F10-OVA tumor-bearing *Batf3*$^{-/-}$ or B6/J mice following co-administration of coRIPK3 AAV2.5 with α-PD-1. N=10-13 mice per group. (**H**) Percentage of mice from panel (**E**) (or naïve controls) that developed B16.F10-OVA tumors upon flank tumor re-challenge injection. N=8-10 mice per group. *p<0.05, **p<0.01, ***p<0.001, ****p<0.0001. Black arrows indicate intratumoral AAV injections. Error bars represent SEM. Data are pooled from 2-4 independent experiments (**A-H**).

### 3.8 Supplemental Tables

Table S1. AAV cloning sequences

| AAV/ Domain Name | Sequence |
|---|---|
| psAAV-eGFP | AAGCTTCCCGGGGGGATCTGGGCCACTCCCTCTCTGCGCGCTCGCT<br>CGCTCACTGAGGCCGGGCGACCAAAGGTCGCCCGACGCCCGGGCTT<br>TGCCCGGGCGGCCTCAGTGAGCGAGCGAGCGCGCAGAGAGGGAGT<br>GGCCAACTCCATCACTAGGGGTTCCTGGAGGGGTGGAGTCGTGACC<br>TAGGGAACAGAGAAACAGGAGAATATGGGCCAAACAGGATATCTG<br>TGGTAAGCAGTTCCTGCCCCGGCTCAGGGCCAAGAACAGTTGGAAC<br>AGCAGAATATGGGCCAAACAGGATATCTGTGGTAAGCAGTTCCTGC<br>CCCGGCTCAGGGCCAAGAACAGATGGTCCCCAGATGCGGTCCCGCC<br>CTCAGCAGTTTCTAGAGAACCATCAGATGTTTCCAGGGTGCCCCAA<br>GGACCTGAAATGACCCTGTGCCTTATTTGAACTAACCAATCAGTTC<br>GCTTCTCGCTTCTGTTCGCGCGCTTCTGCTCCCCGAGCTCTATATAA<br>GCAGAGCTCGTTTAGTGAACCGTCAGATCGCCTGGAGACGCCATCC<br>ACGCTGTTTTGACTTCCATAGAAGGATCCTCGAGGCCACCATGGTG<br>AGCAAGGGCGAGGAGCTGTTCACCGGGGTGGTGCCCATCCTGGTCG<br>AGCTGGACGGCGACGTAAACGGCCACAAGTTCAGCGTGTCCGGCG<br>AGGGCGAGGGCGATGCCACCTACGGCAAGCTGACCCTGAAGTTCAT<br>CTGCACCACCGGCAAGCTGCCCGTGCCCTGGCCCACCCTCGTGACC<br>ACCCTGACCTACGGCGTGCAGTGCTTCAGCCGCTACCCCGACCACA<br>TGAAGCAGCACGACTTCTTCAAGTCCGCCATGCCCGAAGGCTACGT<br>CCAGGAGCGCACCATCTTCTTCAAGGACGACGGCAACTACAAGACC<br>CGCGCCGAGGTGAAGTTCGAGGGCGACACCCTGGTGAACCGCATC<br>GAGCTGAAGGGCATCGACTTCAAGGAGGACGGCAACATCCTGGGG<br>CACAAGCTGGAGTACAACTACAACAGCCACAACGTCTATATCATGG<br>CCGACAAGCAGAAGAACGGCATCAAGGTGAACTTCAAGATCCGCC<br>ACAACATCGAGGACGGCAGCGTGCAGCTCGCCGACCACTACCAGC<br>AGAACACCCCCATCGGCGACGGCCCCGTGCTGCTGCCCGACAACCA<br>CTACCTGAGCACCCAGTCCGCCCTGAGCAAAGACCCCAACGAGAA<br>GCGCGATCACATGGTCCTGCTGGAGTTCGTGACCGCCGCCGGGATC<br>ACTCTCGGCATGGACGAGCTGTACAAGTAAGCGGCCGCAATTCACC<br>CCACCAGTGCAGGCTGCCTATCAGAAAGTGGTGGCTGGTGTGGCTA<br>ATGCCCTGGCCCACAAGTATCACTAAGCTCGCTTTCTTGCTGTCCAA<br>TTTCTATTAAAGGTTCCTTTGTTCCCTAAGTCCAACTACTAAACTGG<br>GGGATATTATGAAGGGCCTTGAGCATCTGGATTCTGCCTAATAAAA<br>AACATTTATTTTCATTGCAATGATGTATTTAAATTATTTCTGAATAT<br>TTTACTAAAAAGGGAATGTGGGAGGTCAGTGCATTTAAAACATAAA<br>GAAATGAAGAGCTAGTTCAAACCTTGGGAAAATACACTATATCTTA<br>AACTCCATGAAAGAAGGTGAGGCTGCAAACAGCTAATGCACATTG<br>GCAACAGCCCCTGATGCCTATGCCTTATTCATCCCTCAGAAAAGGA<br>TTCAAGTAGAGGCTTGATTTGGAGGTTAAAGTTTTGCTATGCTGTAT<br>TTTACATTACTTATTGTTTTAGCTGTCCTCATGAATGTCTTTTCACTA<br>CCCATTTGCTTATCCTGCATCTCTCAGCCTTGACTCCACTCAGTTCTC<br>TTGCTTAGAGATACCACCTTTCCCCTGAAGTGTTCCTTCCATGTTTT<br>ACGGCGAGATGGTTTCTCCTCGCCTGGCCACTCAGCCTTAGTTGTCT<br>CTGTTGTCTTATAGAGGTCTACTTGAAGAAGGAAAAACAGGGGGCA |

| | |
|---|---|
| | TGGTTTGACTGTCCTGTGAGCCCTTCTTCCCTGCCTCCCCCACTCAC<br>AGTGACACTAGTCCACTCCCTCTCTGCGCGCTCGCTCGCTCACTGAG<br>GCCGGGCGACCAAAGGTCGCCCGACGCCCGGGCTTTGCCCGGGCG<br>GCCTCAGTGAGCGAGCGAGCGCGCAGAGAGGGACAGATCCGGGCC<br>CGCATGCGTCGACAATTCACTGGCCGTCGTTTTACAACGTCGTGACT<br>GGGAAAACCCTGGCGTTACCCAACTTAATCGCCTTGCAGCACATCC<br>CCCTTTCGCCAGCTGGCGTAATAGCGAAGAGGCCCGCACCGATCGC<br>CCTTCCCAACAGTTGCGCAGCCTGAATGGCGAATGGCGCCTGATGC<br>GGTATTTTCTCCTTACGCATCTGTGCGGTATTTCACACCGCATATGG<br>TGCACTCTCAGTACAATCTGCTCTGATGCCGCATAGTTAAGCCAGC<br>CCCGACACCCGCCAACACCCGCTGACGCGCCCTGACGGGCTTGTCT<br>GCTCCCGGCATCCGCTTACAGACAAGCTGTGACCGTCTCCGGGAGC<br>TGCATGTGTCAGAGGTTTTCACCGTCATCACCGAAACGCGCGAGAC<br>GAAAGGGCCTCGTGATACGCCTATTTTTATAGGTTAATGTCATGAT<br>AATAATGGTTTCTTAGACGTCAGGTGGCACTTTTCGGGGAAATGTG<br>CGCGGAACCCCTATTTGTTTATTTTTCTAAATACATTCAAATATGTA<br>TCCGCTCATGAGACAATAACCCTGATAAATGCTTCAATAATATTGA<br>AAAAGGAAGAGTATGAGTATTCAACATTTCCGTGTCGCCCTTATTC<br>CCTTTTTTGCGGCATTTTGCCTTCCTGTTTTTGCTCACCCAGAAACGC<br>TGGTGAAAGTAAAAGATGCTGAAGATCAGTTGGGTGCACGAGTGG<br>GTTACATCGAACTGGATCTCAACAGCGGTAAGATCCTTGAGAGTTT<br>TCGCCCCGAAGAACGTTTTCCAATGATGAGCACTTTTAAAGTTCTGC<br>TATGTGGCGCGGTATTATCCCGTATTGACGCCGGGCAAGAGCAACT<br>CGGTCGCCGCATACACTATTCTCAGAATGACTTGGTTGAGTACTCA<br>CCAGTCACAGAAAAGCATCTTACGGATGGCATGACAGTAAGAGAA<br>TTATGCAGTGCTGCCATAACCATGAGTGATAACACTGCGGCCAACT<br>TACTTCTGACAACGATCGGAGGACCGAAGGAGCTAACCGCTTTTTT<br>GCACAACATGGGGGATCATGTAACTCGCCTTGATCGTTGGGAACCG<br>GAGCTGAATGAAGCCATACCAAACGACGAGCGTGACACCACGATG<br>CCTGTAGCAATGGCAACAACGTTGCGCAAACTATTAACTGGCGAAC<br>TACTTACTCTAGCTTCCCGGCAACAATTAATAGACTGGATGGAGGC<br>GGATAAAGTTGCAGGACCACTTCTGCGCTCGGCCCTTCCGGCTGGC<br>TGGTTTATTGCTGATAAATCTGGAGCCGGTGAGCGTGGGTCTCGCG<br>GTATCATTGCAGCACTGGGGCCAGATGGTAAGCCCTCCCGTATCGT<br>AGTTATCTACACGACGGGGAGTCAGGCAACTATGGATGAACGAAA<br>TAGACAGATCGCTGAGATAGGTGCCTCACTGATTAAGCATTGGTAA<br>CTGTCAGACCAAGTTTACTCATATATACTTTAGATTGATTTAAAACT<br>TCATTTTTAATTTAAAAGGATCTAGGTGAAGATCCTTTTTGATAATC<br>TCATGACCAAAATCCCTTAACGTGAGTTTTCGTTCCACTGAGCGTCA<br>GACCCCGTAGAAAAGATCAAAGGATCTTCTTGAGATCCTTTTTTTCT<br>GCGCGTAATCTGCTGCTTGCAAACAAAAAAACCACCGCTACCAGCG<br>GTGGTTTGTTTGCCGGATCAAGAGCTACCAACTCTTTTTCCGAAGGT<br>AACTGGCTTCAGCAGAGCGCAGATACCAAATACTGTTCTTCTAGTG<br>TAGCCGTAGTTAGGCCACCACTTCAAGAACTCTGTAGCACCGCCTA<br>CATACCTCGCTCTGCTAATCCTGTTACCAGTGGCTGCTGCCAGTGGC<br>GATAAGTCGTGTCTTACCGGGTTGGACTCAAGACGATAGTTACCGG<br>ATAAGGCGCAGCGGTCGGGCTGAACGGGGGGTTCGTGCACACAGC<br>CCAGCTTGGAGCGAACGACCTACACCGAACTGAGATACCTACAGCG<br>TGAGCTATGAGAAAGCGCCACGCTTCCCGAAGGGAGAAAGGCGGA<br>CAGGTATCCGGTAAGCGGCAGGGTCGGAACAGGAGAGCGCACGAG<br>GGAGCTTCCAGGGGGAAACGCCTGGTATCTTTATAGTCCTGTCGGG |

| | |
|---|---|
| | TTTCGCCACCTCTGACTTGAGCGTCGATTTTTGTGATGCTCGTCAGG<br>GGGGCGGAGCCTATGGAAAAACGCCAGCAACGCGGCCTTTTTACG<br>GTTCCTGGCCTTTTGCTGGCCTTTTGCTCACATGTTCTTTCCTGCGTT<br>ATCCCCTGATTCTGTGGATAACCGTATTACCGCCTTTGAGTGAGCTG<br>ATACCGCTCGCCGCAGCCGAACGACCGAGCGCAGCGAGTCAGTGA<br>GCGAGGAAGCGGAAGAGCGCCCAATACGCAAACCGCCTCTCCCCG<br>CGCGTTGGCCGATTCATTAATGCAGCTGGCACGACAGGTTTCCCGA<br>CTGGAAAGCGGGCAGTGAGCGCAACGCAATTAATGTGAGTTAGCTC<br>ACTCATTAGGCACCCCAGGCTTTACACTTTATGCTTCCGGCTCGTAT<br>GTTGTGTGGAATTGTGAGCGGATAACAATTTCACACAGGAAACAGC<br>TATGACCATGATTACGCCAAGCTCTCGAGATCTAGA |
| 2L6HC3-13<br>(“co” domain) | CATATGGGTACGAAATACGAACTGCGCCGTGCTCTGGAAGAACTGG<br>AAAAAGCCCTGCGTGAACTGAAAAAATCGCTGGACGAACTGGAAC<br>GTAGCCTGGAAGAACTGGAGAAAAACCCGTCTGAAGATGCGCTGG<br>TCGAAAACAACCGTCTGAACGTGGAAAACAACAAAATCATCGTGG<br>AAGTTCTGCGCATTATCGCGGAAGTTCTGAAAATTAACGCCAAAAG<br>TGACTAA |
| psAAV RIPK3-<br>2L6HC3-13<br>(“coRIPK3”) | CAGCTGCGCGCTCGCTCGCTCACTGAGGCCGCCCGGGCAAAGCCCG<br>GGCGTCGGGCGACCTTTGGTCGCCCGGCCTCAGTGAGCGAGCGAGC<br>GCGCAGAGAGGGAGTGGCCAACTCCATCACTAGGGGTTCCTTGTAG<br>TTAATGATTAACCCGCCATGCTACTTATCTACGGAGTCGTGACCTAG<br>GGAACAGAGAAACAGGAGAATATGGGCCAAACAGGATATCTGTGG<br>TAAGCAGTTCCTGCCCCGGCTCAGGGCCAAGAACAGTTGGAACAGC<br>AGAATATGGGCCAAACAGGATATCTGTGGTAAGCAGTTCCTGCCCC<br>GGCTCAGGGCCAAGAACAGATGGTCCCCAGATGCGGTCCCGCCCTC<br>AGCAGTTTCTAGAGAACCATCAGATGTTTCCAGGGTGCCCCAAGGA<br>CCTGAAATGACCCTGTGCCTTATTTGAACTAACCAATCAGTTCGCTT<br>CTCGCTTCTGTTCGCGCGCTTCTGCTCCCCGAGCTCTATATAAGCAG<br>AGCTCGTTTAGTGAACCGTCAGATCGCCTGGAGACGCCATCCACGC<br>TGTTTTGACTTCCTCGAACCATGTCTTCTGTCAAGTTATGGCCTACT<br>GGTGCGTCAGCGGTTCCTCTGGTGAGCCGTGAAGAACTGAAGAAGC<br>TGGAGTTTGTGGGTAAAGGAGGGTTCGGAGTCGTGTTCCGGGCACA<br>CCACAGAACATGGAACCATGATGTAGCAGTCAAGATCGTGAACTCG<br>AAGAAGATATCCTGGGAGGTGAAGGCTATGGTTAATCTTCGTAATG<br>AGAACGTTCTGCTCCTGCTGGGGGTCACTGAGGACCTCCAGTGGGA<br>CTTCGTGTCCGGGCAGGCTCTGGTGACAAGATTCATGGAGAATGGC<br>TCCCTCGCAGGGCTGCTGCAACCCGAGTGCCCTCGGCCCTGGCCAC<br>TCCTCTGTCGCCTGCTGCAGGAAGTGGTGCTGGGGATGTGCTACCT<br>ACACAGCTTGAACCCTCCGCTCCTGCACCGGGACCTCAAGCCCTCT<br>AACATTCTGCTGGATCCAGAGCTCCACGCCAAGCTAGCAGATTTTG<br>GCCTGTCCACGTTTCAGGGAGGGTCCCAGTCAGGGTCAGGATCAGG<br>ATCAGGATCCAGGGACTCTGGGGGCACCCTAGCGTACTTGGACCCA<br>GAGCTGTTATTTGATGTCAACCTGAAGGCTTCTAAAGCGAGTGATG<br>TCTACAGCTTTGGGATCCTCGTGTGGGCAGTGCTGGCTGGCAGAGA<br>AGCTGAGTTGGTAGACAAGACTTCACTAATCCGGGAAACAGTGTGT<br>GACAGGCAGAGTCGTCCTCCACTGACAGAGCTGCCTCCAGGTAGCC<br>CTGAGACTCCCGGCTTGGAAAAACTGAAGGAGTTAATGATTCATTG<br>CTGGGGTTCCCAGTCCGAAAACAGGCCATCCTTCCAGGACTGCGAA<br>CCAAAAACCAATGAAGTTTACAATCTGGTAAAGGACAAGGTAGAT<br>GCTGCTGTCTCCGAGGTAAAGCATTATCTGTCTCAGCACAGAAGCA |

| | |
|---|---|
| | GCGGCAGAAACTTGTCTGCCAGAGAGCCAAGCCAAAGAGGCACAG<br>AAATGGATTGCCCGAGGGAAACCATGGTTTCTAAAATGCTGGACCG<br>CCTGCATTTGGAGGAACCCTCCGGACCAGTTCCTGGAAAATGTCCT<br>GAGAGGCAAGCACAGGACACATCAGTTGGGCCTGCCACACCAGCA<br>AGGACATCTTCTGACCCCGTGGCTGGCACTCCTCAGATTCCACATA<br>CTTTACCCTTCAGAGGCACAACACCTGGGCCAGTCTTTACTGAGAC<br>TCCCGGTCCTCACCCCCAAAGGAATCAGGGAGATGGAAGACACGG<br>CACTCCTTGGTATCCCTGGACCCCACCGAATCCAATGACAGGGCCA<br>CCGGCTCTCGTCTTCAACAACTGTTCTGAAGTGCAGATTGGGAACT<br>ACAACTCCTTGGTAGCACCACCAAGAACTACTGCCTCAAGTTCGGC<br>CAAGTATGACCAAGCACAGTTCGGCAGGGGTAGGGGCTGGCAGCC<br>CTTCCACAAGCGTACGGGTTCCGAAGGATCAGAAGGGAGTGGTTCT<br>CATATGGGTACGAAATACGAACTGCGCCGTGCTCTGGAAGAACTGG<br>AAAAAGCCCTGCGTGAACTGAAAAAATCGCTGGACGAACTGGAAC<br>GTAGCCTGGAAGAACTGGAGAAAAACCCGTCTGAAGATGCGCTGG<br>TCGAAAACAACCGTCTGAACGTGGAAAACAACAAAATCATCGTGG<br>AAGTTCTGCGCATTATCGCGGAAGTTCTGAAAATTAACGCCAAAAG<br>TGACTAAGGCCGCATAATCAACCTCTGGATTACAAAATTTGTGAAA<br>GATTGACTGGTATTCTTAACTATGTTGCTCCTTTTACGCTATGTGGA<br>TACGCTGCTTTAATGCCTTTGTATCATGCTATTGCTTCCCGTATGGC<br>TTTCATTTTCTCCTCCTTGTATAAATCCTGGTTAGTTCTTGCCACGGC<br>GGAACTCATCGCCGCCTGCCTTGCCCGCTGCTGGACAGGGGCTCGG<br>CTGTTGGGCACTGACAATTCCGTGGTGTTTATTTGTGAAATTTGTGA<br>TGCTATTGCTTTATTTGTAACCATCTAGCTTTATTTGTGAAATTTGTG<br>ATGCTATTGCTTTATTTGTAACCATTATAAGCTGCAATAAACAAGTT<br>AACAACAACAATTGCATTCATTTTATGTTTCAGGTTCAGGGGGAGA<br>TGTGGGAGGTTTTTTGTAGATAAGTAGCATGGCGGGTTAATCATTA<br>ACTACAAGGAACCCCTAGTGATGGAGTTGGCCACTCCCTCTCTGCG<br>CGCTCGCTCGCTCACTGAGGCCGGGCGACCAAAGGTCGCCCGACGC<br>CCGGGCTTTGCCCGGGCGGCCTCAGTGAGCGAGCGAGCGCGCCAGC<br>TGGCGTAATAGCGAAGAGGCCCGCACCGATCGCCCTTCCCAACAGT<br>TGCGCAGCCTGAATGGCGAATGGCGATTCCGTTGCAATGGCTGGCG<br>GTAATATTGTTCTGGATATTACCAGCAAGGCCGATAGTTTGAGTTCT<br>TCTACTCAGGCAAGTGATGTTATTACTAATCAAAGAAGTATTGCGA<br>CAACGGTTAATTTGCGTGATGGACAGACTCTTTTACTCGGTGGCCTC<br>ACTGATTATAAAAACACTTCTCAGGATTCTGGCGTACCGTTCCTGTC<br>TAAAATCCCTTTAATCGGCCTCCTGTTTAGCTCCCGCTCTGATTCTA<br>ACGAGGAAAGCACGTTATACGTGCTCGTCAAAGCAACCATAGTACG<br>CGCCCTGTAGCGGCGCATTAAGCGCGGCGGGTGTGGTGGTTACGCG<br>CAGCGTGACCGCTACACTTGCCAGCGCCCTAGCGCCCGCTCCTTTC<br>GCTTTCTTCCCTTCCTTTCTCGCCACGTTCGCCGGCTTTCCCCGTCAA<br>GCTCTAAATCGGGGGCTCCCTTTAGGGTTCCGATTTAGTGCTTTACG<br>GCACCTCGACCCCAAAAAACTTGATTAGGGTGATGGTTCACGTAGT<br>GGGCCATCGCCCTGATAGACGGTTTTTCGCCCTTTGACGTTGGAGTC<br>CACGTTCTTTAATAGTGGACTCTTGTTCCAAACTGGAACAACACTCA<br>ACCCTATCTCGGTCTATTCTTTTGATTTATAAGGGATTTTGCCGATTT<br>CGGCCTATTGGTTAAAAAATGAGCTGATTTAACAAAAATTTAACGC<br>GAATTTTAACAAAATATTAACGTTTACAATTTAAATATTTGCTTATA<br>CAATCTTCCTGTTTTTGGGGCTTTTCTGATTATCAACCGGGGTACAT<br>ATGATTGACATGCTAGTTTTACGATTACCGTTCATCGATTCTCTTGT<br>TTGCTCCAGACTCTCAGGCAATGACCTGATAGCCTTTGTAGAGACC |

| | |
|---|---|
| | TCTCAAAAATAGCTACCCTCTCCGGCATGAATTTATCAGCTAGAAC<br>GGTTGAATATCATATTGATGGTGATTTGACTGTCTCCGGCCTTTCTC<br>ACCCGTTTGAATCTTTACCTACACATTACTCAGGCATTGCATTTAAA<br>ATATATGAGGGTTCTAAAAATTTTTATCCTTGCGTTGAAATAAAGG<br>CTTCTCCCGCAAAAGTATTACAGGGTCATAATGTTTTTGGTACAACC<br>GATTTAGCTTTATGCTCTGAGGCTTTATTGCTTAATTTTGCTAATTCT<br>TTGCCTTGCCTGTATGATTTATTGGATGTTGGAATCGCCTGATGCGG<br>TATTTTCTCCTTACGCATCTGTGCGGTATTTCACACCGCATATGGTG<br>CACTCTCAGTACAATCTGCTCTGATGCCGCATAGTTAAGCCAGCCC<br>CGACACCCGCCAACACCCGCTGACGCGCCCTGACGGGCTTGTCTGC<br>TCCCGGCATCCGCTTACAGACAAGCTGTGACCGTCTCCGGGAGCTG<br>CATGTGTCAGAGGTTTTCACCGTCATCACCGAAACGCGCGAGACGA<br>AAGGGCCTCGTGATACGCCTATTTTTATAGGTTAATGTCATGATAAT<br>AATGGTTTCTTAGACGTCAGGTGGCACTTTTCGGGGAAATGTGCGC<br>GGAACCCCTATTTGTTTATTTTTCTAAATACATTCAAATATGTATCC<br>GCTCATGAGACAATAACCCTGATAAATGCTTCAATAATATTGAAAA<br>AGGAAGAGTATGAGTATTCAACATTTCCGTGTCGCCCTTATTCCCTT<br>TTTTGCGGCATTTTGCCTTCCTGTTTTTGCTCACCCAGAAACGCTGG<br>TGAAAGTAAAAGATGCTGAAGATCAGTTGGGTGCACGAGTGGGTT<br>ACATCGAACTGGATCTCAACAGCGGTAAGATCCTTGAGAGTTTTCG<br>CCCCGAAGAACGTTTTCCAATGATGAGCACTTTTAAAGTTCTGCTAT<br>GTGGCGCGGTATTATCCCGTATTGACGCCGGGCAAGAGCAACTCGG<br>TCGCCGCATACACTATTCTCAGAATGACTTGGTTGAGTACTCACCA<br>GTCACAGAAAAGCATCTTACGGATGGCATGACAGTAAGAGAATTAT<br>GCAGTGCTGCCATAACCATGAGTGATAACACTGCGGCCAACTTACT<br>TCTGACAACGATCGGAGGACCGAAGGAGCTAACCGCTTTTTTGCAC<br>AACATGGGGGATCATGTAACTCGCCTTGATCGTTGGGAACCGGAGC<br>TGAATGAAGCCATACCAAACGACGAGCGTGACACCACGATGCCTGT<br>AGCAATGGCAACAACGTTGCGCAAACTATTAACTGGCGAACTACTT<br>ACTCTAGCTTCCCGGCAACAATTAATAGACTGGATGGAGGCGGATA<br>AAGTTGCAGGACCACTTCTGCGCTCGGCCCTTCCGGCTGGCTGGTTT<br>ATTGCTGATAAATCTGGAGCCGGTGAGCGTGGGTCTCGCGGTATCA<br>TTGCAGCACTGGGGCCAGATGGTAAGCCCTCCCGTATCGTAGTTAT<br>CTACACGACGGGGAGTCAGGCAACTATGGATGAACGAAATAGACA<br>GATCGCTGAGATAGGTGCCTCACTGATTAAGCATTGGTAACTGTCA<br>GACCAAGTTTACTCATATATACTTTAGATTGATTTAAAACTTCATTT<br>TTAATTTAAAAGGATCTAGGTGAAGATCCTTTTTGATAATCTCATGA<br>CCAAAATCCCTTAACGTGAGTTTTCGTTCCACTGAGCGTCAGACCCC<br>GTAGAAAAGATCAAAGGATCTTCTTGAGATCCTTTTTTTCTGCGCGT<br>AATCTGCTGCTTGCAAACAAAAAAACCACCGCTACCAGCGGTGGTT<br>TGTTTGCCGGATCAAGAGCTACCAACTCTTTTTCCGAAGGTAACTG<br>GCTTCAGCAGAGCGCAGATACCAAATACTGTCCTTCTAGTGTAGCC<br>GTAGTTAGGCCACCACTTCAAGAACTCTGTAGCACCGCCTACATAC<br>CTCGCTCTGCTAATCCTGTTACCAGTGGCTGCTGCCAGTGGCGATAA<br>GTCGTGTCTTACCGGGTTGGACTCAAGACGATAGTTACCGGATAAG<br>GCGCAGCGGTCGGGCTGAACGGGGGGTTCGTGCACACAGCCCAGC<br>TTGGAGCGAACGACCTACACCGAACTGAGATACCTACAGCGTGAGC<br>TATGAGAAAGCGCCACGCTTCCCGAAGGGAGAAAGGCGGACAGGT<br>ATCCGGTAAGCGGCAGGGTCGGAACAGGAGAGCGCACGAGGGAGC<br>TTCCAGGGGGAAACGCCTGGTATCTTTATAGTCCTGTCGGGTTTCGC<br>CACCTCTGACTTGAGCGTCGATTTTTGTGATGCTCGTCAGGGGGGC |

| | |
|---|---|
| | GGAGCCTATGGAAAAACGCCAGCAACGCGGCCTTTTTACGGTTCCT<br>GGCCTTTTGCTGGCCTTTTGCTCACATGTTCTTTCCTGCGTTATCCCC<br>TGATTCTGTGGATAACCGTATTACCGCCTTTGAGTGAGCTGATACCG<br>CTCGCCGCAGCCGAACGACCGAGCGCAGCGAGTCAGTGAGCGAGG<br>AAGCGGAAGAGCGCCCAATACGCAAACCGCCTCTCCCCGCGCGTTG<br>GCCGATTCATTAATG |
| psAAV<br>RIPK3ΔRHIM-<br>2L6HC3-13<br>("coRIPK3ΔC") | CAGCTGCGCGCTCGCTCGCTCACTGAGGCCGCCCGGGCAAAGCCCG<br>GGCGTCGGGCGACCTTTGGTCGCCCGGCCTCAGTGAGCGAGCGAGC<br>GCGCAGAGAGGGAGTGGCCAACTCCATCACTAGGGGTTCCTTGTAG<br>TTAATGATTAACCCGCCATGCTACTTATCTACGGAGTCGTGACCTAG<br>GGAACAGAGAAACAGGAGAATATGGGCCAAACAGGATATCTGTGG<br>TAAGCAGTTCCTGCCCCGGCTCAGGGCCAAGAACAGTTGGAACAGC<br>AGAATATGGGCCAAACAGGATATCTGTGGTAAGCAGTTCCTGCCCC<br>GGCTCAGGGCCAAGAACAGATGGTCCCCAGATGCGGTCCCGCCCTC<br>AGCAGTTTCTAGAGAACCATCAGATGTTTCCAGGGTGCCCCAAGGA<br>CCTGAAATGACCCTGTGCCTTATTTGAACTAACCAATCAGTTCGCTT<br>CTCGCTTCTGTTCGCGCGCTTCTGCTCCCCGAGCTCTATATAAGCAG<br>AGCTCGTTTAGTGAACCGTCAGATCGCCTGGAGACGCCATCCACGC<br>TGTTTTGACTTCCTCGAACCATGTCTTCTGTCAAGTTATGGCCTACT<br>GGTGCGTCAGCGGTTCCTCTGGTGAGCCGTGAAGAACTGAAGAAGC<br>TGGAGTTTGTGGGTAAAGGAGGGTTCGGAGTCGTGTTCCGGGCACA<br>CCACAGAACATGGAACCATGATGTAGCAGTCAAGATCGTGAACTCG<br>AAGAAGATATCCTGGGAGGTGAAGGCTATGGTTAATCTTCGTAATG<br>AGAACGTTCTGCTCCTGCTGGGGGTCACTGAGGACCTCCAGTGGGA<br>CTTCGTGTCCGGGCAGGCTCTGGTGACAAGATTCATGGAGAATGGC<br>TCCCTCGCAGGGCTGCTGCAACCCGAGTGCCCTCGGCCCTGGCCAC<br>TCCTCTGTCGCCTGCTGCAGGAAGTGGTGCTGGGGATGTGCTACCT<br>ACACAGCTTGAACCCTCCGCTCCTGCACCGGGACCTCAAGCCCTCT<br>AACATTCTGCTGGATCCAGAGCTCCACGCCAAGCTAGCAGATTTTG<br>GCCTGTCCACGTTTCAGGGAGGGTCCCAGTCAGGGTCAGGATCAGG<br>ATCAGGATCCAGGGACTCTGGGGGCACCCTAGCGTACTTGGACCCA<br>GAGCTGTTATTTGATGTCAACCTGAAGGCTTCTAAAGCGAGTGATG<br>TCTACAGCTTTGGGATCCTCGTGTGGGCAGTGCTGGCTGGCAGAGA<br>AGCTGAGTTGGTAGACAAGACTTCACTAATCCGGGAAACAGTGTGT<br>GACAGGCAGAGTCGTCCTCCACTGACAGAGCTGCCTCCAGGTAGCC<br>CTGAGACTCCCGGCTTGGAAAAACTGAAGGAGTTAATGATTCATTG<br>CTGGGGTTCCCAGTCCGAAAACAGGCCATCCTTCCAGGACTGCGAA<br>CCAAAAACCAATGAAGTTTACAATCTGGTAAAGGACAAGGTAGAT<br>GCTGCTGTCTCCGAGGTAAAGCATTATCTGTCTCAGCACAGAAGCA<br>GCGGCAGAAACTTGTCTGCCAGAGAGCCAAGCCAAAGAGGCACAG<br>AAATGGATTGCCCGAGGGAAACCATGGTTTCTAAAATGCTGGACCG<br>CCTGCATTTGGAGGAACCCTCCGGACCAGTTCCTGGAAAATGTCCT<br>GAGAGGCAAGCACAGGACACATCAGTTGGGCCTGCCACACCAGCA<br>AGGACATCTTCTGACCCCGTGGCTGGCACTCCTCAGATTCCACATA<br>CTTTACCCTTCAGAGGCACAACACCTGGGCCAGTCTTTACTGAGAC<br>TCCCGGTCCTCACCCCCAAAGGAATCAGGGAGATGGAAGACACGG<br>CACTCCTTGGTATCCCTGGACCCCACCGAATCCAATGACGTACGGG<br>TTCCGAAGGATCAGAAGGGAGTGGTTCTCATATGGGTACGAAATAC<br>GAACTGCGCCGTGCTCTGGAAGAACTGGAAAAAGCCCTGCGTGAA<br>CTGAAAAAATCGCTGGACGAACTGGAACGTAGCCTGGAAGAACTG<br>GAGAAAAACCCGTCTGAAGATGCGCTGGTCGAAAACAACCGTCTG |

| | |
|---|---|
| | AACGTGGAAAACAACAAAATCATCGTGGAAGTTCTGCGCATTATCG<br>CGGAAGTTCTGAAAATTAACGCCAAAAGTGACTAAGGCCGCATAAT<br>CAACCTCTGGATTACAAAATTTGTGAAAGATTGACTGGTATTCTTA<br>ACTATGTTGCTCCTTTTACGCTATGTGGATACGCTGCTTTAATGCCT<br>TTGTATCATGCTATTGCTTCCCGTATGGCTTTCATTTTCTCCTCCTTG<br>TATAAATCCTGGTTAGTTCTTGCCACGGCGGAACTCATCGCCGCCTG<br>CCTTGCCCGCTGCTGGACAGGGGCTCGGCTGTTGGGCACTGACAAT<br>TCCGTGGTGTTTATTTGTGAAATTTGTGATGCTATTGCTTTATTTGTA<br>ACCATCTAGCTTTATTTGTGAAATTTGTGATGCTATTGCTTTATTTGT<br>AACCATTATAAGCTGCAATAAACAAGTTAACAACAACAATTGCATT<br>CATTTTATGTTTCAGGTTCAGGGGGAGATGTGGGAGGTTTTTTGTAG<br>ATAAGTAGCATGGCGGGTTAATCATTAACTACAAGGAACCCCTAGT<br>GATGGAGTTGGCCACTCCCTCTCTGCGCGCTCGCTCGCTCACTGAG<br>GCCGGGCGACCAAAGGTCGCCCGACGCCCGGGCTTTGCCCGGGCG<br>GCCTCAGTGAGCGAGCGAGCGCGCCAGCTGGCGTAATAGCGAAGA<br>GGCCCGCACCGATCGCCCTTCCCAACAGTTGCGCAGCCTGAATGGC<br>GAATGGCGATTCCGTTGCAATGGCTGGCGGTAATATTGTTCTGGAT<br>ATTACCAGCAAGGCCGATAGTTTGAGTTCTTCTACTCAGGCAAGTG<br>ATGTTATTACTAATCAAAGAAGTATTGCGACAACGGTTAATTTGCG<br>TGATGGACAGACTCTTTTACTCGGTGGCCTCACTGATTATAAAAAC<br>ACTTCTCAGGATTCTGGCGTACCGTTCCTGTCTAAAATCCCTTTAAT<br>CGGCCTCCTGTTTAGCTCCCGCTCTGATTCTAACGAGGAAAGCACG<br>TTATACGTGCTCGTCAAAGCAACCATAGTACGCGCCCTGTAGCGGC<br>GCATTAAGCGCGGCGGGTGTGGTGGTTACGCGCAGCGTGACCGCTA<br>CACTTGCCAGCGCCCTAGCGCCCGCTCCTTTCGCTTTCTTCCCTTCCT<br>TTCTCGCCACGTTCGCCGGCTTTCCCCGTCAAGCTCTAAATCGGGGG<br>CTCCCTTTAGGGTTCCGATTTAGTGCTTTACGGCACCTCGACCCCAA<br>AAAACTTGATTAGGGTGATGGTTCACGTAGTGGGCCATCGCCCTGA<br>TAGACGGTTTTTCGCCCTTTGACGTTGGAGTCCACGTTCTTTAATAG<br>TGGACTCTTGTTCCAAACTGGAACAACACTCAACCCTATCTCGGTCT<br>ATTCTTTTGATTTATAAGGGATTTTGCCGATTTCGGCCTATTGGTTA<br>AAAAATGAGCTGATTTAACAAAAATTTAACGCGAATTTTAACAAAA<br>TATTAACGTTTACAATTTAAATATTTGCTTATACAATCTTCCTGTTTT<br>TGGGGCTTTTCTGATTATCAACCGGGGTACATATGATTGACATGCTA<br>GTTTTACGATTACCGTTCATCGATTCTCTTGTTTGCTCCAGACTCTCA<br>GGCAATGACCTGATAGCCTTTGTAGAGACCTCTCAAAAATAGCTAC<br>CCTCTCCGGCATGAATTTATCAGCTAGAACGGTTGAATATCATATTG<br>ATGGTGATTTGACTGTCTCCGGCCTTTCTCACCCGTTTGAATCTTTA<br>CCTACACATTACTCAGGCATTGCATTTAAAATATATGAGGGTTCTA<br>AAAATTTTTATCCTTGCGTTGAAATAAAGGCTTCTCCCGCAAAAGT<br>ATTACAGGGTCATAATGTTTTTGGTACAACCGATTTAGCTTTATGCT<br>CTGAGGCTTTATTGCTTAATTTTGCTAATTCTTTGCCTTGCCTGTATG<br>ATTTATTGGATGTTGGAATCGCCTGATGCGGTATTTTCTCCTTACGC<br>ATCTGTGCGGTATTTCACACCGCATATGGTGCACTCTCAGTACAATC<br>TGCTCTGATGCCGCATAGTTAAGCCAGCCCCGACACCCGCCAACAC<br>CCGCTGACGCGCCCTGACGGGCTTGTCTGCTCCCGGCATCCGCTTAC<br>AGACAAGCTGTGACCGTCTCCGGGAGCTGCATGTGTCAGAGGTTTT<br>CACCGTCATCACCGAAACGCGCGAGACGAAAGGGCCTCGTGATAC<br>GCCTATTTTTATAGGTTAATGTCATGATAATAATGGTTTCTTAGACG<br>TCAGGTGGCACTTTTCGGGGAAATGTGCGCGGAACCCCTATTTGTTT<br>ATTTTTCTAAATACATTCAAATATGTATCCGCTCATGAGACAATAAC |

| | |
|---|---|
| | CCTGATAAATGCTTCAATAATATTGAAAAAGGAAGAGTATGAGTAT<br>TCAACATTTCCGTGTCGCCCTTATTCCCTTTTTTGCGGCATTTTGCCT<br>TCCTGTTTTTGCTCACCCAGAAACGCTGGTGAAAGTAAAAGATGCT<br>GAAGATCAGTTGGGTGCACGAGTGGGTTACATCGAACTGGATCTCA<br>ACAGCGGTAAGATCCTTGAGAGTTTTCGCCCCGAAGAACGTTTTCC<br>AATGATGAGCACTTTTAAAGTTCTGCTATGTGGCGCGGTATTATCCC<br>GTATTGACGCCGGGCAAGAGCAACTCGGTCGCCGCATACACTATTC<br>TCAGAATGACTTGGTTGAGTACTCACCAGTCACAGAAAAGCATCTT<br>ACGGATGGCATGACAGTAAGAGAATTATGCAGTGCTGCCATAACCA<br>TGAGTGATAACACTGCGGCCAACTTACTTCTGACAACGATCGGAGG<br>ACCGAAGGAGCTAACCGCTTTTTTGCACAACATGGGGGATCATGTA<br>ACTCGCCTTGATCGTTGGGAACCGGAGCTGAATGAAGCCATACCAA<br>ACGACGAGCGTGACACCACGATGCCTGTAGCAATGGCAACAACGTT<br>GCGCAAACTATTAACTGGCGAACTACTTACTCTAGCTTCCCGGCAA<br>CAATTAATAGACTGGATGGAGGCGGATAAAGTTGCAGGACCACTTC<br>TGCGCTCGGCCCTTCCGGCTGGCTGGTTTATTGCTGATAAATCTGGA<br>GCCGGTGAGCGTGGGTCTCGCGGTATCATTGCAGCACTGGGGCCAG<br>ATGGTAAGCCCTCCCGTATCGTAGTTATCTACACGACGGGGAGTCA<br>GGCAACTATGGATGAACGAAATAGACAGATCGCTGAGATAGGTGC<br>CTCACTGATTAAGCATTGGTAACTGTCAGACCAAGTTTACTCATATA<br>TACTTTAGATTGATTTAAAACTTCATTTTTAATTTAAAAGGATCTAG<br>GTGAAGATCCTTTTTGATAATCTCATGACCAAAATCCCTTAACGTGA<br>GTTTTCGTTCCACTGAGCGTCAGACCCCGTAGAAAAGATCAAAGGA<br>TCTTCTTGAGATCCTTTTTTTCTGCGCGTAATCTGCTGCTTGCAAAC<br>AAAAAAACCACCGCTACCAGCGGTGGTTTGTTTGCCGGATCAAGAG<br>CTACCAACTCTTTTTCCGAAGGTAACTGGCTTCAGCAGAGCGCAGA<br>TACCAAATACTGTCCTTCTAGTGTAGCCGTAGTTAGGCCACCACTTC<br>AAGAACTCTGTAGCACCGCCTACATACCTCGCTCTGCTAATCCTGTT<br>ACCAGTGGCTGCTGCCAGTGGCGATAAGTCGTGTCTTACCGGGTTG<br>GACTCAAGACGATAGTTACCGGATAAGGCGCAGCGGTCGGGCTGA<br>ACGGGGGGTTCGTGCACACAGCCCAGCTTGGAGCGAACGACCTAC<br>ACCGAACTGAGATACCTACAGCGTGAGCTATGAGAAAGCGCCACG<br>CTTCCCGAAGGGAGAAAGGCGGACAGGTATCCGGTAAGCGGCAGG<br>GTCGGAACAGGAGAGCGCACGAGGGAGCTTCCAGGGGGAAACGCC<br>TGGTATCTTTATAGTCCTGTCGGGTTTCGCCACCTCTGACTTGAGCG<br>TCGATTTTTGTGATGCTCGTCAGGGGGGCGGAGCCTATGGAAAAAC<br>GCCAGCAACGCGGCCTTTTTACGGTTCCTGGCCTTTTGCTGGCCTTT<br>TGCTCACATGTTCTTTCCTGCGTTATCCCCTGATTCTGTGGATAACC<br>GTATTACCGCCTTTGAGTGAGCTGATACCGCTCGCCGCAGCCGAAC<br>GACCGAGCGCAGCGAGTCAGTGAGCGAGGAAGCGGAAGAGCGCCC<br>AATACGCAAACCGCCTCTCCCCGCGCGTTGGCCGATTCATTAATG |

Table S2. Nanostring expression data

| | $Log_2FC$ (AAV/eGFP) | |
|---|---|---|
| **Gene Target** | **coRIPK3ΔC** | **coRIPK3** |
| *Rock2* | -0.111031312 | 0.111031312 |
| *Rapgef2* | -0.042644337 | 0.111031312 |
| *Pdgfa* | -0.150559677 | 0.028569152 |
| *Tlr1* | -0.137503524 | 0.23878686 |
| *C9* | -0.028569152 | 0.189033824 |
| *Alox15* | -0.070389328 | 0.111031312 |
| *Hspb1* | -0.097610797 | 0.137503524 |
| *Il12a* | -0.042644337 | 0.084064265 |
| *Il1b* | -0.298658316 | 0.070389328 |
| *Il2* | -0.275007047 | 0.097610797 |
| *Mx1* | -0.367371066 | 0.111031312 |
| *Gpr44* | -0.275007047 | 0.056583528 |
| *Myl2* | -0.275007047 | 0.014355293 |
| *Cfb* | -0.23878686 | 0.014355293 |
| *Ltb4r1* | -0.333423734 | 0.084064265 |
| *Ppp1r12b* | -0.250961574 | 0.124328135 |
| *Ccr1* | -0.23878686 | 0.097610797 |
| *Ccl2* | -0.422233001 | 0.111031312 |
| *Mef2a* | -0.432959407 | 0.163498732 |
| *Lta* | -0.286881148 | 0.275007047 |
| *Il23r* | -0.310340121 | 0.298658316 |
| *Nod2* | -0.070389328 | 0.35614381 |
| *Tlr8* | -0.545968369 | 0.097610797 |
| *Tlr5* | -0.613531653 | 0.028569152 |
| *Arg1* | -0.443606651 | 0.23878686 |
| *Il13* | -0.516015147 | 0.189033824 |
| *Cd86* | -0.333423734 | 0.333423734 |
| *Cd40* | -0.495695163 | 0.286881148 |
| *Prkcb* | -0.201633861 | 0.097610797 |
| *Tlr7* | -0.389566812 | 0.622930351 |
| *Hc* | -0.941106311 | 0.056583528 |
| *Ltb* | -1.028569152 | 0.150559677 |
| *Ptgfr* | -0.310340121 | 0.097610797 |
| *Nlrp3* | -0.321928095 | 0.028569152 |
| *Mafg* | -0.214124805 | 0.056583528 |
| *Smad7* | -0.014355293 | 0.124328135 |
| *Irf3* | -0.124328135 | 0.084064265 |
| *Alox5* | -0.137503524 | 0.014355293 |
| *Tnfaip3* | -0.097610797 | 0.111031312 |
| *Prkca* | -0.124328135 | 0.056583528 |
| *Keap1* | -0.124328135 | 0.042644337 |
| *C3ar1* | -0.176322773 | 0.321928095 |
| | | |

| | $Log_2FC$ (AAV/eGFP) | |
|---|---|---|
| **Gene Target** | **coRIPK3ΔC** | **coRIPK3** |
| *C3* | -0.23878686 | 0.214124805 |
| *C8a* | -0.084064265 | 0.275007047 |
| *Defa-rs1* | -0.028569152 | 0.22650853 |
| *Cxcl9* | -0.070389328 | 0.084064265 |
| *Mmp3* | -0.163498732 | 0.286881148 |
| *Tslp* | -0.286881148 | 0.137503524 |
| *Tlr9* | -0.454175893 | 0.411426246 |
| *Il1r1* | -0.35614381 | 0.526068812 |
| *Cxcl1* | -0.485426827 | 0.565597176 |
| *Cd4* | -0.545968369 | 0.028569152 |
| *C1qb* | -0.516015147 | 0.176322773 |
| *Cxcl3* | -0.622930351 | 0.22650853 |
| *Cd163* | -0.526068812 | 0.070389328 |
| *Il12b* | -0.422233001 | 0.23878686 |
| *Ptger2* | -0.150559677 | 0.333423734 |
| *Ccl3* | -1.137503524 | 0.90303827 |
| *Ifng* | -0.871843649 | 0.790772038 |
| *C7* | -0.839959587 | 0.214124805 |
| *Nfatc3* | 0 | 0.150559677 |
| *Stat3* | 0.056583528 | 0.137503524 |
| *Bcl6* | 0.137503524 | 0.056583528 |
| *Ifit3* | 0.137503524 | 0.097610797 |
| *Ifi44* | 0.124328135 | 0.097610797 |
| *Ccr3* | 0.23878686 | 0.124328135 |
| *Ly96* | 0.367371066 | 0.214124805 |
| *H2-Eb1* | 0.056583528 | 0.310340121 |
| *Creb1* | 0.189033824 | 0.367371066 |
| *Nos2* | 0.176322773 | 0.310340121 |
| *Ccl22* | 0.084064265 | 0.475084883 |
| *Ccr7* | 0.070389328 | 0.454175893 |
| *Tlr3* | 0.084064265 | 0.35614381 |
| *Irf7* | 0.201633861 | 0.555816155 |
| *Ifi27l2a* | 0.084064265 | 0.516015147 |
| *Il7* | 0.344828497 | 0.263034406 |
| *Cxcr2* | 0.275007047 | 0.163498732 |
| *Ptgs2* | 0.275007047 | 0.201633861 |
| *Ifna1* | 0.23878686 | 0.321928095 |
| *Cxcr4* | 0.163498732 | 0.124328135 |
| *Il17a* | 0.22650853 | 0.070389328 |
| *Flt1* | 0.070389328 | 0.22650853 |
| *Trem2* | 0.516015147 | 0.097610797 |
| *Tlr6* | 0.475084883 | 0.847996907 |
| *Cfd* | 0.124328135 | 0.613531653 |
| *Pik3c2g* | 0.378511623 | 0.50589093 |
| *Ccl17* | 0.411426246 | 0.604071324 |
| *Il18rap* | 0.555816155 | 0.704871964 |
| *Ccl4* | 0.575312331 | 0.695993813 |

| | $Log_2FC$ (AAV/eGFP) | |
|---|---|---|
| **Gene Target** | **coRIPK3ΔC** | **coRIPK3** |
| *Il1rn* | 0.604071324 | 0.516015147 |
| *Cxcl5* | 0.189033824 | 0.124328135 |
| *Alox12* | 1.182692298 | 0.310340121 |
| *Ccr2* | 0.956056652 | 1.448900951 |
| *Mbl2* | 1.13093087 | 1.655351829 |
| *Csf2* | 0.604071324 | 1.344828497 |
| *Mrc1* | 0.097610797 | -0.831877241 |
| *Tnfsf14* | 0.584962501 | -0.097610797 |
| *Mx2* | 0.056583528 | -0.275007047 |
| *Cebpb* | 0.014355293 | 0.214124805 |
| *Ddit3* | 0.189033824 | 0.344828497 |
| *Ptgir* | 0.22650853 | 0.333423734 |
| *Rps6ka5* | 0.176322773 | 0.22650853 |
| *Ccl21a* | 0.111031312 | 0.310340121 |
| *Tbxa2r* | 0.150559677 | 0.250961574 |
| *Retnla* | 0.286881148 | 0.042644337 |
| *C4a* | 0.485426827 | 0.028569152 |
| *Masp2* | 0.189033824 | 0.678071905 |
| *H2-Ea-ps* | 0.084064265 | 0.565597176 |
| *Il22* | 0.042644337 | 0.555816155 |
| *C6* | 0.545968369 | 0.310340121 |
| *Maff* | 0.097610797 | -0.189033824 |
| *Oas1a* | 0.014355293 | -0.097610797 |
| *Ripk2* | 0.014355293 | -0.150559677 |
| *Ccl7* | 0.163498732 | -0.275007047 |
| *Nox1* | 0.176322773 | -0.310340121 |

Table S3. Primer sequences for qRT-PCR

| **Target** | | **Sequence (5' → 3')** |
|---|---|---|
| *Ccl2* | Fwd | TGG CTC AGC CAG ATG CAG T |
| | Rev | TTG GGA TCA TCT TGC TGG TG |
| *Ccl3* | Fwd | CCA AGT CTT CTC AGC GCC AT |
| | Rev | TCC GGC TGT AGG AGA AGC AG |
| *Ccl4* | Fwd | TCT TGC TCG TGG CTG CCT |
| | Rev | GGG AGG GTC AGA GCC CA |
| *Ifng* | Fwd | AAC GCT ACA CAC TGC ATC TTG G |
| | Rev | GCC GTG GCA GTA ACA GCC |
| *Nod2* | Fwd | CAT CTG GTC ACC AAC ATT CG |
| | Rev | GAA GGG GAG AAG CCA ATT TC |
| *Nos2* | Fwd | CTT TGC CAC GGA CGA GAC |
| | Rev | TCA TTG TAC TCT GAG GGC TGA C |

# Chapter 4

Summary and future directions

## 4.1 Summary

### Ectopic administration of necroptotic cells stimulates anti-tumor immunity

Although the signaling events that induce different forms of programmed cell death (PCD) are well-defined, the downstream immune responses to dying cells in the context of cancer remain relatively unexplored. Necroptosis occurs following activation of the receptor-interacting protein kinases RIPK1 and RIPK3, leading to lytic cell death accompanied by *de novo* production of pro-inflammatory mediators. In this study, we show that ectopic introduction of necroptotic cells to the tumor microenvironment (TME) promotes $BATF3^+$ cDC1- and $CD8^+$ leukocyte-dependent anti-tumor immunity accompanied by increased tumor antigen loading by tumor-associated antigen presenting cells. This tumor control requires signaling through the RIPK1/RIPK3 necrosome complex, but not the release of immunogenic damage-associated molecular patterns (DAMPs) following cell lysis, indicating that necroptosis likely modulates anti-tumor immune responses through an unidentified NF-κB-dependent transcriptional target produced by the dying cells. Lastly, we demonstrate that immune stimulation by necroptotic cells synergizes with co-administration of immune checkpoint blockade reagents to promote durable tumor control, suggesting that strategies to elicit necrosome signaling within the TME could yield promising combination treatments with existing immunotherapy. Collectively, these findings provide intriguing proof-of-concept studies that support a role for RIPK1/RIPK3 activation as a beneficial proximal target in the initiation of tumor immunity.

### Immunogenic necroptosis can be targeted *in situ* using adeno-associated viruses (AAVs)

Extending from our work examining ectopic introduction of necroptosis to the tumor microenvironment, we next explored strategies to study the effects of tumor cell necroptosis *in*

*situ*. We report the development of constitutively-active forms of the necroptosis-inducing enzyme RIPK3, and show that delivery of a gene encoding this enzyme to tumor cells using adeno-associated viruses (AAVs) induces tumor cell necroptosis that is accompanied by RIPK1-dependent upregulation of an active NF-κB transcriptional signature. The resulting tumor cell death synergizes with immune checkpoint blockade *in vivo* to promote $BATF3^+$ cDC1- and $CD8^+$ leukocyte-dependent tumor clearance that is resistant to rechallenge, suggesting the formation of durable immune memory. These findings show that enforced activation of the RIPK1/RIPK3 necrosome within tumor cells using AAVs recapitulates the therapeutic effects observed following ectopic administration of necroptotic cells. Considering that successful tumor immunotherapy regimens will require the rational application of combinatorial treatment modalities, we propose that maximizing the immunogenicity of dying cells within the tumor microenvironment through specific activation of the necroptotic pathway using gene therapy tools such as AAVs represents a beneficial treatment approach that may warrant further clinical development.

## 4.2 Conclusions and future directions

### Contributions of RIPK1/RIPK3 activation to anti-tumor immunity

This dissertation outlines a critical role for activation of the RIPK1/RIPK3 signaling complex in stimulating NF-κB-dependent anti-tumor immune responses irrespective of cellular lysis and DAMP release. These findings are consistent with a growing body of evidence supporting a role for death-independent functions of RIPK1/RIPK3 in driving immune responses to necrosome signaling *in vivo*[3]. This includes RIPK1/NF-κB-dependent signals that drive the immunogenicity of necroptotic fibroblasts in a $CD8^+$ T cell cross-priming vaccination model[10], RIPK3-dependent neuronal production of protective inflammatory chemokines during West Nile virus infection[11], the RIPK3/IRF1/IRG1-driven acquisition of an antiviral metabolic state in neurons during Zika virus infection[12], and exacerbated autoimmune pathologies observed in *Caspase8*$^{-/-}$*Mlkl*$^{-/-}$ mice compared to *Caspase8*$^{-/-}$*Ripk3*$^{-/-}$ mice[51]. Collectively, these findings lend support to the idea that RIPK3 activation drives the immunogenicity of necroptotic cells independently of (or in addition to) MLKL-mediated cellular lysis and passive release of DAMPs. As the cell death signaling field moves towards applying knowledge of mechanistic *in vitro* studies towards examining the consequences of PCD pathway engagement *in vivo*, there is a growing appreciation of death-independent functions of RIPK3 activation in promoting immune responses to dying cells.

An obvious continuation of this work is identification of the specific RIPK1/RIPK3/NF-κB-dependent signal (or signals) produced by necroptotic cells responsible for their immunogenicity within the TME. This remains an outstanding question raised by other reports of death-independent immunogenicity of necroptotic cells[10-12,51], in which the mechanism by which RIPK1 and/or RIPK3 upregulate pro-inflammatory gene expression remain poorly understood.

Notably, both necroptotic fibroblast and AAV-induced tumor cell necroptosis models exhibit upregulation of a variety of NF-κB-dependent inflammatory chemokines and cytokines (Ref. 10 and Chapter 3 Fig.1D, respectively). This complements reports of RIPK3-dependent chemokine expression in the brain during neurotropic flavivirus infection[11], and potentially represents a conserved RIPK3-dependent signaling program that contributes to the immunogenicity of RIPK1/RIPK3 activation across different cell types and disease models. Consistent with this, we observe increased intratumoral levels of the dendritic cell-attracting chemokines CCL3, CCL4, and CCL5 following administration of necroptotic cells (Chapter 2 Fig.5B) that is correlated with increased recruitment of $CD103^+$ cDC1's in the tumor microenvironment (Chapter 2 Fig.5A). However, the source of these chemokines and whether their production is required for the therapeutic effect of necroptotic cells remains unknown. Future experiments that determine the requirement for specific chemokine/chemokine receptor signaling axes in mediating the therapeutic effect of necroptotic cells will yield important information related to the underlying mechanism of tumor control following necroptosis induction in the TME. Furthermore, as inflammatory chemokine expression is often attributed to canonical NF-κB activation via TAK1/IKK-mediated phosphorylation and degradation of IκBα[218], testing the necessity of these canonical NF-κB signaling components in driving immune responses to necroptotic cells remains an important future direction in with respect to mechanistically defining the molecular determinants of necroptotic cell immunogenicity.

In addition to chemokine production by necroptotic cells that could promote leukocyte infiltration into the TME, alternative immunostimulatory signals may function by directly affecting the activation status of APCs already localized within the TME. We report increased proportions of tumor-associated phagocytes that are loaded with tumor-derived fluorophore

(Chapter 2 Fig.5D), suggesting that exposure to necroptosis in the TME can stimulate phagocytes such that they (a) increase their rate of phagocytosis or macropinocytosis, and/or (b) differentially compartmentalize ingested antigens in a manner that promotes antigen preservation/retention over time. Notably, increased phagocytosis is a hallmark of APC activation[219]. APC activation can be potently stimulated following exposure to necroptotic fibroblasts: *in vitro* co-culture induces the expression of DC maturation markers[10], and we observe enhanced phenotypic and functional activation of tumor-associated DCs and macrophages following intratumoral injection of necroptotic cells (Chapter 2, Fig.5G-H). Therefore, activating stimuli derived from necroptotic cells could function locally by increasing the activation status of APCs present within the TME to increase their rates of phagocytosis, independently of any chemokine-driven recruitment of additional leukocytes to the TME. Obvious candidate signals in this context would be pro-inflammatory cytokines produced downstream of canonical NF-κB activation[218] that can subsequently promote inflammatory APC polarization in a paracrine fashion, including IL-2[220], IL-12[221], and TNF-α[222-223]. Additionally, type I IFN signaling in leukocytes is required for tumor control by necroptotic cells (Chapter 2, Fig.3A), though this could be partially attributed to defective baseline recruitment of leukocytes to the TME (Chapter 2, Fig.S3A right panel). However, we have not comprehensively ruled out a role for IFNα/β functioning in this system by promoting the maturation status of tumor-associated APCs. Indeed, type I IFN has been shown to potentiate the activation status of DCs[224-225], indicating that signaling through IFNAR1 expressed on tumor APCs could help drive the observed increase in their activation status. Future work will be necessary to determine the identity of potentially RIPK1/RIPK3/NF-κB-dependent gene targets such as cytokines that would potentiate the maturation of tumor-associated APC subsets.

Regarding antigen compartmentalization, a previous study has reported that while apoptotic bodies are taken up in tightly-sealed phagosomes via a "zipper"-like mechanism of classical phagocytosis, necrotic cell debris is internalized via macropinocytosis, resulting in concurrent uptake of extracellular contents adjacent to cellular debris[190]. These differences in internalization mechanisms could potentially explain our observed increase in tumor antigen loading by tumor APCs, as phagocytes clearing necroptotic debris would coincidentally take up tumor-derived cellular debris present within the extracellular space of the TME via macropinocytosis. Interestingly, pinocytosis of exogenous antigen has been associated with increased antigen presentation on MHC-I to stimulate $CD8^+$ T cell responses, in contrast to exogenous antigen internalized via classical receptor-mediated endocytosis (phagocytosis) that is preferentially processed for presentation on MHC-II[227]. This suggests that processes that promote macropinocytosis by tumor APCs may preferentially stimulate $CD8^+$ T cell responses required for tumor immunity. However, the biological relevance of differential internalization mechanisms employed by tumor APCs responding to apoptotic versus necroptotic debris remains to be determined. Presumably, increased sampling of the TME/increased tumor antigen loading associated with necroptotic cell clearance is not sufficient for driving anti-tumor effects of necroptotic cells, as administered lytic necrotic cells would also be cleared using macropinocytosis, yet lack any therapeutic effects in our tumor models (Chapter 2, Fig.3D; Chapter 3, Fig.2A and Fig. Fig.2C). Therefore, determining how increased antigen loading in the TME could potentially synergize with other inflammatory cues derived from necroptotic cells to enhance the antigen presentation functionality of tumor-associated APCs remains an intriguing avenue for future research.

These proposed mechanisms underlying the immunogenicity of necroptotic cells should not be considered mutually exclusive from one another. Since multiple signals are likely produced downstream of RIPK1/RIPK3 activation, it is possible that engaging this form of PCD in the TME may potentiate anti-tumor immunity in a combinatorial fashion. This could involve (1) promoting tumor antigen loading via macropinocytosis associated with necroptotic cell clearance, (2) enhancing APC maturation through the release of inflammatory cytokines, and/or (3) increasing the recruitment of beneficial leukocyte subsets via chemokine production (Figure 1). Indeed, identification of the specific signals required for tumor control by necroptotic cells will provide valuable insight related to the development of future reductionist therapies. Such strategies would aim to maximize the immunogenicity of PCD engagement by producing only the beneficial immunogenic molecules produced by necroptotic cells, without the release of potentially deleterious DAMPs following cellular lysis[90-93].

**Using adeno-associated viruses (AAVs) to target necroptosis to the tumor microenvironment *in vivo***

Extending from our proof of concept studies using a model of intratumoral necroptotic cell administration, this dissertation additionally details the development of recombinant AAVs used to enforce necroptotic signaling in the TME that promotes $BATF3^+$ cDC1 and $CD8^+$ leukocyte-dependent tumor control. This represents the first reported usage of engineered versions of RIPK3 fused to *in silico*-designed constitutively oligomerizing domains[209], whose expression results in RIPK1/RIPK3 activation and signaling within target cells to induce necroptosis regardless of the expression status of endogenous PCD signaling pathway components. These findings join existing gene therapy approaches to transduce tumor cells *in*

*vivo* using adenoviral-based vectors encoding inducible versions of caspase-9[144] or caspase-3[145] in order to trigger apoptosis in previously refractory tumor cells. Collectively, these strategies represent gene therapy-based approaches to render transformed cells that have evaded PCD signaling susceptible once again to death induction, regardless of the expression status of endogenous PCD pathway components (Figure 2). Considering the results presented in this dissertation, we propose that gene therapy strategies that maximize the immunogenicity of tumor cell death through engagement of RIPK1/RIPK3 signaling in comparison to apoptotic signaling through caspases may warrant further development.

Despite the advantages of using AAVs as gene therapy vectors[194-196], there still remain several potential issues that will require further investigation. First, although AAVs exhibit low frequencies of host genomic integration, there are reports of rare integration events that can lead to subsequent genotoxic stress[228-229]; as intravenously-administered AAVs efficiently transduce liver hepatocytes[208], these studies primarily focus on liver genotoxicity. These insertions are typically random, but concern is raised when viral genome integration occurs at proto-oncogenes, which could conceivably upregulate oncogene expression due to ITR transactivation[230-231]. Second, though AAVs are less immunogenic compared to other viral vectors for *in vivo* usage[196], AAV capsid proteins can still stimulate humoral immunity and the production of capsid-specific antibodies that can neutralize or opsonize AAV particles in future rounds of administration[232-233]. Additionally, as latent AAV infection circulates in a high percentage of the human population[234], some individuals may have pre-existing B cell responses to certain AAV serotypes[235]. These types of immune responses can lead to dangerous inflammatory side effects that warrant screening patients for either pre-existing or induced AAV-reactive antibodies[195,235]. In addition to this off-target toxicity, AAV-neutralizing humoral

responses obviously negate the efficacy of dosing regimens that would involve repeated rounds of AAV transduction, as one might expect would be employed for the treatment of tumors. Furthermore, AAV-mediated expression of a transgene can lead to B or T cell responses mounted against the engineered protein itself, as this product can be perceived as a foreign peptide[236]. Notably, since the AAV products described here would immediately lead to cell death, we would expect that transgene-specific immune responses would be minimal as the engineered protein would not be stably expressed over time. However, genotoxicity stemming from genomic AAV integration or lymphocyte reactivity to immunogenic AAV capsid proteins remain important factors to consider in future work adapting the AAV-mediated delivery of oligomerizable RIPK3 constructs that we present here. We do note that, as a gross check on systemic inflammation resulting from AAV toxicity, mice receiving intratumoral AAV injections did not show any apparent signs of septic shock (ruffled fur/hunching, decrease in body temperature, or purulent eyes) at time points <12 hours post-AAV administration (data not shown). However, more rigorous examination of potential off-target effects of these death-inducing AAVs remains a critical area of study for any future research that employs these tools.

Considering potential issues with AAV vectors, it is important to consider alternative forms of gene delivery vehicles that could also be explored as tools to enforce expression of the constitutively-oligomerizing version of RIPK3 (coRIPK3) presented in this dissertation. One such tool that could be adapted for future research is oncolytic virotherapy. Oncolytic viruses encompass a class of modified viruses that are engineered to increase their tumor cell tropism while minimizing infection of non-neoplastic cells[237-238]. One of the primary mechanisms of action of oncolytic viruses is their ability to directly kill tumor cells, reducing tumor burden and promoting the release of tumor-associated antigens that potentially contribute to epitope

spreading[237-239]. However, virally-induced cytotoxicity is often insufficient as a primary therapeutic agent to restrict tumor outgrowth[238]. Indeed, the only currently FDA-approved oncolytic virotherapy is talimogene laherparepvec (T-Vec), an engineered version of herpes simplex virus-1 (HSV-1) that targets both tumor cell killing as well as concurrent expression of immunostimulatory GM-CSF[240-241]. Therefore, engineering of oncolytic viruses to express immunostimulatory signaling molecules instead of simply killing off tumor cells may represent the most effective form of oncolytic virotherapy. The development of oncolytic viruses that encode both coRIPK3 along with DC- or T cell-attracting chemokines such as CCL3/4/5 or CXCL9/10 would be an intriguing potential strategy for effectively "arming" oncolytic viruses. Additionally, exploration of other gene delivery strategies using tools such as cationic lipid[242] or peptide[243] nanoparticles for mRNA delivery may also warrant future examination. Together, future work on these gene therapy approaches could yield a repertoire of therapeutic agents that would function by rendering death-resistant tumor cell clones susceptible to immunogenic forms of PCD, including necroptosis (Figure 2). As with any form of gene therapy, targeting necroptosis to the TME via AAV, oncolytic viruses, or nanoparticle-based mRNA transfection systems would all likely require direct intratumoral administration to restrict the therapeutic effects to the tumor tissue itself and minimize off-target toxicity effects[196,238,244]. The development of targeted forms of these gene therapies that could be administered systemically but specifically traffic to tumor cells represents an important future direction at the intersection of both gene therapy and immunotherapy fields.

Lastly, we stress the need to apply our findings to murine tumor models that more closely recapitulate symptoms of human disease. Although syngeneic flank tumors provide a relatively rapid and affordable murine model of cancer outgrowth, these tumors do not faithfully represent

many biological elements of the TME that likely determine the efficacy of immunotherapeutic agents in human tumors[245-246]. Several key tumor immunotherapy proof of concept findings were first demonstrated in syngeneic flank tumor models; however, these results need to be subsequently tested in more sophisticated animal models of disease in order to fully evaluate their translational potential. Genetically-engineered mouse (GEM) models are generated using transgenic mice that bear similar genetic lesions observed in particular subtypes of human cancers. As such, GEM models provide the most accurate representation of human tumor biology, recapitulating characteristics related to oncogenic transformation, tumor development and establishment of the TME, and tumor-immune interactions[246]. Inflammatory signals can play a paradoxical role in the TME[39]; furthermore, the consequences of necroptotic pathway signaling are likely to be highly cell type- and tissue context-specific[176]. Therefore, examining how pro-inflammatory signals produced downstream of RIPK1/RIPK3 activation in translationally relevant tumor models represents an essential continuation of the findings presented in this dissertation. The AAVs reported here provide tractable tools that can be easily applied to GEM models that yield tumors accessible for intratumoral injection. Testing how enforced activation of RIPK3 in the TME of GEM tumor models affects anti-tumor immune responses constitutes a critical future step in determining if specific targeting of tumor cell necroptosis warrants future development as a novel immunotherapeutic agent.

### 4.3 Figures

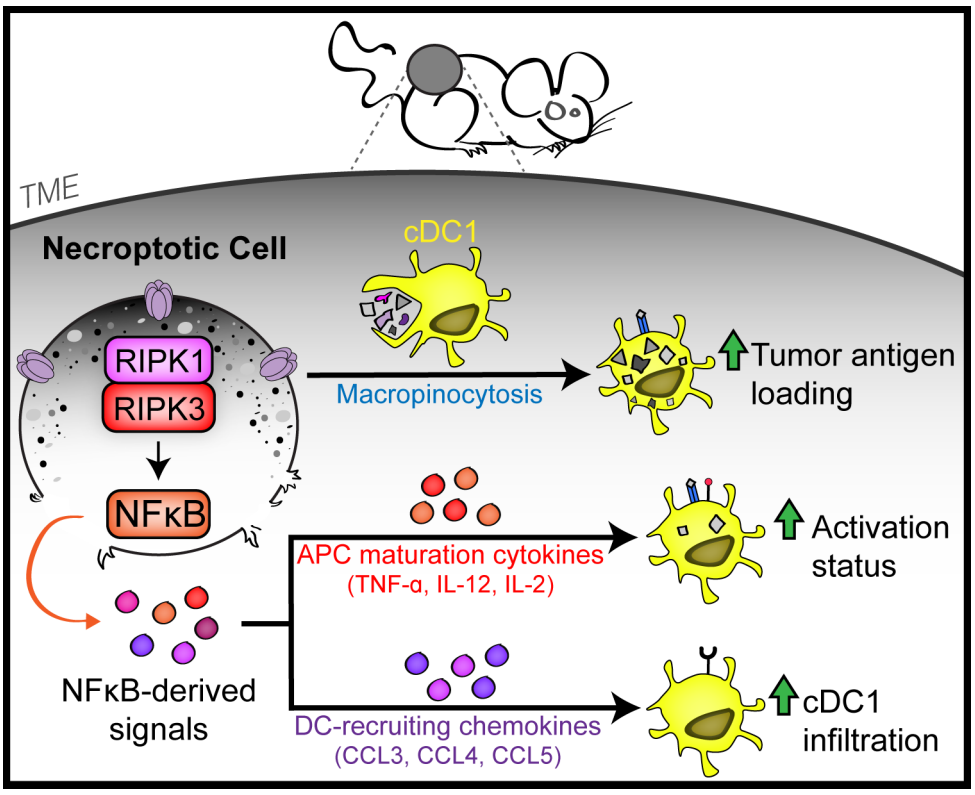


**Figure 1. Potential mechanisms underlying immunogenicity of necroptotic cell death.** Following induction of necroptosis in the tumor microenvironment, multiple signals could be produced that contribute to anti-tumor immunity. Possible mechanisms could include (1) increased sampling of the tumor microenvironment via macropinocytosis associated with the clearance of necroptotic cell debris, (2) potentiating APC activation through the release of inflammatory cytokines by necroptotic cells, and/or (3) enhancing recruitment of beneficial DC populations via production of chemokines by necroptotic cells.

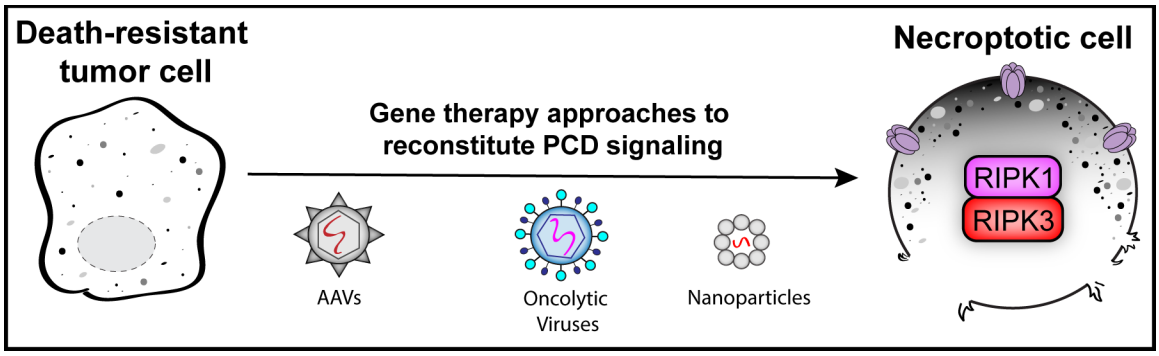


**Figure 2. Gene therapy strategies to reconstitute immunogenic cell death signaling pathways in transformed tumor cells.** Tumor cells subvert cell death signaling pathways as a common mechanism of oncogenic transformation, yielding death-resistant tumor cell clones. Gene therapy approaches that can be used to reinforce expression of programmed cell death (PCD) signaling components in tumor cells include adeno-associated viruses (AAVs), oncolytic viruses, or nanoparticles. Upon therapy application, expression of PCD signaling enzymes such as pro-necroptotic RIPK1/RIPK3 renders target cells susceptible to death induction, irrespective of the expression status of endogenous PCD signaling pathways.

# References


1. Galluzzi L, Vitale I, Aaronson SA, Abrams JM, Adam D, Agostinis P, et al. Molecular mechanisms of cell death: recommendations of the Nomenclature Committee on Cell Death 2018. *Cell Death Differ* 2018; **25**(3): 486-541.
2. Elmore S. Apoptosis: a review of programmed cell death. *Toxicol Pathol* 2007; **35**(4): 495-516.
3. Yatim N, Cullen S, Albert ML. Dying cells actively regulate adaptive immune responses. *Nat Rev Immunol* 2017; **17**(4): 262-75.
4. Grootjans S, Vanden Berghe T, Vandenabeele P. Initiation and execution mechanisms of necroptosis: an overview. *Cell Death Differ* 2017; **24**(7): 1184-95.
5. Weinlich R, Oberst A, Beere HM, Green DR. Necroptosis in development, inflammation and disease. *Nat Rev Mol Cell Biol* 2017; **18**(2): 127-36.
6. Orzalli MH, Kagan JC. Apoptosis and Necroptosis as Host Defense Strategies to Prevent Viral Infection. *Trends Cell Biol* 2017; **27**(11): 800-9.
7. Vanden Berghe T, Hassannia B, Vandenabeele P. An outline of necrosome triggers. *Cell Mol Life Sci* 2016; **73**(11-12): 2137-52.
8. Wallach D, Kang TB, Dillon CP, Green DR. Programmed necrosis in inflammation: Toward identification of the effector molecules. *Science* 2016; **352**(6281): aaf2154.
9. Czabotar PE, Lessene G, Strasser A, Adams JM. Control of apoptosis by the BCL-2 protein family: implications for physiology and therapy. *Nat Rev Mol Cell Biol* 2014; **15**(1): 49-63.
10. Yatim N, Jusforgues-Saklani H, Orozco S, Schulz O, Barreira da Silva R, Reis e Sousa C, et al. RIPK1 and NF-kappaB signaling in dying cells determines cross-priming of CD8(+) T cells. *Science* 2015; **350**(6258): 328-34.
11. Daniels BP, Snyder AG, Olsen TM, Orozco S, Oguin TH, 3rd, Tait SWG, et al. RIPK3 Restricts Viral Pathogenesis via Cell Death-Independent Neuroinflammation. *Cell* 2017; **169**(2): 301-13.e11.
12. Daniels BP, Kofman SB, Smith JR, Norris GT, Snyder AG, Kolb JP, et al. The nucleotide sensor ZBP1 and kinase RIPK3 induce the enzyme IRG1 to promote an antiviral metabolic state in neurons. *Immunity*. 2019; **50**(1): 64-76.
13. Newton K, Dugger DL, Maltzman A, Greve JM, Hedehus M, Martin-McNulty B, et al. RIPK3 deficiency or catalytically inactive RIPK1 provides greater benefit than MLKL deficiency in mouse models of inflammation and tissue injury. *Cell Death Differ.* 2016; **23**(9): 1565-1576.
14. Dickens LS, Powley IR, Hughes MA, MacFarlane M. The 'complexities' of life and death: death receptor signalling platforms. *Exp Cell Res* 2012; **318**(11): 1269-77.
15. Taylor RC, Cullen SP, Martin SJ. Apoptosis: controlled demolition at the cellular level. *Nat Rev Mol Cell Biol* 2008; **9**(3): 231-41.
16. Ucker DS, Levine JS. Exploitation of Apoptotic Regulation in Cancer. *Front Immunol* 2018; **9**: 241.
17. Yuan S, Akey CW. Apoptosome structure, assembly, and procaspase activation. *Structure* 2013; **21**(4): 501-15.
18. Strasser A, Harris AW, Huang DC, Krammer PH, Cory S. Bcl-2 and Fas/APO-1 regulate distinct pathways to lymphocyte apoptosis. *Embo j* 1995; **14**(24): 6136-47.

19. Jost PJ, Grabow S, Gray D, McKenzie MD, Nachbur U, Huang DC, et al. XIAP discriminates between type I and type II FAS-induced apoptosis. *Nature* 2009; **460**(7258): 1035-9.
20. Ozturk S, Schleich K, Lavrik IN. Cellular FLICE-like inhibitory proteins (c-FLIPs): fine-tuners of life and death decisions. *Exp Cell Res* 2012; **318**(11): 1324-31.
21. Hughes MA, Powley IR, Jukes-Jones R, Horn S, Feoktistova M, Fairall L, et al. Co-operative and Hierarchical Binding of c-FLIP and Caspase-8: A Unified Model Defines How c-FLIP Isoforms Differentially Control Cell Fate. *Mol Cell* 2016; **61**(6): 834-49.
22. Lopez J, Tait SW. Mitochondrial apoptosis: killing cancer using the enemy within. *Br J Cancer* 2015; **112**(6): 957-62.
23. Shakeri R, Kheirollahi A, Davoodi J. Apaf-1: Regulation and function in cell death. *Biochimie* 2017; **135**: 111-25.
24. Bosurgi L, Hughes LD, Rothlin CV, Ghosh S. Death begets a new beginning. *Immunol Rev* 2017; **280**(1): 8-25.
25. Kumar S, Calianese D, Birge RB. Efferocytosis of dying cells differentially modulate immunological outcomes in tumor microenvironment. *Immunol Rev* 2017; **280**(1): 149-64.
26. Elkon KB. Cell Death, Nucleic Acids, and Immunity: Inflammation Beyond the Grave. *Arthritis Rheumatol* 2018.
27. Nagata S, Hanayama R, Kawane K. Autoimmunity and the clearance of dead cells. *Cell* 2010; **140**(5): 619-30.
28. Baumann I, Kolowos W, Voll RE, Manger B, Gaipl U, Neuhuber WL, et al. Impaired uptake of apoptotic cells into tingible body macrophages in germinal centers of patients with systemic lupus erythematosus. *Arthritis Rheum* 2002; **46**(1): 191-201.
29. Ting AT, Bertrand MJM. More to Life than NF-kappaB in TNFR1 Signaling. *Trends Immunol* 2016; **37**(8): 535-45.
30. Oberst A, Dillon CP, Weinlich R, McCormick LL, Fitzgerald P, Pop C, et al. Catalytic activity of the caspase-8-FLIP(L) complex inhibits RIPK3-dependent necrosis. *Nature* 2011; **471**(7338): 363-7.
31. Kaiser WJ, Upton JW, Long AB, Livingston-Rosanoff D, Daley-Bauer LP, Hakem R, et al. RIP3 mediates the embryonic lethality of caspase-8-deficient mice. *Nature* 2011; **471**(7338): 368-72.
32. Upton JW, Kaiser WJ, Mocarski ES. Virus inhibition of RIP3-dependent necrosis. *Cell Host Microbe* 2010; **7**(4): 302-13.
33. Stupack DG. Caspase-8 as a therapeutic target in cancer. *Cancer Lett* 2013; **332**(2): 133-40.
34. Thapa RJ, Ingram JP, Ragan KB, Nogusa S, Boyd DF, Benitez AA, et al. DAI Senses Influenza A Virus Genomic RNA and Activates RIPK3-Dependent Cell Death. *Cell Host Microbe* 2016; **20**(5): 674-81.
35. Kaiser WJ, Sridharan H, Huang C, Mandal P, Upton JW, Gough PJ, et al. Toll-like receptor 3-mediated necrosis via TRIF, RIP3, and MLKL. *J Biol Chem* 2013; **288**(43): 31268-79.
36. He S, Liang Y, Shao F, Wang X. Toll-like receptors activate programmed necrosis in macrophages through a receptor-interacting kinase-3-mediated pathway. *Proc Natl Acad Sci U S A* 2011; **108**(50): 20054-9.
37. Najjar M, Saleh D, Zelic M, Nogusa S, Shah S, Tai A, et al. RIPK1 and RIPK3 Kinases Promote Cell-Death-Independent Inflammation by Toll-like Receptor 4. *Immunity* 2016; **45**(1): 46-59.
38. Linkermann A, Green DR. Necroptosis. *N Engl J Med* 2014; **370**(5): 455-65.

39. Murphy JM, Czabotar PE, Hildebrand JM, Lucet IS, Zhang JG, Alvarez-Diaz S, et al. The pseudokinase MLKL mediates necroptosis via a molecular switch mechanism. *Immunity* 2013; **39**(3): 443-53.
40. Zhang Y, Chen X, Gueydan C, Han J. Plasma membrane changes during programmed cell deaths. *Cell Res* 2018; **28**(1): 9-21.
41. Li T, Chen ZJ. The cGAS-cGAMP-STING pathway connects DNA damage to inflammation, senescence, and cancer. *J Exp Med* 2018; **215**(5): 1287-99.
42. Ahrens S, Zelenay S, Sancho D, Hanc P, Kjaer S, Feest C, et al. F-actin is an evolutionarily conserved damage-associated molecular pattern recognized by DNGR-1, a receptor for dead cells. *Immunity* 2012; **36**(4): 635-45.
43. Sancho D, Joffre OP, Keller AM, Rogers NC, Martinez D, Hernanz-Falcon P, et al. Identification of a dendritic cell receptor that couples sensing of necrosis to immunity. *Nature* 2009; **458**(7240): 899-903.
44. Scaffidi P, Misteli T, Bianchi ME. Release of chromatin protein HMGB1 by necrotic cells triggers inflammation. *Nature* 2002; **418**(6894): 191-5.
45. Hreggvidsdottir HS, Lundberg AM, Aveberger AC, Klevenvall L, Andersson U, Harris HE. High mobility group box protein 1 (HMGB1)-partner molecule complexes enhance cytokine production by signaling through the partner molecule receptor. *Mol Med* 2012; **18**: 224-30.
46. Lee BH, Hwang DM, Palaniyar N, Grinstein S, Philpott DJ, Hu J. Activation of P2X(7) receptor by ATP plays an important role in regulating inflammatory responses during acute viral infection. *PLoS One* 2012; **7**(4): e35812.
47. Riteau N, Baron L, Villeret B, Guillou N, Savigny F, Ryffel B, et al. ATP release and purinergic signaling: a common pathway for particle-mediated inflammasome activation. *Cell Death Dis* 2012; **3**: e403.
48. Obeid M, Panaretakis T, Tesniere A, Joza N, Tufi R, Apetoh L, et al. Leveraging the immune system during chemotherapy: moving calreticulin to the cell surface converts apoptotic death from "silent" to immunogenic. *Cancer Res* 2007; **67**(17): 7941-4.
49. Gardai SJ, McPhillips KA, Frasch SC, Janssen WJ, Starefeldt A, Murphy-Ullrich JE, et al. Cell-surface calreticulin initiates clearance of viable or apoptotic cells through trans-activation of LRP on the phagocyte. *Cell* 2005; **123**(2): 321-34.
50. Shi J, Gao W, Shao F. Pyroptosis: Gasdermin-Mediated Programmed Necrotic Cell Death. *Trends Biochem Sci* 2017; **42**(4): 245-54.
51. Alvarez-Diaz S, Dillon CP, Lalaoui N, Tanzer MC, Rodriguez DA, Lin A, et al. The Pseudokinase MLKL and the Kinase RIPK3 Have Distinct Roles in Autoimmune Disease Caused by Loss of Death-Receptor-Induced Apoptosis. *Immunity* 2016; **45**(3): 513-26.
52. Vince JE, Wong WW, Gentle I, Lawlor KE, Allam R, O'Reilly L, et al. Inhibitor of apoptosis proteins limit RIP3 kinase-dependent interleukin-1 activation. *Immunity* 2012; **36**(2): 215-27.
53. Upton JW, Shubina M, Balachandran S. RIPK3-driven cell death during virus infections. *Immunol Rev* 2017; **277**(1): 90-101.
54. Hanahan D, Weinberg RA. Hallmarks of cancer: the next generation. *Cell* 2011; **144**(5): 646-74.
55. Matsuura K, Canfield K, Feng W, Kurokawa M. Metabolic Regulation of Apoptosis in Cancer. *Int Rev Cell Mol Biol* 2016; **327**: 43-87.
56. Yaacoub K, Pedeux R, Tarte K, Guillaudeux T. Role of the tumor microenvironment in regulating apoptosis and cancer progression. *Cancer Lett* 2016; **378**(2): 150-9.

57. Fernald K, Kurokawa M. Evading apoptosis in cancer. *Trends Cell Biol* 2013; **23**(12): 620-33.
58. Kaiser AM, Attardi LD. Deconstructing networks of p53-mediated tumor suppression in vivo. *Cell Death Differ* 2018; **25**(1): 93-103.
59. Liao D, Johnson RS. Hypoxia: a key regulator of angiogenesis in cancer. *Cancer Metastasis Rev* 2007; **26**(2): 281-90.
60. Bhattarai D, Xu X, Lee K. Hypoxia-inducible factor-1 (HIF-1) inhibitors from the last decade (2007 to 2016): A "structure-activity relationship" perspective. *Med Res Rev* 2017.
61. Dunn GP, Old LJ, Schreiber RD. The three Es of cancer immunoediting. *Annu Rev Immunol* 2004; **22**: 329-60.
62. French LE, Tschopp J. Defective death receptor signaling as a cause of tumor immune escape. *Semin Cancer Biol* 2002; **12**(1): 51-5.
63. Otten HG, van Ginkel WG, Hagenbeek A, Petersen EJ. Prevalence and clinical significance of resistance to perforin- and FAS-mediated cell death in leukemia. *Leukemia* 2004; **18**(8): 1401-5.
64. Kythreotou A, Siddique A, Mauri FA, Bower M, Pinato DJ. PD-L1. *J Clin Pathol* 2018; **71**(3): 189-94.
65. Ichim G, Tait SW. A fate worse than death: apoptosis as an oncogenic process. *Nat Rev Cancer* 2016; **16**(8): 539-48.
66. Garg AD, Romano E, Rufo N, Agostinis P. Immunogenic versus tolerogenic phagocytosis during anticancer therapy: mechanisms and clinical translation. *Cell Death Differ* 2016; **23**(6): 938-51.
67. Labi V, Erlacher M, Krumschnabel G, Manzl C, Tzankov A, Pinon J, et al. Apoptosis of leukocytes triggered by acute DNA damage promotes lymphoma formation. *Genes Dev* 2010; **24**(15): 1602-7.
68. Michalak EM, Vandenberg CJ, Delbridge AR, Wu L, Scott CL, Adams JM, et al. Apoptosis-promoted tumorigenesis: gamma-irradiation-induced thymic lymphomagenesis requires Puma-driven leukocyte death. *Genes Dev* 2010; **24**(15): 1608-13.
69. Richards CH, Mohammed Z, Qayyum T, Horgan PG, McMillan DC. The prognostic value of histological tumor necrosis in solid organ malignant disease: a systematic review. *Future Oncol* 2011; **7**(10): 1223-35.
70. Steinbach JP, Wolburg H, Klumpp A, Probst H, Weller M. Hypoxia-induced cell death in human malignant glioma cells: energy deprivation promotes decoupling of mitochondrial cytochrome c release from caspase processing and necrotic cell death. *Cell Death Differ* 2003; **10**(7): 823-32.
71. Vaupel P, Mayer A. Hypoxia in cancer: significance and impact on clinical outcome. *Cancer Metastasis Rev* 2007; **26**(2): 225-39.
72. Kumar V, Gabrilovich DI. Hypoxia-inducible factors in regulation of immune responses in tumour microenvironment. *Immunology* 2014; **143**(4): 512-9.
73. Tonnus W, Linkermann A. The in vivo evidence for regulated necrosis. *Immunol Rev* 2017; **277**(1): 128-49.
74. He S, Huang S, Shen Z. Biomarkers for the detection of necroptosis. *Cell Mol Life Sci* 2016; **73**(11-12): 2177-81.
75. Jouan-Lanhouet S, Riquet F, Duprez L, Vanden Berghe T, Takahashi N, Vandenabeele P. Necroptosis, in vivo detection in experimental disease models. *Semin Cell Dev Biol* 2014; **35**: 2-13.

76. Koo GB, Morgan MJ, Lee DG, Kim WJ, Yoon JH, Koo JS, et al. Methylation-dependent loss of RIP3 expression in cancer represses programmed necrosis in response to chemotherapeutics. *Cell Res* 2015; **25**(6): 707-25.
77. Moriwaki K, Bertin J, Gough PJ, Orlowski GM, Chan FK. Differential roles of RIPK1 and RIPK3 in TNF-induced necroptosis and chemotherapeutic agent-induced cell death. *Cell Death Dis* 2015; **6**: e1636.
78. Bozec D, Iuga AC, Roda G, Dahan S, Yeretssian G. Critical function of the necroptosis adaptor RIPK3 in protecting from intestinal tumorigenesis. *Oncotarget* 2016; **7**(29): 46384-400.
79. Li L, Yu S, Zang C. Low Necroptosis Process Predicts Poor Treatment Outcome of Human Papillomavirus Positive Cervical Cancers by Decreasing Tumor-Associated Macrophages M1 Polarization. *Gynecol Obstet Invest* 2018; **83**(3): 259-67.
80. Hockendorf U, Yabal M, Herold T, Munkhbaatar E, Rott S, Jilg S, et al. RIPK3 Restricts Myeloid Leukemogenesis by Promoting Cell Death and Differentiation of Leukemia Initiating Cells. *Cancer Cell* 2016; **30**(1): 75-91.
81. Kasof GM, Prosser JC, Liu D, Lorenzi MV, Gomes BC. The RIP-like kinase, RIP3, induces apoptosis and NF-kappaB nuclear translocation and localizes to mitochondria. *FEBS Lett* 2000; **473**(3): 285-91.
82. Mutirangura A, Pornthanakasem W, Sriuranpong V, Supiyaphun P, Voravud N. Loss of heterozygosity on chromosome 14 in nasopharyngeal carcinoma. *Int J Cancer* 1998; **78**(2): 153-6.
83. Papaemmanuil E, Hosking FJ, Vijayakrishnan J, Price A, Olver B, Sheridan E, et al. Loci on 7p12.2, 10q21.2 and 14q11.2 are associated with risk of childhood acute lymphoblastic leukemia. *Nat Genet* 2009; **41**(9): 1006-10.
84. Newton K, Sun X, Dixit VM. Kinase RIP3 is dispensable for normal NF-kappa Bs, signaling by the B-cell and T-cell receptors, tumor necrosis factor receptor 1, and Toll-like receptors 2 and 4. *Mol Cell Biol* 2004; **24**(4): 1464-9.
85. Wu J, Huang Z, Ren J, Zhang Z, He P, Li Y, et al. Mlkl knockout mice demonstrate the indispensable role of Mlkl in necroptosis. *Cell Res* 2013; **23**(8): 994-1006.
86. Gerl R, Vaux DL. Apoptosis in the development and treatment of cancer. *Carcinogenesis* 2005; **26**(2): 263-70.
87. Seifert L, Werba G, Tiwari S, Giao Ly NN, Alothman S, Alqunaibit D, et al. The necrosome promotes pancreatic oncogenesis via CXCL1 and Mincle-induced immune suppression. *Nature* 2016; **532**(7598): 245-9.
88. Seifert L, Miller G. Molecular Pathways: The Necrosome-A Target for Cancer Therapy. *Clin Cancer Res* 2017; **23**(5): 1132-6.
89. Hanggi K, Vasilikos L, Valls AF, Yerbes R, Knop J, Spilgies LM, et al. RIPK1/RIPK3 promotes vascular permeability to allow tumor cell extravasation independent of its necroptotic function. *Cell Death Dis* 2017; **8**(2): e2588.
90. Ahn J, Xia T, Konno H, Konno K, Ruiz P, Barber GN. Inflammation-driven carcinogenesis is mediated through STING. *Nat Commun* 2014; **5**: 5166.
91. Lemos H, Mohamed E, Huang L, Ou R, Pacholczyk G, Arbab AS, et al. STING Promotes the Growth of Tumors Characterized by Low Antigenicity via IDO Activation. *Cancer Res* 2016; **76**(8): 2076-81.
92. Huang C, Luo Y, Zhao J, Yang F, Zhao H, Fan W, et al. Shikonin kills glioma cells through necroptosis mediated by RIP-1. *PLoS One* 2013; **8**(6): e66326.

93. Eil R, Vodnala SK, Clever D, Klebanoff CA, Sukumar M, Pan JH, et al. Ionic immune suppression within the tumour microenvironment limits T cell effector function. *Nature* 2016; **537**(7621): 539-43.
94. Grivennikov SI, Greten FR, Karin M. Immunity, inflammation, and cancer. *Cell* 2010; **140**(6): 883-99.
95. Krysko O, Aaes TL, Kagan VE, D'Herde K, Bachert C, Leybaert L, et al. Necroptotic cell death in anti-cancer therapy. *Immunol Rev* 2017; **280**(1): 207-19.
96. Wang T, Jin Y, Yang W, Zhang L, Jin X, Liu X, et al. Necroptosis in cancer: An angel or a demon? *Tumour Biol* 2017; **39**(6): 1010428317711539.
97. Lalaoui N, Brumatti G. Relevance of necroptosis in cancer. *Immunol Cell Biol* 2017; **95**(2): 137-45.
98. Chen D, Yu J, Zhang L. Necroptosis: an alternative cell death program defending against cancer. *Biochim Biophys Acta* 2016; **1865**(2): 228-36.
99. Fulda S. Therapeutic exploitation of necroptosis for cancer therapy. *Semin Cell Dev Biol* 2014; **35**: 51-6.
100. Souers AJ, Leverson JD, Boghaert ER, Ackler SL, Catron ND, Chen J, et al. ABT-199, a potent and selective BCL-2 inhibitor, achieves antitumor activity while sparing platelets. *Nat Med* 2013; **19**(2): 202-8.
101. Oltersdorf T, Elmore SW, Shoemaker AR, Armstrong RC, Augeri DJ, Belli BA, et al. An inhibitor of Bcl-2 family proteins induces regression of solid tumours. *Nature* 2005; **435**(7042): 677-81.
102. Kotschy A, Szlavik Z, Murray J, Davidson J, Maragno AL, Le Toumelin-Braizat G, et al. The MCL1 inhibitor S63845 is tolerable and effective in diverse cancer models. *Nature* 2016; **538**(7626): 477-82.
103. Ludwig LM, Nassin ML, Hadji A, LaBelle JL. Killing Two Cells with One Stone: Pharmacologic BCL-2 Family Targeting for Cancer Cell Death and Immune Modulation. *Front Pediatr* 2016; **4**: 135.
104. Derakhshan A, Chen Z, Van Waes C. Therapeutic Small Molecules Target Inhibitor of Apoptosis Proteins in Cancers with Deregulation of Extrinsic and Intrinsic Cell Death Pathways. *Clin Cancer Res* 2017; **23**(6): 1379-87.
105. Casares N, Pequignot MO, Tesniere A, Ghiringhelli F, Roux S, Chaput N, et al. Caspase-dependent immunogenicity of doxorubicin-induced tumor cell death. *J Exp Med* 2005; **202**(12): 1691-701.
106. Spisek R, Charalambous A, Mazumder A, Vesole DH, Jagannath S, Dhodapkar MV. Bortezomib enhances dendritic cell (DC)-mediated induction of immunity to human myeloma via exposure of cell surface heat shock protein 90 on dying tumor cells: therapeutic implications. *Blood* 2007; **109**(11): 4839-45.
107. Tesniere A, Schlemmer F, Boige V, Kepp O, Martins I, Ghiringhelli F, et al. Immunogenic death of colon cancer cells treated with oxaliplatin. *Oncogene* 2010; **29**(4): 482-91.
108. Obeid M, Panaretakis T, Joza N, Tufi R, Tesniere A, van Endert P, et al. Calreticulin exposure is required for the immunogenicity of gamma-irradiation and UVC light-induced apoptosis. *Cell Death Differ* 2007; **14**(10): 1848-50.
109. Garg AD, Krysko DV, Vandenabeele P, Agostinis P. Hypericin-based photodynamic therapy induces surface exposure of damage-associated molecular patterns like HSP70 and calreticulin. *Cancer Immunol Immunother* 2012; **61**(2): 215-21.

110. Vandenabeele P, Vandecasteele K, Bachert C, Krysko O, Krysko DV. Immunogenic Apoptotic Cell Death and Anticancer Immunity. *Adv Exp Med Biol* 2016; **930**: 133-49.
111. Twyman-Saint Victor C, Rech AJ, Maity A, Rengan R, Pauken KE, Stelekati E, et al. Radiation and dual checkpoint blockade activate non-redundant immune mechanisms in cancer. *Nature* 2015; **520**(7547): 373-7.
112. Jain MV, Paczulla AM, Klonisch T, Dimgba FN, Rao SB, Roberg K, et al. Interconnections between apoptotic, autophagic and necrotic pathways: implications for cancer therapy development. *J Cell Mol Med* 2013; **17**(1): 12-29.
113. Rongvaux A, Jackson R, Harman CC, Li T, West AP, de Zoete MR, et al. Apoptotic caspases prevent the induction of type I interferons by mitochondrial DNA. *Cell* 2014; **159**(7): 1563-77.
114. White MJ, McArthur K, Metcalf D, Lane RM, Cambier JC, Herold MJ, et al. Apoptotic caspases suppress mtDNA-induced STING-mediated type I IFN production. *Cell* 2014; **159**(7): 1549-62.
115. Giampazolias E, Zunino B, Dhayade S, Bock F, Cloix C, Cao K, et al. Mitochondrial permeabilization engages NF-kappaB-dependent anti-tumour activity under caspase deficiency. *Nat Cell Biol* 2017; **19**(9): 1116-29.
116. Lee H, Shin EA, Lee JH, Ahn D, Kim CG, Kim JH, et al. Caspase inhibitors: a review of recently patented compounds (2013-2015). *Expert Opin Ther Pat* 2018; **28**(1): 47-59.
117. Ni HM, McGill MR, Chao X, Woolbright BL, Jaeschke H, Ding WX. Caspase inhibition prevents tumor necrosis factor-alpha-induced apoptosis and promotes necrotic cell death in mouse hepatocytes in vivo and in vitro. *Am J Pathol* 2016; **186**(10): 2623-36.
118. MacKenzie SH, Schipper JL, Clark AC. The potential for caspases in drug discovery. *Curr Opin Drug Discov Devel* 2010; **13**(5): 568-76.
119. Cho YS, Park HL. Exploitation of necroptosis for treatment of caspase-compromised cancers. *Oncol Lett* 2017; **14**(2): 1207-14.
120. Cho E, Lee JK, Park E, Seo CH, Luchian T, Park Y. Antitumor activity of HPA3P through RIPK3-dependent regulated necrotic cell death in colon cancer. *Oncotarget* 2018; **9**(8): 7902-17.
121. Fu Z, Deng B, Liao Y, Shan L, Yin F, Wang Z, et al. The anti-tumor effect of shikonin on osteosarcoma by inducing RIP1 and RIP3 dependent necroptosis. *BMC Cancer* 2013; **13**: 580.
122. Xuan Y, Hu X. Naturally-occurring shikonin analogues--a class of necroptotic inducers that circumvent cancer drug resistance. *Cancer Lett* 2009; **274**(2): 233-42.
123. Han W, Li L, Qiu S, Lu Q, Pan Q, Gu Y, et al. Shikonin circumvents cancer drug resistance by induction of a necroptotic death. *Mol Cancer Ther* 2007; **6**(5): 1641-9.
124. Cekay MJ, Roesler S, Frank T, Knuth AK, Eckhardt I, Fulda S. Smac mimetics and type II interferon synergistically induce necroptosis in various cancer cell lines. *Cancer Lett* 2017; **410**: 228-37.
125. McCabe KE, Bacos K, Lu D, Delaney JR, Axelrod J, Potter MD, et al. Triggering necroptosis in cisplatin and IAP antagonist-resistant ovarian carcinoma. *Cell Death Dis* 2014; **5**: e1496.
126. Steinhart L, Belz K, Fulda S. Smac mimetic and demethylating agents synergistically trigger cell death in acute myeloid leukemia cells and overcome apoptosis resistance by inducing necroptosis. *Cell Death Dis* 2013; **4**: e802.

127. Jing L, Song F, Liu Z, Li J, Wu B, Fu Z, et al. MLKL-PITPalpha signaling-mediated necroptosis contributes to cisplatin-triggered cell death in lung cancer A549 cells. *Cancer Lett* 2018; **414**: 136-46.
128. Xu Y, Lin Z, Zhao N, Zhou L, Liu F, Cichacz Z, et al. Receptor interactive protein kinase 3 promotes Cisplatin-triggered necrosis in apoptosis-resistant esophageal squamous cell carcinoma cells. *PLoS One* 2014; **9**(6): e100127.
129. Yang H, Ma Y, Chen G, Zhou H, Yamazaki T, Klein C, et al. Contribution of RIP3 and MLKL to immunogenic cell death signaling in cancer chemotherapy. *Oncoimmunology* 2016; **5**(6): e1149673.
130. Chesi M, Mirza NN, Garbitt VM, Sharik ME, Dueck AC, Asmann YW, et al. IAP antagonists induce anti-tumor immunity in multiple myeloma. *Nat Med* 2016; **22**(12): 1411-20.
131. He GW, Gunther C, Thonn V, Yu YQ, Martini E, Buchen B, et al. Regression of apoptosis-resistant colorectal tumors by induction of necroptosis in mice. *J Exp Med* 2017; **214**(6): 1655-62.
132. Rodriguez-Madoz JR, Zabala M, Alfaro M, Prieto J, Kramer MG, Smerdou C. Short-term intratumoral interleukin-12 expressed from an alphaviral vector is sufficient to induce an efficient antitumoral response against spontaneous hepatocellular carcinomas. *Hum Gene Ther* 2014; **25**(2): 132-43.
133. Murugesan SR, King CR, Osborn R, Fairweather WR, O'Reilly EM, Thornton MO, et al. Combination of human tumor necrosis factor-alpha (hTNF-alpha) gene delivery with gemcitabine is effective in models of pancreatic cancer. *Cancer Gene Ther* 2009; **16**(11): 841-7.
134. Zitvogel L, Tahara H, Cai Q, Storkus WJ, Muller G, Wolf SF, et al. Construction and characterization of retroviral vectors expressing biologically active human interleukin-12. *Hum Gene Ther* 1994; **5**(12): 1493-506.
135. Riediger C, Wingender G, Knolle P, Aulmann S, Stremmel W, Encke J. Fms-like tyrosine kinase 3 receptor ligand (Flt3L)-based vaccination administered with an adenoviral vector prevents tumor growth of colorectal cancer in a BALB/c mouse model. *J Cancer Res Clin Oncol* 2013; **139**(12): 2097-110.
136. Tandon M, Vemula SV, Sharma A, Ahi YS, Mittal S, Bangari DS, et al. EphrinA1-EphA2 interaction-mediated apoptosis and FMS-like tyrosine kinase 3 receptor ligand-induced immunotherapy inhibit tumor growth in a breast cancer mouse model. *J Gene Med* 2012; **14**(2): 77-89.
137. Hou S, Kou G, Fan X, Wang H, Qian W, Zhang D, et al. Eradication of hepatoma and colon cancer in mice with Flt3L gene therapy in combination with 5-FU. *Cancer Immunol Immunother* 2007; **56**(10): 1605-13.
138. Liu A, Guardino A, Chinsangaram L, Goldstein MJ, Panicali D, Levy R. Therapeutic vaccination against murine lymphoma by intratumoral injection of recombinant fowlpox virus encoding CD40 ligand. *Cancer Res* 2007; **67**(14): 7037-44.
139. Kikuchi T, Crystal RG. Anti-tumor immunity induced by in vivo adenovirus vector-mediated expression of CD40 ligand in tumor cells. *Hum Gene Ther* 1999; **10**(8): 1375-87.
140. del Campo AB, Aptsiauri N, Mendez R, Zinchenko S, Vales A, Paschen A, et al. Efficient recovery of HLA class I expression in human tumor cells after beta2-microglobulin gene transfer using adenoviral vector: implications for cancer immunotherapy. *Scand J Immunol* 2009; **70**(2): 125-35.

141. Hung KS, Hong CY, Lee J, Lin SK, Huang SC, Wang TM, et al. Expression of p16(INK4A) induces dominant suppression of glioblastoma growth in situ through necrosis and cell cycle arrest. *Biochem Biophys Res Commun* 2000; **269**(3): 718-25.
142. Caruso M, Panis Y, Gagandeep S, Houssin D, Salzmann JL, Klatzmann D. Regression of established macroscopic liver metastases after in situ transduction of a suicide gene. *Proc Natl Acad Sci U S A* 1993; **90**(15): 7024-8.
143. Culver KW, Ram Z, Wallbridge S, Ishii H, Oldfield EH, Blaese RM. In vivo gene transfer with retroviral vector-producer cells for treatment of experimental brain tumors. *Science* 1992; **256**(5063): 1550-2.
144. Xie X, Zhao X, Liu Y, Zhang J, Matusik RJ, Slawin KM, et al. Adenovirus-mediated tissue-targeted expression of a caspase-9-based artificial death switch for the treatment of prostate cancer. *Cancer Res* 2001; **61**(18): 6795-804.
145. Shariat SF, Desai S, Song W, Khan T, Zhao J, Nguyen C, et al. Adenovirus-mediated transfer of inducible caspases: a novel "death switch" gene therapeutic approach to prostate cancer. *Cancer Res* 2001; **61**(6): 2562-71.
146. Srivastava S, Riddell SR. Chimeric Antigen Receptor T Cell Therapy: Challenges to Bench-to-Bedside Efficacy. *J Immunol*. 2018; **200**(2): 459-68.
147. Lim WA, June CH. The Principles of Engineering Immune Cells to Treat Cancer. *Cell*. 2017; **168**(4): 724-40.
148. Johnson LA, June CH. Driving gene-engineered T cell immunotherapy of cancer. *Cell Res*. 2017; **27**(1): 38-58.
149. Fesnak AD, June CH, Levine BL. Engineered T cells: the promise and challenges of cancer immunotherapy. *Nat Rev Cancer*. 2016; **16**(9): 566-81.
150. Vance RE, Eichberg MJ, Portnoy DA, Raulet DH. Listening to each other: Infectious disease and cancer immunology. *Sci Immunol*. 2017; **2**(7): 10.1126/sciimmunol.aai9339.
151. Vatner RE, Janssen EM. STING, DCs and the link between innate and adaptive tumor immunity. *Mol Immunol*. 2017; 10.1016/j.molimm.2017.12.011.
152. Corrales L, Matson V, Flood B, Spranger S, Gajewski TF. Innate immune signaling and regulation in cancer immunotherapy. *Cell Res*. 2017; **27**(1): 96-108.
153. Rakoff-Nahoum S, Medzhitov R. Toll-like receptors and cancer. *Nat Rev Cancer*. 2009; **9**(1): 57-63.
154. Corrales L, McWhirter SM, Dubensky TW, Jr., Gajewski TF. The host STING pathway at the interface of cancer and immunity. *J Clin Invest*. 2016; **126**(7): 2404-11.
155. Binnewies M, Roberts EW, Kersten K, Chan V, Fearon DF, Merad M, et al. Understanding the tumor immune microenvironment (TIME) for effective therapy. *Nat Med*. 2018; **24**(5): 541-50.
156. Anderson KG, Stromnes IM, Greenberg PD. Obstacles Posed by the Tumor Microenvironment to T cell Activity: A Case for Synergistic Therapies. *Cancer Cell*. 2017; **31**(3): 311-25.
157. Bayat Mokhtari R, Homayouni TS, Baluch N, Morgatskaya E, Kumar S, Das B, et al. Combination therapy in combating cancer. *Oncotarget*. 2017; **8**(23): 38022-43.
158. Park CG, Hartl CA, Schmid D, Carmona EM, Kim HJ, Goldberg MS. Extended release of perioperative immunotherapy prevents tumor recurrence and eliminates metastases. *Sci Transl Med*. 2018; **10**(433): 10.1126/scitranslmed.aar1916.

159. Baird JR, Friedman D, Cottam B, Dubensky TW, Jr., Kanne DB, Bambina S, et al. Radiotherapy Combined with Novel STING-Targeting Oligonucleotides Results in Regression of Established Tumors. *Cancer Res*. 2016; **76**(1): 50-6.
160. Corrales L, Glickman LH, McWhirter SM, Kanne DB, Sivick KE, Katibah GE, et al. Direct Activation of STING in the Tumor Microenvironment Leads to Potent and Systemic Tumor Regression and Immunity. *Cell Rep*. 2015; **11**(7):1018-30.
161. Li T, Cheng H, Yuan H, Xu Q, Shu C, Zhang Y, et al. Antitumor Activity of cGAMP via Stimulation of cGAS-cGAMP-STING-IRF3 Mediated Innate Immune Response. *Sci Rep*. 2016; **6**: 10.1038/srep19049.
162. Yu X, Wang H, Li X, Guo C, Yuan F, Fisher PB, et al. Activation of the MDA-5-IPS-1 Viral Sensing Pathway Induces Cancer Cell Death and Type I IFN-Dependent Antitumor Immunity. *Cancer Res*. 2016; **76**(8): 2166-76.
163. Bath-Hextall F, Ozolins M, Armstrong SJ, Colver GB, Perkins W, Miller PS, et al. Surgical excision versus imiquimod 5% cream for nodular and superficial basal-cell carcinoma (SINS): a multicentre, non-inferiority, randomised controlled trial. *The Lancet Oncology*. 2014; **15**(1): 96-105.
164. Akalu YT, Rothlin CV, Ghosh S. TAM receptor tyrosine kinases as emerging targets of innate immune checkpoint blockade for cancer therapy. *Immunol Rev*. 2017; **276**(1): 165-77.
165. von Massenhausen A, Sanders C, Thewes B, Deng M, Queisser A, Vogel W, et al. MERTK as a novel therapeutic target in head and neck cancer. *Oncotarget*. 2016; **7**(22): 32678-94.
166. Li Y, Ye X, Tan C, Hongo JA, Zha J, Liu J, et al. Axl as a potential therapeutic target in cancer: role of Axl in tumor growth, metastasis and angiogenesis. *Oncogene*. 2009; **28**(39): 3442-55.
167. Holland SJ, Pan A, Franci C, Hu Y, Chang B, Li W, et al. R428, a selective small molecule inhibitor of Axl kinase, blocks tumor spread and prolongs survival in models of metastatic breast cancer. *Cancer Res*. 2010; **70**(4):1544-54.
168. Cummings CT, Zhang W, Davies KD, Kirkpatrick GD, Zhang D, DeRyckere D, et al. Small Molecule Inhibition of MERTK Is Efficacious in Non-Small Cell Lung Cancer Models Independent of Driver Oncogene Status. *Mol Cancer Ther*. 2015; **14**(9): 2014-22.
169. Dagogo-Jack I, Shaw AT. Tumour heterogeneity and resistance to cancer therapies. *Nat Rev Clin Oncol* 2018; **15**(2): 81-94.
170. Zappasodi R, Merghoub T, Wolchok JD. Emerging Concepts for Immune Checkpoint Blockade-Based Combination Therapies. *Cancer Cell*. 2018; **33**(4): 581-98.
171. June CH, Warshauer JT, Bluestone JA. Is autoimmunity the Achilles' heel of cancer immunotherapy? *Nat Med* 2017; **23**(5): 540-7.
172. Yang L, Yu H, Dong S, Zhong Y, Hu S. Recognizing and managing on toxicities in cancer immunotherapy. *Tumour Biol* 2017; **39**(3): 10.1177/1010428317694542.
173. Puzanov I, Diab A, Abdallah K, Bingham CO, 3rd, Brogdon C, Dadu R, et al. Managing toxicities associated with immune checkpoint inhibitors: consensus recommendations from the Society for Immunotherapy of Cancer (SITC) Toxicity Management Working Group. *J Immunother Cancer* 2017; **5**(1): 95.
174. Sharma P, Hu-Lieskovan S, Wargo JA, Ribas A. Primary, Adaptive, and Acquired Resistance to Cancer Immunotherapy. *Cell* 2017; **168**(4): 707-23.
175. Binder DC, Fu YX, Weichselbaum RR. Radiotherapy and immune checkpoint blockade: potential interactions and future directions. *Trends Mol Med.* 2015; **21**(8): 463-65.

176. Messmer MN, Snyder AG, Oberst A. Comparing the effects of different cell death programs in tumor progression and immunotherapy. *Cell Death Differ.* 2018; **26**(1): 10.1038/s41418-018-0214-4.
177. Kazama H, Ricci JE, Herndon JM, Hoppe G, Green DR, Ferguson TA. Induction of immunological tolerance by apoptotic cells requires caspase-dependent oxidation of high-mobility group box-1 protein. *Immunity.* 2008; **29**(1): 21-32.
178. Love Aaes T, Kaczmarek A, Delvaeye T, De Craene B, De Koker S, Heyndrickx L, et al. Vaccination with necroptotic cancer cells induces efficient anti-tumor immunity. *Cell Rep.* 2016; **15**(2): 274-87.
179. Nailwal H, Chan FK. Necroptosis in anti-viral inflammation. *Cell Death Differ.* 2018; **26**(1): 4-13.
180. Orozco S, Yatim N, Werner MR, Tran H, Gunja SY, Tait SWG, et al. RIPK1 both positively and negatively regulates RIPK3 oligomerization and necroptosis. *Cell Death Differ*. 2014; **21**(10): 1511-21.
181. Moore MW, Carbone FR, Bevan MJ. Introduction of soluble protein into the class I pathway of antigen processing and presentation. *Cell*. 1988; **54**(6): 777-85.
182. Spranger S, Dai D, Horton B, Gajewski TF. Tumor-residing Batf3 dendritic cells are required for effector T cell trafficking and adoptive T cell therapy. *Cancer Cell.* 2017; **31**(5): 711-23.
183. Gutierrez KD, Davis MA, Daniels BP, Olsen TM, Ralli-Jain P, Tait SWG, et al. MLKL activation triggers NLRP3-mediated processing and release of IL-1β independently of gasdermin-D. *J Immunol*. 2017; **198**(5): 2156-64.
184. Remijsen Q, Goossens V, Grootjans S, Van den Haute C, Vanlangenakker N, Dondelinger Y, et al. Depletion of RIPK3 or MLKL blocks TNF-driven necroptosis and switches towards a delayed RIPK1 kinase-dependent apoptosis. *Cell Death Dis.* 2014; **5**: 10.1038/cddis.2013.531.
185. Mandal P, Berger SB, Pillay S, Moriwaki K, Huang C, Guo H, et al. RIP3 induces apoptosis independent of pronecrotic kinase activity. *Mol Cell*. 2014; **56**(4): 481-95.
186. Broz ML, Binnewies M, Boldajipour B, Nelson AE, Pollack JL, Erle DJ, et al. Dissecting the tumor myeloid compartment reveals rare activating antigen-presenting cells critical for T cell immunity. *Cancer Cell.* 2014; **26**(5): 638-52.
187. Salmon H, Idoyaga J, Rahman A, Leboeuf M, Remark R, Jordan S, et al. Expansion and activation of $CD103^+$ dendritic cell progenitors at the tumor site enhances tumor responses to therapeutic PD-L1 and BRAF inhibition. *Immunity.* 2016; **44**(4): 924-38.
188. Bottcher P, Bonavita E, Chakravarty P, Blees H, Cabeza-Cabrerizo M, Sammicheli S, et al. NK cells stimulate recruitment of cDC1 into the tumor microenvironment promoting cancer immune control. *Cell.* 2018; **172**(5): 1022-37.
189. Saleh D, Najjar M, Zelic M, Shah S, Nogusa S, Polykratis A, et al. Kinase activities of RIPK1 and RIPK3 can direct IFN-β synthesis induced by lipopolysaccharide. *J Immunol.* 2017; **198**(11): 4435-47.
190. Krysko DV, Denecker G, Festjens N, Gabriels S, Parthoens E, D'herde K, et al. Macrophages use different internalization mechanisms to clear apoptotic and necrotic cells. *Cell Death Differ.* 2006; **13**(12): 2011-22.
191. Seehawer M, Heinzmann F, D'Artista L, Harbig J, Roux P, Hoenicke L, et al. Necroptosis microenvironment directs lineage commitment in liver cancer. *Nature.* 2018; **562**(7725): 69-75.

192. Gray EE, Winship D, Snyder JM, Child SJ, Geballe AP, Stetson DB. The AIM2-like receptors are dispensable for the interferon response to intracellular DNA. *Immunity*. 2016; **45**(2): 255-66.
193. Sanjana NE, Shalem O, Zhang F. Improved vectors and genome-wide libraries for CRISPR screening. *Nat Methods*. 2014; **11**(8): 783-4.
194. Naso MF, Tomkowicz B, Perry III WL, Strohl WR. Adeno-associated virus (AAV) as a vector for gene therapy. 2017; **31**(7): 317-34.
195. Buning H, Schmidt M. Adeno-associated vector toxicity – to be or not to be? *Mol Ther.* 2015; **23**(11): 1673-1675.
196. Colella P, Ronzitti G, Mingozzi F. Emerging issues in AAV-mediated *in vivo* gene therapy. *Mol Ther Methods Clin Dev*. 2018; **8**: 87-104.
197. Dong B, Nakai H, Xiao W. Characterizaton of genome integrity for oversized recombinant AAV vector. *Mol Ther*. 2010; **18**(1): 87-92.
198. Zhong L, Li B, Mah CS, Govindasamy L, Agbandje-McKenna M, Cooper M, et al. Next generation of adeno-associated virus 2 vectors: point mutations in tyrosines lead to high-efficiency transduction at lower doses. *Proc Natl Acad Sci.* 2008; **105**(22): 7827-7832.
199. Gabriel N, Hareendran S, Sen D, Gadkari RA, Sudha G, Selot R, et al. Bioengineering of AAV2 capsid at specific serine, threonine, or lysine residues improves its transduction efficiency in vitro and in vivo. *Hum Gene Ther Methods*. 2013; **24**(2): 80-93.
200. Mitchell AM, Li C, Samulski RJ. Arsenic trioxide stabilizes accumulations of adeno-associated virus virions at the perinuclear region, increasing transduction in vitro and in vivo. *J Virol.* 2013; **87**(8): 4571-4583.
201. Wang LN, Wang Y, Lu Y, Yin ZF, Zhang YH, Aslanidi GV, et al. Pristimerin enhances recombinant adeno-associated virus vector-mediated transgene expression in human cell lines in vitro and murine hepatocytes in vivo. *J Integr Med.* 2014; **12**(1): 20-34.
202. Faust SM, Bell P, Cutler BJ, Ashley SN, Zhu Y, Rabinowitz JE, et al. CpG-depleted adeno-associated virus vectors evade immune detection. *J Clin Invest.* 2013; **123**(7): 2994-3001.
203. Papadakis ED, Nicklin SA, Baker AH, White SJ. Promoters and control elements: designing expression cassettes for gene therapy. *Curr Gene Ther*. 2004; **4**(1): 89-113.
204. Choi JH, Yu NK, Baek GC, Bakes J, Seo D, Nam HJ, et al. Optimization of AAV expression cassettes to improve packaging capacity and transgene expression in neurons. *Mol Brain*. 2014; **7**: 17.
205. Weinmann J, Grimm D. Next-generation AAV vectors for clinical use: an ever-accelerating race. *Virus Genes*. 2017; **53**(5): 707-713.
206. Hubbard N, Haing D, Sommer K, Song Y, Khan I, Clough C, et al. Targeted gene editing restores regulated CD40L function in X-linked hyper-IgM syndrome. *Blood.* 2016; **127**(21), 2513-22.
207. Sather BD, Romano Ibarra GS, Sommer K, Curinga G, Hale M, Khan IF, et al. Efficient modification of CCR5 in primary human hematopoietic cells using a megaTAL nuclease and AAV donor template. *Sci Transl Med.* 2015; **7**(307): 10.1126/scitranslmed.aac5530.
208. Nathwani AC, Tuddenham EGD, Rangarajan S, Rosales C, McIntosh J, Linch DC, et al. Adenovirus-associated virus vector-mediated gene transfer in hemophilia B. *N Engl J Med.* 2011; **365**(25): 2357-65.
209. Boyken SE, Chen Z, Groves B, Langan RA, Oberdorfer G, Ford A, et al. De novo design of protein homo-oligomers with modular hydrogen-bond network-mediated specificity. *Science.* 2016; **352**(6286), 680-7.

210. Bowles DE, McPhee SW, Li C, Gray SJ, Samulski JJ, Camp AS, et al. Phase 1 gene therapy for Duchenne muscular dystrophy using a translational optimized AAV vector. *Mol Ther.* 2012; **20**(2): 443-55.
211. Weinstein JN, Collisson EA, Mills GB, Shaw KM, Ozenberger BA, Ellrott K, et al. The Cancer Genome Atlas pan-cancer analysis project. *Nat Genet.* 2013; **45**(10), 1113-20.
212. Anaya J. OncoLnc: linking TCGA survival data to mRNAs, miRNAs, and lncRNAs. *PeerJ Comp Sci.* 2016; **2**: e67.
213. Van Hoecke L, Van Lint S, Roose K, Van Parys A, Vandenabeele P, Grooten J, et al. Treatment with mRNA coding for the necroptosis mediator MLKL induces antitumor immunity directed against neo-epitopes. 2018; **9**(1): 3417.
214. Ott PA, Hodi FS, Kaufman HL, Wigginton JM, Wolchok JD. Combination immunotherapy: a road map. *J Immunother of Cancer*. 2017; **5**(16): 10.1186/s40425-017-0218-5.
215. Kearse M, Moir R, Wilson A, Stones-Havas S, Cheung M, Sturrock S, et al. Geneious Basic: an integrated and extendable desktop software platform for the organization and analysis of sequence data. *Bioinformatics.* 2012; **28**(12): 1647-9.
216. Khan IF, Hirata RK, Russel DW. AAV-mediated gene targeting methods for human cells. *Nat Protocol.* 2011; **6**(4): 482-501.
217. Brault M, Olsen TM, Martinez J, Stetson DB, Oberst A. Intracellular nucleic acid sensing triggers necroptosis through synergistic type I IFN and TNF signaling. *J Immunol.* 2018; **200**(8): 2748-56.
218. Liu T, Zhang L, Joo D, Sun SC. NF-κB signaling in inflammation. *Signal Transduct Target Ther.* 2017; **2**(17023): 10.1038/sigtrans.2017.23.
219. Martinez FO, Gordon S. The M1 and M2 paradigm of macrophage activation: time for reassessment. *F1000Prime Rep.* 2014; **6**(13): 10.12703/P6-13.
220. Han X, Wilbanks GD, Devaja O, Ruperlia V, Raju KS. IL-2 enhances standard IFNgamma/LPS activation of macrophage cytotoxicity to human ovarian carcinoma in vitro: a potential for adoptive cellular immunotherapy. *Gynecol Oncol.* 1999; **75**(2): 198-210.
221. Grohmann U, Belladonna ML, Vacca C, Bianchi R, Fallarino F, Orabona C, et al. Positive regulatory role of IL-12 in macrophages and modulation by IFN-gamma. *J Immunol*. 2001; **167**(1): 221-227.
222. Brunner C, Seiderer J, Schlamp A, Bidlingmaier M, Eigler A, Haimerl W, et al. Enhanced dendritic cell maturation by TNF-alpha or cytidine-phosphate-guanosine DNA drives T cell activation in vitro and therapeutic anti-tumor immune responses in vivo. *J Immunol.* 2000; **165**(11): 6278-6286.
223. Parameswaran N and Patial S. Tumor necrosis factor-α signaling in macrophages. *Crit Rev Eukaryot Gene Expr*. 2010; **20**(2): 87-103.
224. Montoya M, Schiavoni G, Mattei F, Gresser I, Belardelli F, Borrow P, et al. Type I interferons produced by dendritic cells promote their phenotypic and functional activation. *Blood*. 2002; **99**(9): 3263-3271.
225. Ding X, Yang W, Shi X, Du P, Su L, Qin Z, et al. TNF receptor 1 mediates dendritic cell maturation and CD8 T cell response through two distinct mechanisms. *J Immunol.* 2011; **187**(3): 1184-1191.
226. Simmons DP, Wearsch PA, Canaday DH, Meyerson HJ, Liu YC, Wang Y, et al. Type I IFN drives a distinctive dendritic cell maturation phenotype that allows continued class II MHC synthesis and antigen processing. *J Immunol*. 2012; **188**(7): 3116-3126.

227. Peppelenbosch MP, DeSmedt M, Pynaert G, van Deventer SJH, Grooten J. Macrophages present pinocytosed exogenous antigen via MHC class I whereas antigen ingested by receptor-mediator endocytosis is presented via MHC class II. *J Immunol.* 2000; **165**(4): 10.4049/jimmunol.165.4.1984.
228. Chandler RJ, LaFave MC, Varshney GK, Trivedi NS, Carrillo-Carrasco N, Senac JS, et al. Vector design influences hepatic genotoxicity after adeno-associated virus gene therapy. *J Clin Invest*. 2015; **125**(2): 870-880.
229. Donsante A, Miller DG, Li Y, Vogler C, Brunt EM, Russell DW, et al. AAV vector integration sites in mouse hepatocellular carcinoma. *Science*. 2007; **317**(5837): 477.
230. Nault JC, Mami I, La Bella T, Datta S, Imbeaud S, Franconi A, et al. Wild-type AAV insertions in hepatocellular carcinoma do not inform debate over genotoxicity risk of vectorized AAV. *Mol Ther.* 2016; **24**(4): 660-661.
231. Logan GJ, Dane AP, Hallwirth CV, Smyth CM, Wilkie EE, Amaya AK, et al. Identification of liver-specific enhancer-promoter activity in the 3' untranslated region of the wild-type AAV2 genome. *Nat Genet.* 2017; **49**(8): 1267-1273.
232. Louis Jeune V, Joergensen JA, Hajjar RJ, Weber T. Pre-existing anti-adeno-associated virus antibodies as a challenge in AAV gene therapy. *Hum Gene Ther Methods*. 2013; **24**(2): 59-67.
233. Sudres M, Cire S, Vasseur V, Brault L, Da Rocha S, Boisgerault F, et al. MyD88 signaling in B cells regulates the production of Th1-dependent antibodies to AAV. *Mol Ther*. 2012; **20**(8): 1571-1581.
234. Thwaite R, Pages G, Chillon M, Boscha A. AAVrh.10 immunogenicity in mice and humans: Relevance of antibody cross-reactivity in human gene therapy. *Gene Ther.* 2015; **22**(2): 196-201.
235. Greenberg B, Butler J, Felker GM, Ponikowski P, Voors A, Pogoda JM, et al. Prevalence of AAV1 neutralizing antibodies an consequences for a clinical trial of gene transfer for advanced heart failure. *Gene Ther*. 2016; **23**(3): 313-319.
236. Mays LE, Wilson JM. The complex and evolving story of T cell activation to AAV vector-encoded transgene products. *Mol Ther*. 2011; **19**(1): 16-27.
237. Russell SJ, Peng K-W, Bell JC. Oncolytic virotherapy. *Nat Biotechnol*. 2012; **30**(7): 658-670.
238. Raja J, Ludwig JM, Gettinger SN, Schalper KA, Kim HS. Oncolytic virus immunotherapy: future prospects for oncology. *J Immunother Canc.* 2018; **6**(1): 140.
239. Goldufsky J, Sivendran S, Harcharik S, Pan M, Bernardo S, Stern RH, et al. Oncolytic virus therapy for cancer. *Oncolytic Virother*. 2013; **2**: 31-46.
240. Senzer NN, Kaufman HL, Amatruda T, Nemunaitis M, Reid T, Daniels G, et al. Phase II clinical trial of a granulocyte-macrophage colony-stimulating factor-encoding, second-generation oncolytic herpesvirus in patients with unresectable metastatic melanoma. *J Clin Oncol*. 2009; **27**(34): 5763-5771.
241. Pol J, Kroemer G, Galluzzi L. First oncolytic virus approved for melanoma immunotherapy. *Taylor & Francis*; 2016.
242. Warashina S, Nakamura T, Sato Y, Fujiwara Y, Hyodo M, Hatakeyama H, et al. A lipid nanoparticle for the efficient delivery of siRNA to dendritic cells. *J Contr Rel*. 2016; **225**: 183-191.

243. Conde J, Bao C, Tan Y, Cui D, Edelman ER, Azevedo HS, et al. Dual targeted immunothrapy via in vivo delivery of biohybrid RNAi-peptide nanoparticles to tumor-associated macorphages and cancer cells. *Adv Func Mater.* 2015; **25**(27): 4183-4194.
244. Velpurisiva P, Gad A, Piel B, Jadia R, Rai P. Nanoparticle design strategies for effective cancer immunotherapy. *J Biomed (Syd)*. 2017; **2**(2): 64-77.
245. Talmadge JE, Singh RK, Fidler IJ, Raz A. Murine models to evaluate novel and conventional therapeutic strategies for cancer. *Am J Pathol*. 2007, **170**(3): 793-804.
246. Day C-P, Merlino G, Van Dyke T. Preclinical mouse cancer models: a maze of opportunities and challenges. *Cell*. 2015; **163**(1): 39-53.